NASA CONTRACTOR REPORT

NASA CR-1621

THEORETICAL FREQUENCY RESPONSE FUNCTIONS AND POWER SPECTRA OF THE XB-70 RESPONSE TO ATMOSPHERIC TURBULENCE

by Thomas E. Stenton

Prepared by
NORTH AMERICAN ROCKWELL CORPORATION
Los Angeles, Calif.
for Langley Research Center

NATIONAL AERONAUTICS AND SPACE ADMINISTRATION • WASHINGTON, D. C. • AUGUST 1970

1. Report No.	2. Government Accession No.	3. Recipient's Catalog No.
NASA CR-1621		

4. Title and Subtitle	5. Report Date
THEORETICAL FREQUENCY RESPONSE FUNCTIONS AND POWER SPECTRA OF THE XB-70 RESPONSE TO ATMOSPHERIC TURBULENCE	August 1970
	6. Performing Organization Code
7. Author(s)	8. Performing Organization Report No.
Thomas E. Stenton	
	10. Work Unit No.
9. Performing Organization Name and Address	720-02-10-01-23
North American Rockwell Corporation Los Angeles, California	11. Contract or Grant No. NAS1-7805
12. Sponsoring Agency Name and Address	13. Type of Report and Period Covered Contractor Report
National Aeronautics and Space Administration Washington, D. C. 20546	14. Sponsoring Agency Code

15. Supplementary Notes

16. Abstract

Responses include normal accelerations at eight locations on the airplane, pitch rate at the center of gravity, a representative fuselage bending moment, and wing tip hinge moment. Calculated results are presented for eight different flight conditions with respect to weight (390,000 to 542,000 lbs.), Mach number (0.4 to 3.0), and altitude (0 to 70,000 ft). Generalized aerodynamic forces on the wing due to motion and sinusoidal gust field were determined from unsteady lifting surface theory. The theoretical frequency responses and spectra are compared with experimental results for one flight condition and with theoretical results obtained by another method.

17. Key Words (Suggested by Author(s))	18. Distribution Statement
Airplane response to atmospheric turbulence XB-70 gust response	UNCLASSIFIED - UNLIMITED

19. Security Classif. (of this report)	20. Security Classif. (of this page)	21. No. of Pages	22. Price*
Unclassified	Unclassified	121	$3.00

*For sale by the Clearinghouse for Federal Scientific and Technical Information
Springfield, Virginia 22151

PREFACE

This report presents the calculated theoretical system response functions and power spectral density functions of certain XB-70 airplane response parameters to be measured in test flights. The work has been accomplished by the Los Angeles Division of North American Rockwell Corporation under Contract NAS 1-7805 with the NASA, Langley Research Center, Hampton, Virginia.
P. F. Wildermuth was the program manager, L. G. Johnson was the project engineer,and T. E. Stenton was the principal investigator. The contract monitor for the NASA was Kermit G. Pratt.

TABLE OF CONTENTS

LIST OF ILLUSTRATIONS

LIST OF ILLUSTRATIONS - Continued

LIST OF TABLES

THEORETICAL FREQUENCY RESPONSE FUNCTIONS

AND POWER SPECTRA OF THE XB-70

RESPONSE TO ATMOSPHERIC TURBULENCE

By Thomas E. Stenton

Los Angeles Division

North American Rockwell Corporation

SUMMARY

Theoretical frequency dependent system response functions and power spectra are presented for the response of certain parameters to atmospheric turbulence encounter by the XB-70 airplane. Calculations are made for 8 different flight conditions, with Mach numbers ranging from 0.4 to 3.0 and altitudes ranging from sea level to 70,000 feet.

Unsteady lifting surface theory was used to predict the generalized forces on the wing due to motion and gust. Quasi-steady theory was used to predict the contributions from the canard and forebody. The responses are assumed to be small perturbations from the trim condition.

Comparisons of responses are made with experimental results obtained from one flight condition and with theoretical results obtained by another method.

INTRODUCTION

The introduction of modern high speed flexible aircraft has focused increasing attention on the problem of accurate determination of theoretical frequency dependent system response functions and power spectra. Attention has been directed particularly toward the use of these functions in the prediction of loads spectra by the method of generalized harmonic analysis, reference 1. More recently, a number of studies have been performed on systems that extend the stability augmentation devices into the lower frequency structural dynamic modes, references 2, 3, 4. These studies have shown that it is possible to selectively gain stabilize by shifting the mode frequencies and to phase stabilize by increasing the damping, and to avoid or filter out control signals from the several modes, significant to the aircraft's dynamics. Such systems are desirable from the standpoint of increasing passenger and crew comfort, and for the purpose of increasing the feasibility of high speed flight at low altitudes where severe turbulence may be encountered.

Although the mathematical representation of a theoretical system response function is well-known and straightforward, its actual accurate determination is extremely complicated because of the very accurate and detailed knowledge that is required about the airplane's characteristics. Precise knowledge is required of the airplane's weight distribution, its flexibility, and the aerodynamic forcing and damping functions.

The present work was performed using the XB-70 airplane as the subject vehicle. The purpose of the work was to perform the calculation of theoretical system response functions and power spectra for (1) acceleration at two designated fuselage stations for comparison with existing flight test measurements, reference 5, (2) acceleration at the pilot station for comparison with existing theoretical data from an alternate method, reference 2, and (3) prediction of various airplane responses for representative flight conditions.

The gust field was assumed to be constant spanwise and to have a velocity, normal to the wing, that varied sinusoidally in the direction of flight. Seven longitudinal modes of motion were assumed, these were: plunge, pitch, and five normal modes of flexibility. Free-free normal modes and frequencies were computed using methods described by references 6, 7, and 8. The unsteady generalized forces were computed for the subsonic regime using a computer program based on the method of reference 9. For the supersonic regime, the program of reference 10 was used. The dynamic equations of motion are formed in the same manner as the flutter equation with the addition of a gust forcing function.

SYMBOLS

$A_i = A_i(x,y)$	deflection of ith mode at point (x,y), feet, positive down
a_n	acceleration, $\ddot{z}/g$, g units, positive up
$B(\omega)$	dynamic response matrix
$\bar{c}$	mean aerodynamic chord, feet
$F_i = F_i(\omega)$	generalized force in ith mode due to impingement of a unit sinusoidal gust
f	frequency, cycles per second
$G_i = G_i(\omega)$	$F_i/(2\rho \times 10^6)$
g	acceleration of gravity
$H = H(\omega)$	system response function
I	imaginary part of a complex number or function
i	$\sqrt{-1}$

i,j	modal subscripts
K	counter described by equation 3
k	reduced frequency, $\omega\bar{c}/2V$
L	scale of turbulence, feet
L	parameter described by equation 3
M	generalized mass, $U^T mU$
m	point mass
Q_{ij}	generalized force in mode i due to deflection in mode j
q_i	generalized coordinate of ith mode
R	real part of a complex number or function
t	time, seconds
U	matrix of modal columns
U^T	the transpose of U
$\bar{u}$	the magnitude of an oscillating function, $u = \bar{u} \cdot \exp(i\omega t)$
$\lvert u \rvert$	absolute value of the complex function u
V	true velocity, feet per second
w	complex downwash
x	streamwise coordinate, feet
y	spanwise coordinate, feet
$\ddot{z}$	acceleration, feet/sec^2, positive down
γ	structural damping parameter
θ	phase angle, degrees
ρ	density, slugs/foot^3
σ	root mean square
$\Phi_o(\omega)$	power spectral density of a response parameter
$\Phi_w(\omega)$	gust spectrum

$\Omega = \omega/V$	spatial frequency, radians per foot
ω	frequency, radians per second

METHOD OF ANALYSIS

Normal Mode Shapes and Frequencies

The normal mode shapes and frequencies were obtained from a computer program based on the methods outlined in references 6, 7, and 8. The dynamic matrix is freed in the rigid motions of pitch and plunge using the method of reference 6. The eigenvalue problem is then solved by a computer program based on the method of reference 7, page 84. The theoretical background for this eigenvalue solution is given in reference 8.

The computer program normalizes the modal columns in such a way that:

$$U^T \, m \, U = I$$

where U is a matrix of modal columns, U^T is the transpose of U, m is a diagonal matrix of point masses in dimensions of pounds/385.92, and I is the identity matrix. The mass diagonal is formed from weights for the one-half airplane.

Generalized masses associated with the structural modes are defined by:

$$M = U^T \, m \, U$$

Since the equations of motion, described in the next section, are written in units of feet-pounds-seconds, and since complete airplane weights are used, the generalized masses obtained from this method are all:

$$1 \times 2 \times 12 = 24$$

For flight conditions 2-1 through 2-3, table III, the mode shapes, frequencies, and generalized masses of reference 2 are used. The generalized masses and modal frequencies are given in table IV. Plots of the mode shapes are depicted in figures 16 through 22. The buttock planes plotted are: 0, 180, 280, 361, 394, 480.8 and 589.2.

The mode shape for the plunge mode is considered to be a positive deflection of one foot everywhere. The mode shape for the pitch mode is a rotation, nose up, about the actual center of gravity such that the slope of the rotation angle is 1.0. It follows that the generalized mass in the plunge mode is the total mass of the airplane in slugs, and that the generalized mass in the pitch mode is the pitching moment of inertia in slug-ft^2.

Equations of Motion

The basic coordinates included in the equations of motion are normal plunging displacement, designated q_1, pitching displacement, designated q_2, and coordinates for the five structural modes of lowest frequency, designated q_3 through q_7. Units of feet, pounds, seconds, radians apply. All deflections are taken positive down, and rotation is positive nose up. Unit deflection in the structural modes is taken to mean a deflection of one foot at the point where the mode shape is + 1. The equation defining the steady-state response of the ith coordinate, q_i, to a unit sinusoidal gust, $1 \cdot \exp(i\omega t)$, impinging on the airplane is:

$$(-\omega^2 + (1 + i\gamma)\,\omega_i^2)\, q_i = \frac{1}{M_i} \sum_{j=1}^{7} Q_{ij}\, q_j + \frac{1}{M_i} F_i \tag{1}$$

where

$q = \overline{q}(\omega) \exp(i\omega t)$ = generalized coordinate

$Q_{ij} = \overline{Q}_{ij}(\omega) \exp(i\omega t)$ = generalized force in mode i due to unit deflection in mode j at frequency ω

$F_i = \overline{F}_i(\omega) \exp(i\omega t)$ = generalized force in mode i due to a unit sinusoidal gust of frequency ω

γ = structural damping parameter

ω_i = ith mode structural frequency

M_i = ith mode generalized mass

Equation (1) is written for each generalized coordinate, q, resulting in the formal matrix equation:

$$\Big(B(\omega)\Big)\, \overline{q}(\omega) = \left[\frac{1}{M}\right] \left\{\overline{F}(\omega)\right\} \tag{2}$$

Equation (2) is formed and solved for the values of ω :

$$\omega = \pi K/L, \qquad K = 0, 1, 2 \text{ --- } K_{max} \tag{3}$$

The parameter K_{max} was 100 for all the computer runs, and L ranged from 6.7 to 7. Solution of equation (2) results in a set of system response functions, $H(\omega)$, for the basic coordinates q_i .

Generalized Forces

The generalized forces, Q_{ij}, and F_i, for the wing were computed in the subsonic regime by a computer program based on the subsonic kernel function method of reference 9. For the supersonic speed regime, the computer program of reference 10 was used. The program of reference 10 employs a network of supersonic Mach boxes overlaid on the wing, together with velocity potential influence coefficients which define the velocity potential at a box center due to unit complex downwashes at other boxes which lie in the forward Mach cone of influence. The velocity potential distribution is thus determined as a function of the distribution of downwash over the wing. Pressure distributions and generalized forces are computed from the velocity potential distribution. The program of reference 10 is an extension of that of reference 11 to account for more general planforms, and for a trailing edge control surface.

The generalized forces were computed for a small number of frequencies (10 in the subsonic case and 8 in the supersonic case). These were then curve fitted to produce values at the frequency points described by equation (3). For the purpose of solving equation (2), the generalized forces were put on digital tape and read off as needed in the solution. This process was employed in order to avoid the excessive amount of computer time that would be required to generate, from the aerodynamic programs, generalized forces for all values of frequency that were required.

The generalized forces for the canard and forebody were generated internally in a quasi-steady manner and were then added to the wing contribution, after first multiplying the part due to gust by an appropriate time-lag function. The canard angle of attack was considered to be defined by the angle of attack at the attach point; the canard was assumed to be otherwise rigid.

The pitching moment resulting from airloads on the canard and forebody are destabilizing and that resulting from airloads on the wing is stabilizing. The total pitching moment at any frequency of oscillation thus results in a small difference between large numbers. It was therefore considered prudent to ratio all pitching moments determined from the aerodynamic programs for the wing by a number determined from known pitching moment characteristics of the wing at zero frequency. After the canard and forebody contributions were added, the total lift and moment were again adjusted to reflect the known short period characteristics of the airplane. These ratios were applied only to the principal part of the lift and moment due to plunge and pitch motions.

The wing contribution to the generalized force due to gust was computed in the same manner as those due to motion, except for this case a special gust downwash mode was entered in the programs, defined by

$$w = 1 \cdot \exp\left(-i\omega\frac{x}{V}\right)$$

where

w = the complex downwash due to gust

ω = frequency, radians per second x = a streamwise spatial dimension, positive aft from the wing apex

V = velocity, feet per second

This gust mode was treated as an oscillatory downwash "mode", but not a deflection mode; for this problem, where there are seven modes of motion and one gust mode, the resulting generalized force matrix consists of seven rows and eight columns, the eighth column being the generalized forces in the various modes of motion due to a sinusoidal gust of unit velocity and frequency ω. The generalized gust forces for the wing alone are presented, for the various flight conditions, in figures 23 through 30 as G_1 thru G_7 where $G_i = F_i/(2\rho \times 10^6)$ and F_i is the generalized force in the ith mode due to impingement of a unit sinusoidal gust.

System Response Functions

System response functions for the various parameters of interest were computed using linear combinations of the system response functions of the generalized coordinates. For example, at frequency ω, the normal acceleration factor at a point (x,y) on the airframe is given by:

$$H(\omega) = a_n(\omega) = \frac{\omega^2}{32.16} \sum_{i=1}^{7} A_i(x,y)\, \bar{q}_i(\omega) \tag{4}$$

where $A(x,y)$ is the mode displacement at the point (x,y) associated with the generalized coordinate q_i. System response functions for fuselage bending moment and tip hinge moment were computed by the mode displacement method as described by reference 12, page 641.

All responses were computed as excursions from the trim condition, and small perturbations are assumed.

Power Spectral Density Functions

Power spectral density functions were computed from the system response functions and the appropriate gust spectra using:

$$\Phi_o(\omega) = \left|H(\omega)\right|^2 \Phi_w(\omega)$$

where

$\left|H(\omega)\right|$ = the absolute value of the system response function

$\Phi_o(\omega)$ = the output spectrum

$\Phi_w(\omega)$ = the gust spectrum

and $\Phi(\omega) = \frac{1}{V}\,\tilde{\Phi}(\Omega)$

Two types of gust spectra were used, (1) the Von Karman spectrum defined by

$$\frac{\tilde{\Phi}_w(\Omega)}{\sigma_w^2} = \frac{L}{\pi} \; \frac{1 + \frac{8\Omega^2}{3}(1.339L)^2}{(1 + \Omega^2(1.339L)^2)^{11/6}}$$

and (2) the Dryden spectrum defined by

$$\frac{\tilde{\Phi}_w(\Omega)}{\sigma_w^2} = \frac{L}{\pi} \; \frac{1 + 3\,\Omega^2 L^2}{(1 + \Omega^2 L^2)^2}$$

For Condition 1-1, the Von Karman spectrum was used with L = 2500. For Condition 2-1, the Dryden spectrum was used with L = 500, and for Conditions 2-2 and 2-3, the Dryden spectrum was used with L = 1000. Plots of these gust spectra are depicted in figure 3.

RESULTS

General Discussion

System response functions and power spectral density functions were computed for various weight cases and flight conditions. The results are presented in figures 4 through 15. Response parameter designations and locations, flight conditions, flexibility data, and figure indices are keyed by tables II through V. For flight Conditions 1-1 and 2-1 through 2-3, only two parameters were considered. These were the normal acceleration factor at the pilot station and at a nominal center of gravity station. The locations of these two stations were dictated by the position of accelerometers located there. The center of gravity station is thus taken to be at fuselage station 1485 although the actual center of gravity is elsewhere, and varies for each weight case. The pilot station is at fuselage station 441. For flight Conditions 3-1 through 3-4, system response functions were computed for eleven parameters listed in table II.

Comparison with Experimental Results

The theoretical power spectral density functions computed for flight Condition 1-1 are compared with the experimental results of reference 5 and the results are presented in figures 5(a) and 5(b). The curves cannot be compared quantitatively, because the RMS of the turbulence encountered on the flight record analyzed in reference 5 is unknown, while the RMS of the turbulence for the present theoretical results is 1.0. The results of reference 5 were therefore normalized to produce the same RMS response as that for the present results. It should also be pointed out that the "peakedness" of the curves of reference 5 is a function of the bandwidth used in reducing the data. The data of reference 5 was analyzed using a bandwidth of .25 cps. Decreasing the bandwidth would result in a higher resolution of the peaks and an increase in magnitude at the peak points. The only real comparison that can be made between the experimental and theoretical results is the frequency at which the peaks occur, and the relative magnitude. The theoretical results indicate that for the response at the pilot station, the power is concentrated in the short period mode, and the first and third structural modes.

Comparison with Other Theoretical Results

The power spectral density functions for the normal acceleration factor at the pilot station for flight Conditions 2-1, 2-2, and 2-3 are presented in figures 7(b), 9(b), and 11(b), where the results are compared to those of reference 2. The comparison varies from poor in the subsonic speed range to excellent at Mach number 3.0. It is believed that this phenomenon is partly related to the fact that the results of reference 2 were obtained using coefficients for all the generalized forces due to motion. These coefficients defined the level of the real part of the generalized force, and the slope of the imaginary part at zero frequency. Such an approach assumes a constant real part of the generalized force, and an imaginary part which is linear with frequency, and at Mach number 3.0, the assumption is nearly valid. In fact, for the cases studied, and for most modes of motion, the generalized forces were nearly linear for values of reduced frequency, $k \leq 0.5$. The maximum values of k required varied from 0.6 for the Mach 3 case to about 4.3 for the Mach 0.4 case. Although the generalized forces become highly nonlinear for the larger values of k, the coefficients used in reference 2 agree with similar coefficients extracted (at low k) from the frequency dependent data used herein. These data were satisfactory for the study objectives of reference 2.

CONCLUDING REMARKS

Theoretical system response functions and power spectra have been computed for the response of certain parameters to atmospheric turbulence encounter by the XB-70 airplane. Comparisons were made with experimental response power spectra obtained from one flight condition, and with theoretical results obtained by another method.

Unsteady lifting surface theory was used to predict the forces due to motion and gust on the wing, and quasi-steady aerodynamics was used to predict the contribution from the canard and forebody. It appears that the use of unsteady lifting theory is mandatory where the frequency range of interest extends to that associated with the flexible modes of motion. The maximum reduced frequency of interest was 4.3 for one case and, for such a large value of k, even the most sophisticated methods for computing generalized forces are suspect.

REFERENCES

1. Houbolt, J. C.; Steiner, R.; and Pratt, K. G.: Dynamic Response of Airplanes to Atmospheric Turbulence Including Flight Data on Input and Response. NASA TR R-199, June 1964.

2. Wykes, John H.; and Mori, Alva S.: An Analysis of Flexible Aircraft Structural Mode Control. Part I. Unclassified Data. AFFDL-TR-65-190, June 1966.

3. Andrew, G. M.; Johnson, J. M., Jr.; and Gardner, F. H.: Gust Alleviator and Rigidity Augmentor for Supersonic Airplanes. Institute of Aerospace Sciences Paper No. 62-1, January 1962.

4. Andrew, G. M.; and Johnson, J. M., Jr.: Automatic Control of Aeroelastic Modes. Institute of Aerospace Sciences Paper No. 62-86, June 1962.

5. Kordes, Eldon E.; and Love, Betty J.: Preliminary Evaluation of XB-70 Airplane Encounter with High Altitude Turbulence. NASA Technical Note D-4209, October 1967.

6. Dugundji, John: On the Calculation of Natural Modes of Free Free Structures. Journal of the Aeronautical Sciences, February 1961.

7. Ralston, Anthony; and Wilf, Herbert S.: Mathematical Methods for Digital Computers. John Wiley and Sons, Inc, New York 1960

8. Jacobi, C. G. J.: Über ein Leichtes Verfahren, die in der Theorie der Säkularstörungen Vorkommenden Gleichungen Numerisch Aufzulözen. J. reine angew, Math., vol. 30, 1846.

9. Watkins, Charles E.; Woolston, D. S.; and Cunningham, H. J.: A Systematic Kernel Function Procedure for Determining Aerodynamic Forces on Oscillating or Steady Finite Wings at Subsonic Speeds. NASA Technical Report R-48, 1959.

10. Donato, Vincent W.; and Huhn, Charles R., Jr.: Supersonic Unsteady Aerodynamics for Wings with Trailing Edge Control Surfaces and Folded Tips. AFFDL-TR-68-30, January 1968.

11. Moore, M. T.; and Andrew, L. V.: Unsteady Aerodynamics for Advanced Configurations. Part IV. Application of the Supersonic Mach Box Method to Intersecting Planar Lifting Surfaces. FDL-TDR-64-152, Part IV, February 1965.

12. Bisplinghoff, Raymond L.; Ashley, Holt; and Halfman, Robert L.: Aeroelasticity. Addison-Wesley Publishing Co., Inc, Cambridge, Mass. c. 1955.

TABLE I.- GEOMETRIC CHARACTERISTICS OF THE XB-70 AIRPLANE

Total wing -	
Total area (includes 2482.34 ft^2 covered by fuselage but not 33.53 ft^2 of the wing ramp area), ft^2	6297.8
Span, ft	105
Aspect ratio	1.751
Taper ratio	0.019
Dihedral angle, deg	0
Root chord (wing station 0), ft	117.76
Tip chord (wing station 630 in.) ft	2.19
Mean aerodynamic chord (wing station 213.85 in.), in.	942.38
Fuselage station of 25-percent wing mean aerodynamic chord, in.	1621.22
Sweepback angle, deg:	
Leading edge	65.57
25-percent element	58.79
Trailing edge	0
Incidence angle, deg:	
Root (fuselage juncture)	0
Tip (fold line and outboard)	-2.60
Airfoil section:	
Root to wing station 186 in.(thickness-chord ratio, 2 percent)	0.30 to 0.70 HEX (MOD)
Wing station 460 in. to 630 in. (thickness-chord ratio, 2.5 percent)	0.30 to 0.70 HEX (MOD)
Inboard wing -	
Area (includes 2482.34 ft^2 covered by fuselage but not 33.53 ft^2 wing ramp area), ft^2	5256.0
Span, ft	63.44
Aspect ratio	0.766
Taper ratio	0.407
Dihedral angle, deg	0
Root chord (wing station 0), ft	117.76
Tip chord (wing station 380.62 in.) ft	47.94
Mean aerodynamic chord (wing station 163.58 in.), in.	1053
Fuselage station of 25-percent wing mean aerodynamic chord, in.	1538.29
Sweepback angle, deg:	
Leading edge	65.57
25-percent element	58.79
Trailing edge	0
Airfoil section:	
Root (thickness-chord ratio, 2 percent)	0.30 to 0.70 HEX (MOD)
Tip (thickness-chord ratio, 2.4 percent)	0.30 to 0.70 HEX (MOD)

TABLE I.- GEOMETRIC CHARACTERISTICS OF THE XB-70 AIRPLANE - Continued

Mean camber (leading edge), deg:		
Butt plane 0		0.15
Butt plane 107 in.		4.40
Butt plane 153 in.		3.15
Butt plane 257 in.		2.33
Butt plane 367 in. to tip		0
Outboard wing -		
Area (one side only), ft^2		520.90
Span, ft		20.78
Aspect ratio		0.829
Taper ratio		0.046
Dihedral angle, deg		0
Root chord (wing station 380.62 in.), ft		47.94
Tip chord (wing station 630 in.), ft		2.19
Mean aerodynamic chord (wing station 467.37 in.), in.		384.25
Sweepback angle, deg:		
Leading edge		65.57
25-percent element		58.79
Trailing edge		0
Airfoil section:		
Root (thickness-chord ratio, 2.4 percent)		0.30 to 0.70 HEX (MOD)
Tip (Thickness-chord ratio, 2.5 percent)		0.30 to 0.70 HEX (MOD)
Down deflection from wing reference plane, deg		0, 25, 65
Skewline of tip fold, deg:		
Leading edge in		1.5
Leading edge down		3
Wing-tip area in wing reference plane (one side only), ft^2:		
Rotated down 25 deg		472.04
Rotated down 65 deg		220.01
	Wing tips	
	Up	Down
Elevons (data for one side):		
Total area aft of hinge line, ft^2	197.7	135.26
Span, ft	20.44	13.98
Inboard chord (equivalent), in.	116	116
Outboard chord (equivalent), in.	116	116
Sweepback angle of hinge line, deg	0	0
Deflection, deg:		
As elevator		-25 to 15
As aileron with elevators at ± 15 deg or less		-15 to 15
As aileron with elevators at -25 deg		-5 to 5
Total		-30 to 30
Canard -		
Area (includes 150.31 ft^2 covered by fuselage), ft^2		415.59
Span, ft		28.81
Aspect ratio		1.997
Taper ratio		0.388

TABLE I.- GEOMETRIC CHARACTERISTICS OF THE XB-70 AIRPLANE - Continued

Dihedral angle, deg	0
Root chord (canard station 0), ft	20.79
Tip chord (canard station 172.86 in.), ft	8.06
Mean aerodynamic chord (canard station 73.71 in.), in.	184.3
Fuselage station of 25-percent canard mean aerodynamic chord, in.	553.73
Sweepback angle, deg:	
Leading edge	31.70
25-percent element	21.64
Trailing edge	-14.91
Incidence angle (nose up), deg	0 to 6
Airfoil section:	
Root (thickness-chord ratio 2.5 percent)	0.34 to 0.66 HEX (MOD)
Tip (thickness-chord ratio 2.52 percent)	0.34 to 0.66 HEX (MOD)
Ratio of canard area to wing area	0.066
Canard flap (one of two):	
Area (aft of hinge line), ft^2	54.69
Ratio of flap area to canard semi-area	0.263
Vertical tail (one of two) -	
Area (includes 8.96 ft^2 blanketed area), ft^2	233.96
Span, ft	15
Aspect ratio	1
Taper ratio	0.30
Root chord (vertical-tail station 0), ft	23.08
Tip chord (vertical-tail station 180 in.), ft	6.92
Mean aerodynamic chord (vertical-tail station 73.85 in.), in.	197.40
Fuselage station of 25-percent vertical-tail mean aerodynamic chord, in.	2188.50
Sweepback angle, deg:	
Leading edge	51.77
25-percent element	45
Trailing edge	10.89
Airfoil section:	
Root thickness-chord ratio 3.75 percent)	0.30 to 0.70 HEX (MOD)
Tip (thickness-chord ratio 2.5 percent)	0.30 to 0.70 HEX (MOD)
Cant angle, deg	0
Ratio vertical tail to wing area	0.037
Rudder travel, deg:	
With gear extended	± 12
With gear retracted	± 3
Fuselage (includes canopy) -	
Length, ft	185.75
Maximum depth (fuselage station 878 in.), in.	106.92
Maximum breadth (fuselage station 855 in.), in.	100
Side area, ft^2	939.72

TABLE I.- GEOMETRIC CHARACTERISTICS OF THE XB-70 AIRPLANE - Concluded

Planform area, ft^2	1184.78
Center of gravity:	
Forward limit, percent mean aerodynamic chord	19.0
Aft limit, percent mean aerodynamic chord	25.0
Duct -	
Length, ft	104.84
Maximum depth (fuselage station 1375 in.), in.	90.75
Maximum breadth (fuselage station 2100 in.), in.	360.70
Side area, ft^2	716.66
Planform area, ft^2	2342.33
Inlet captive area (each), $in.^2$	5600
Surface areas (net wetted), ft^2:	
Fuselage and canopy	2871.24
Duct	4956.66
Wing, wing tips, and wing ramp	7658.44
Vertical tails (two)	936.64
Canard	530.83
Tail pipes	340.45
Total	17,294.26
Engines	6 YJ93-GE-3
Landing gear -	
Tread, ft	23.17
Wheelbase, in.	554.50
Tire size:	
Main gear (8)	40 x 17.5-18
Nose gear (2)	40 x 17.5-18

TABLE II.- RESPONSE PARAMETER LOCATIONS, XB-70-1 AIRPLANE

Response parameter	Instrumentation parameter number	Location: Fuselage station, in.	Location: Butt plane, in.
Normal acceleration at center of gravity station	A490	1485	-11 (3)
Normal acceleration at pilot station	A488	441 (1),(2)	-12 (3)
Normal acceleration at nose instrumentation package	A486	195	-6 (3)
Normal acceleration at wing apex station	A900	1284	0
Normal acceleration at aft fuselage station	A912	2037	4 (3)
Normal acceleration at left hand wing tip	A496	2200	520
Normal acceleration at forward wing tip hinge line	A492	1820	375
Normal acceleration at aft wing tip hinge line	A494	2172	375
Rate of pitch at center of gravity	M209		0
Fuselage bending moment at station 1040		1040	
Wing tip hinge moment			375

(1) Used station 438 for Condition 1-1 per reference 5.
(2) Used station 432 for Conditions 2-1, 2-2, and 2-3 per reference 2.
(3) Butt plane 0 used in analyses.

TABLE III.- FLIGHT CONDITIONS

Condition number	Mach number, M	Altitude h, ft	Tip position, δ_T, deg	Airplane weight, W, lb	Center of gravity, fus. sta. in.	Turbulence spectra type	Scale of turbulence L, ft
1-1	2.40	55 000	65	411 144	1602.44	Von Karman	2500
2-1	0.40	0	0	542 029	1598.38	Dryden	500
2-2	0.90	25 000	0	542 029	1598.38	Dryden	1000
2-3	3.00	70 000	65	394 578	1596.40	Dryden	1000
3-1	0.80	20 000	0	480 000	1592.08		
3-2	1.40	30 000	65	450 000	1587.00		
3-3	2.10	50 000	65	420 000	1597.50		
3-4	2.60	65 000	65	390 000	1589.26		

TABLE IV.- GENERALIZED MASSES AND FREQUENCIES, STRUCTURAL MODES

Condition number	Airplane weight W, lb	Generalized mass, slugs					Frequency, cycles per second				
		Mode 1	Mode 2	Mode 3	Mode 4	Mode 5	Mode 1	Mode 2	Mode 3	Mode 4	Mode 5
1-1	411 144	24.0	24.0	24.0	24.0	24.0	1.77	3.4	3.71	5.48	6.02
2-1 (1)	542 029	788.84	90.34	3861.39	212.69	42.63	1.79	3.01	3.82	5.10	6.49
2-2 (1)	542 029	788.84	90.34	3861.39	212.69	42.63	1.79	3.01	3.82	5.10	6.49
2-3 (1)	394 578	2699.45	119.62	1754.17	131.65	22.94	2.00	3.34	4.13	5.70	6.38
3-1	480 000	24.0	24.0	24.0	24.0	24.0	1.65	3.07	3.56	5.03	6.07
3-2	450 000	24.0	24.0	24.0	24.0	24.0	1.69	3.39	3.55	5.36	5.85
3-3	420 000	24.0	24.0	24.0	24.0	24.0	1.72	3.40	3.66	5.41	5.88
3-4	390 000	24.0	24.0	24.0	24.0	24.0	1.75	3.42	3.79	5.61	5.92

(1) Data for these conditions from reference 2.

TABLE V.- FIGURE INDEX

Condition number	System response functions	Power spectral densities	Mode shapes	Generalized gust forces
1-1	4(a) and 4(b)	5(a) and 5(b)	16	23
2-1	6(a) and 6(b)	7(a) and 7(b)	17	24
2-2	8(a) and 8(b)	9(a) and 9(b)	17	25
2-3	10(a) and 10(b)	11(a) and 11(b)	18	26
3-1	12(a) thru 12(k)		19	27
3-2	13(a) thru 13(k)		20	28
3-3	14(a) thru 14(k)		21	29
3-4	15(a) thru 15(k)		22	30

TABLE VI.- CONVERSION TO INTERNATIONAL SYSTEM (SI) UNITS

To convert from	to	multiply by
foot	meter	0.30480
foot^2	meter^2	0.09290
foot/second	meter/second	0.30480
inch	meter	0.02540
inch pound	meter kilogram	0.01152
pound (avoirdupois)	kilogram	0.45359
slug	kilogram	14.59390

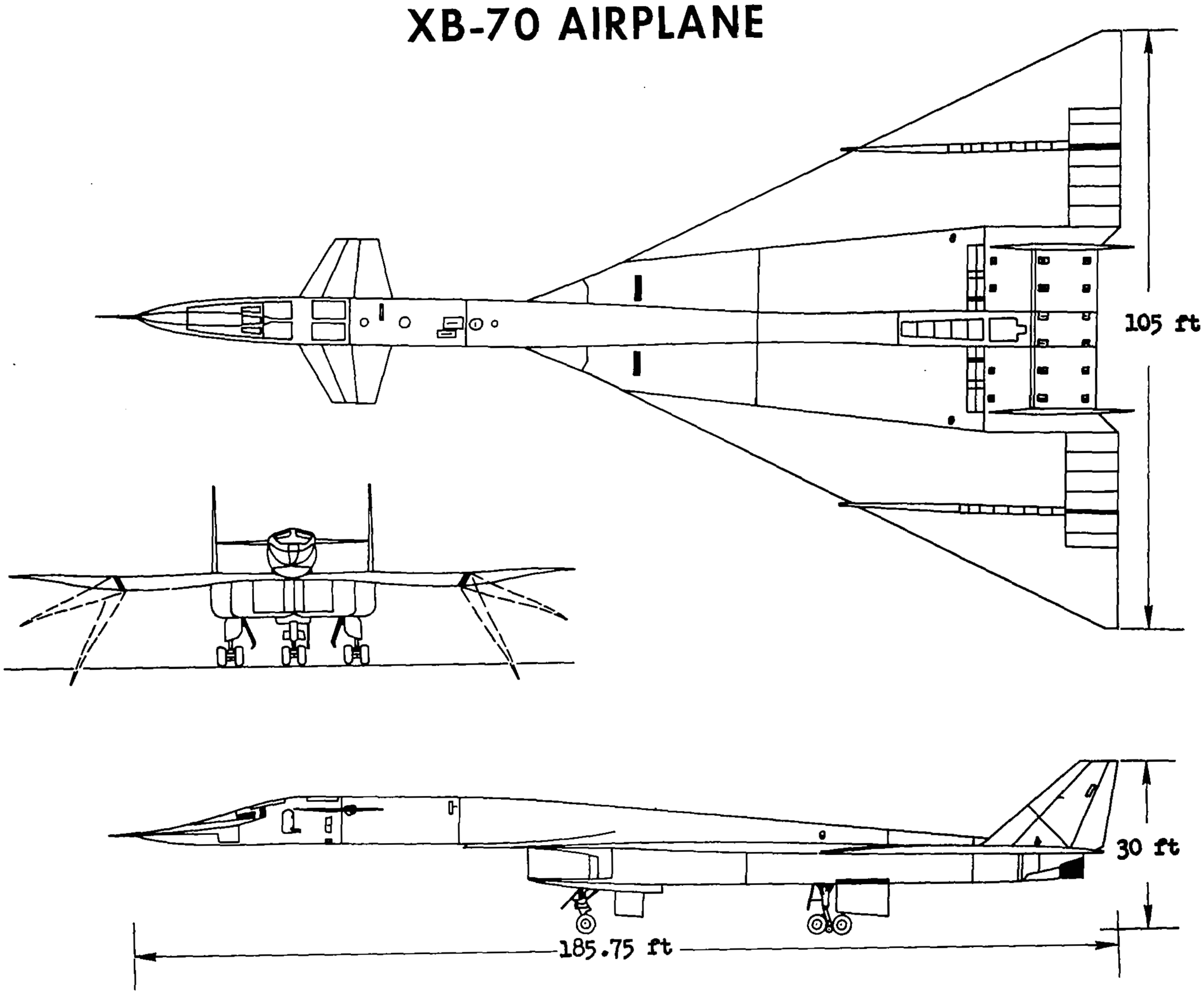

Figure 1.- Three-view drawing of the XB-70-1 airplane.

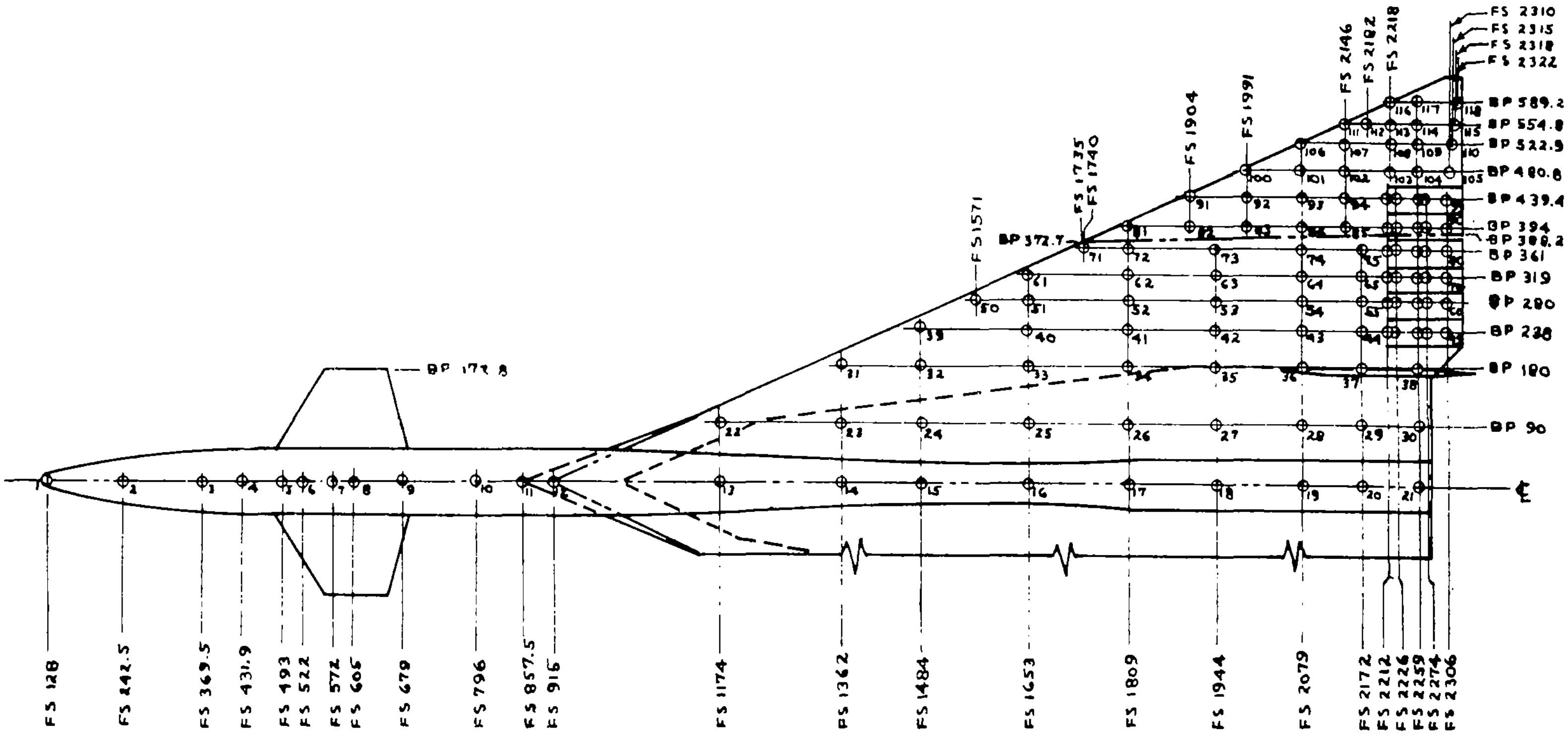

Figure 2.- XB-70 geometry and mode shape grid.

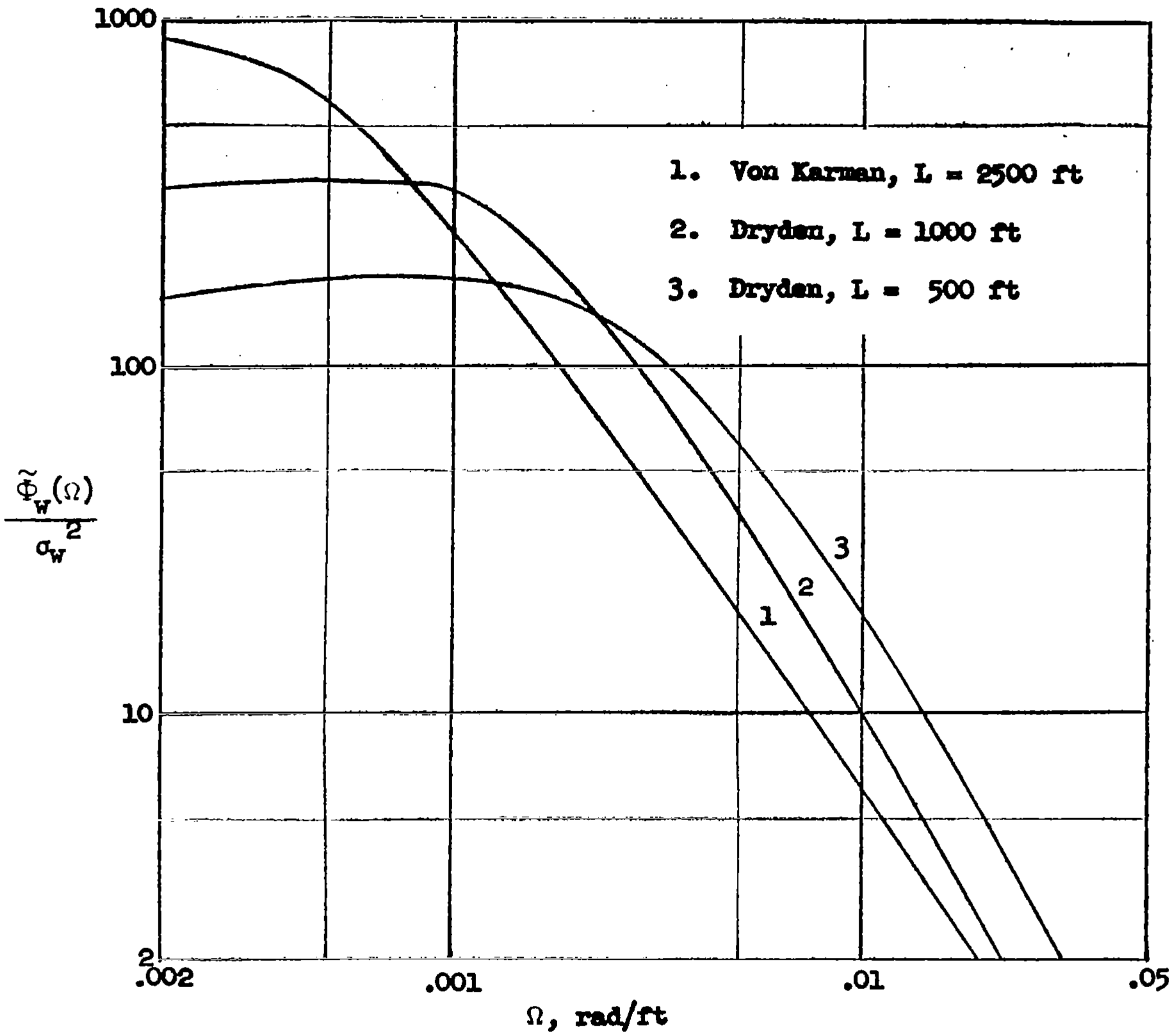

Figure 3.- Atmospheric turbulence spectra.

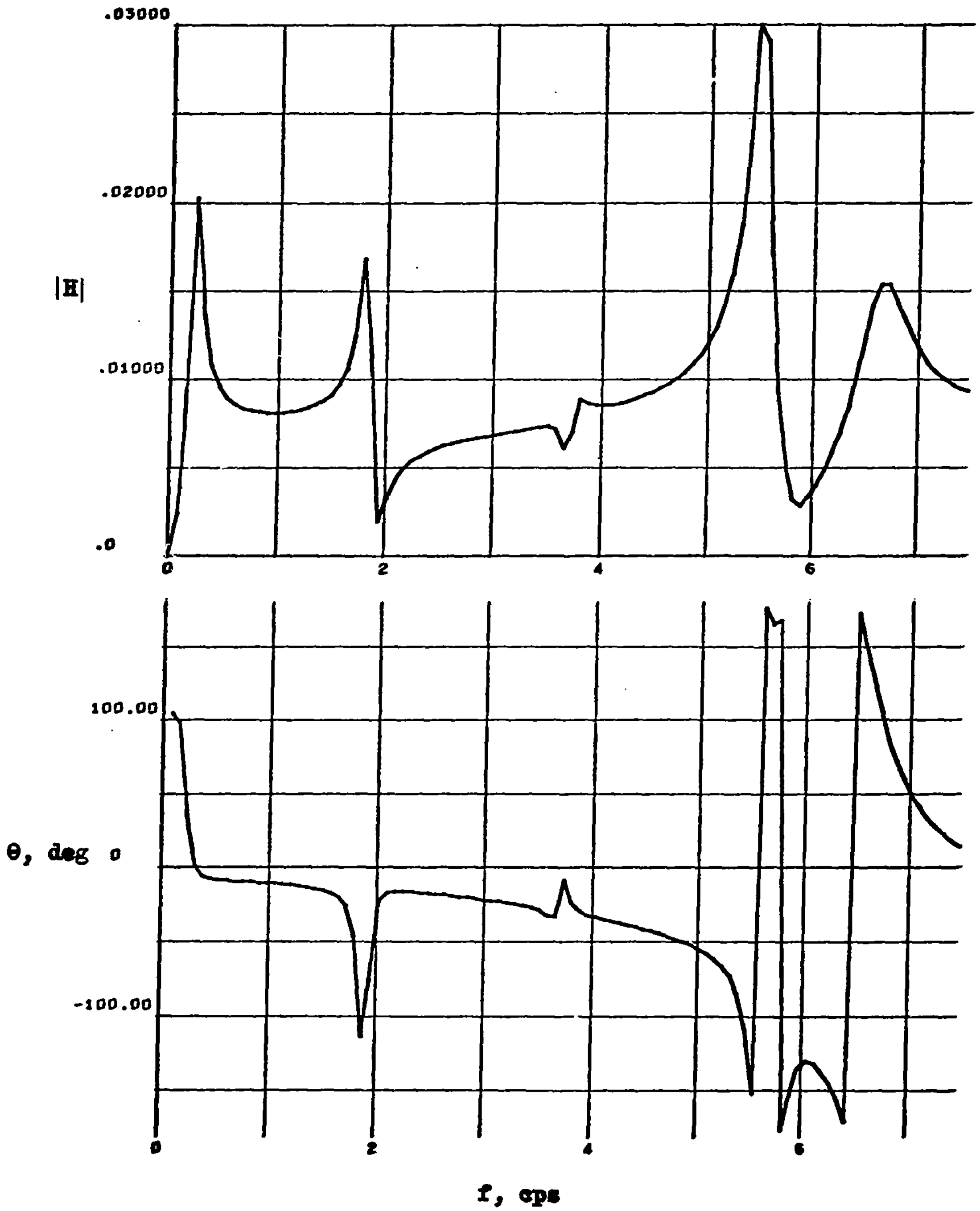

(a) Acceleration at the center of gravity station.

Figure 4.- System response functions for Condition 1-1.

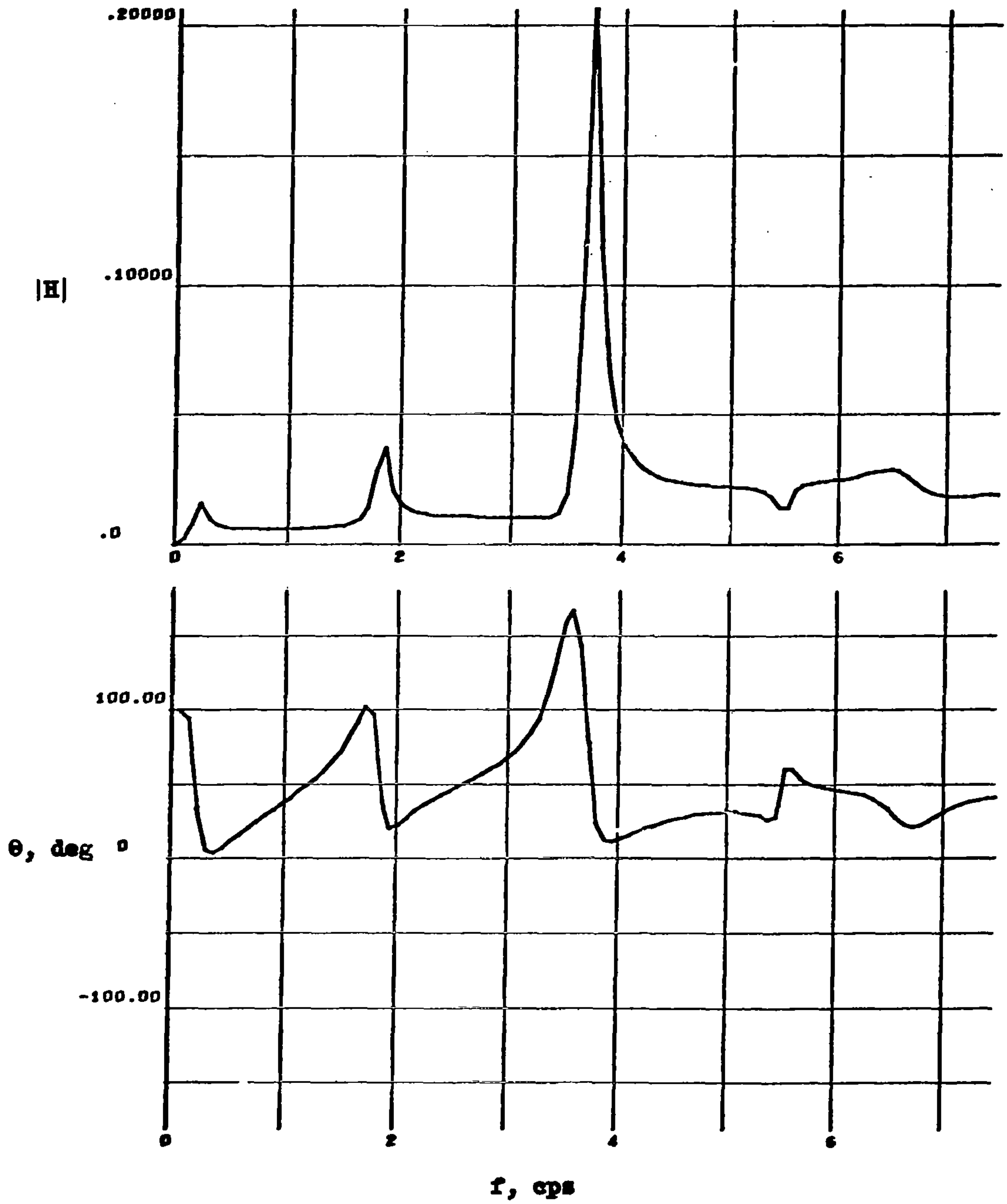

(b) Acceleration at the pilot station.

Figure 4.- Concluded.

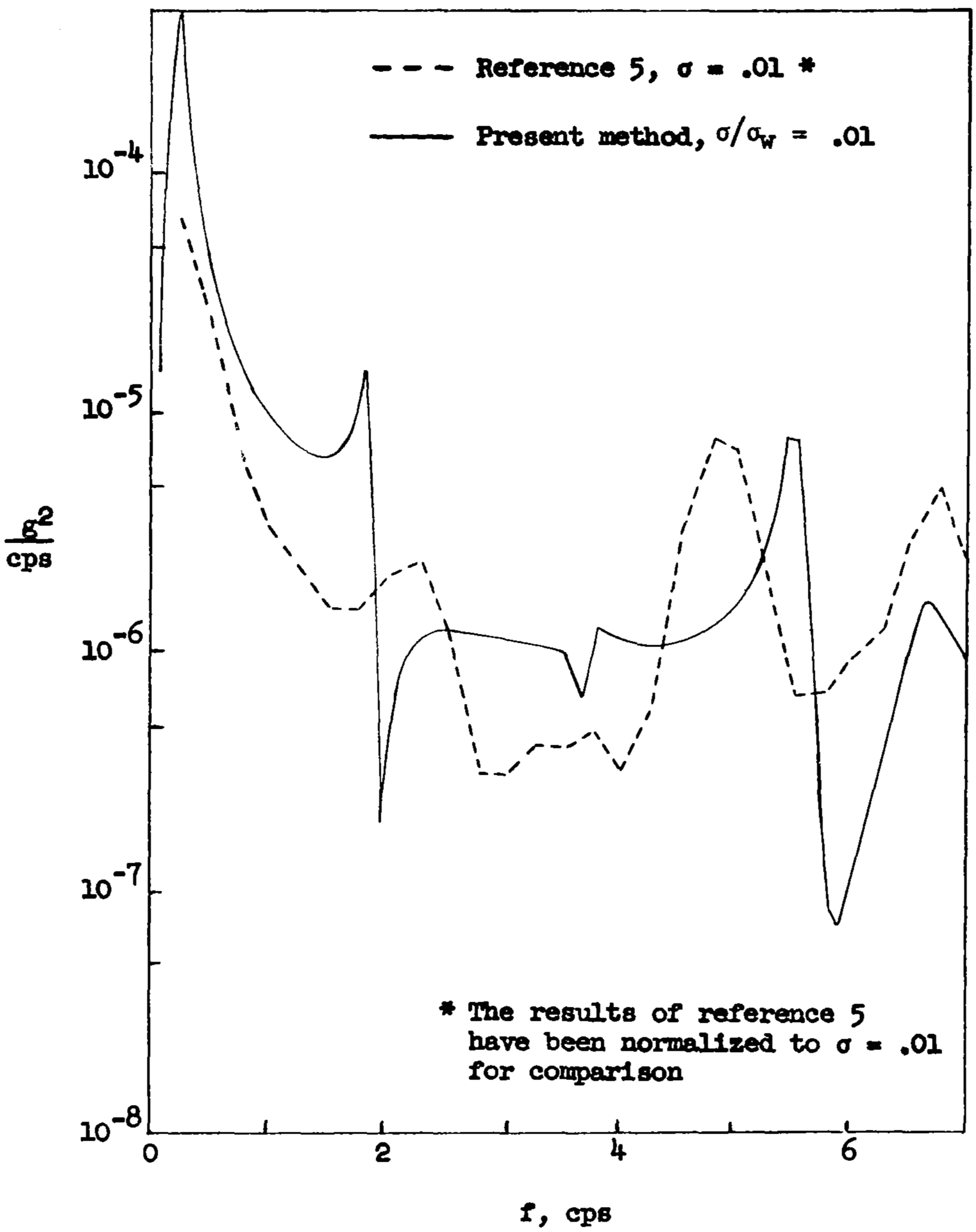

(a) Acceleration at the center of gravity station compared with reference 5.

Figure 5.- Power spectra for Condition 1-1.

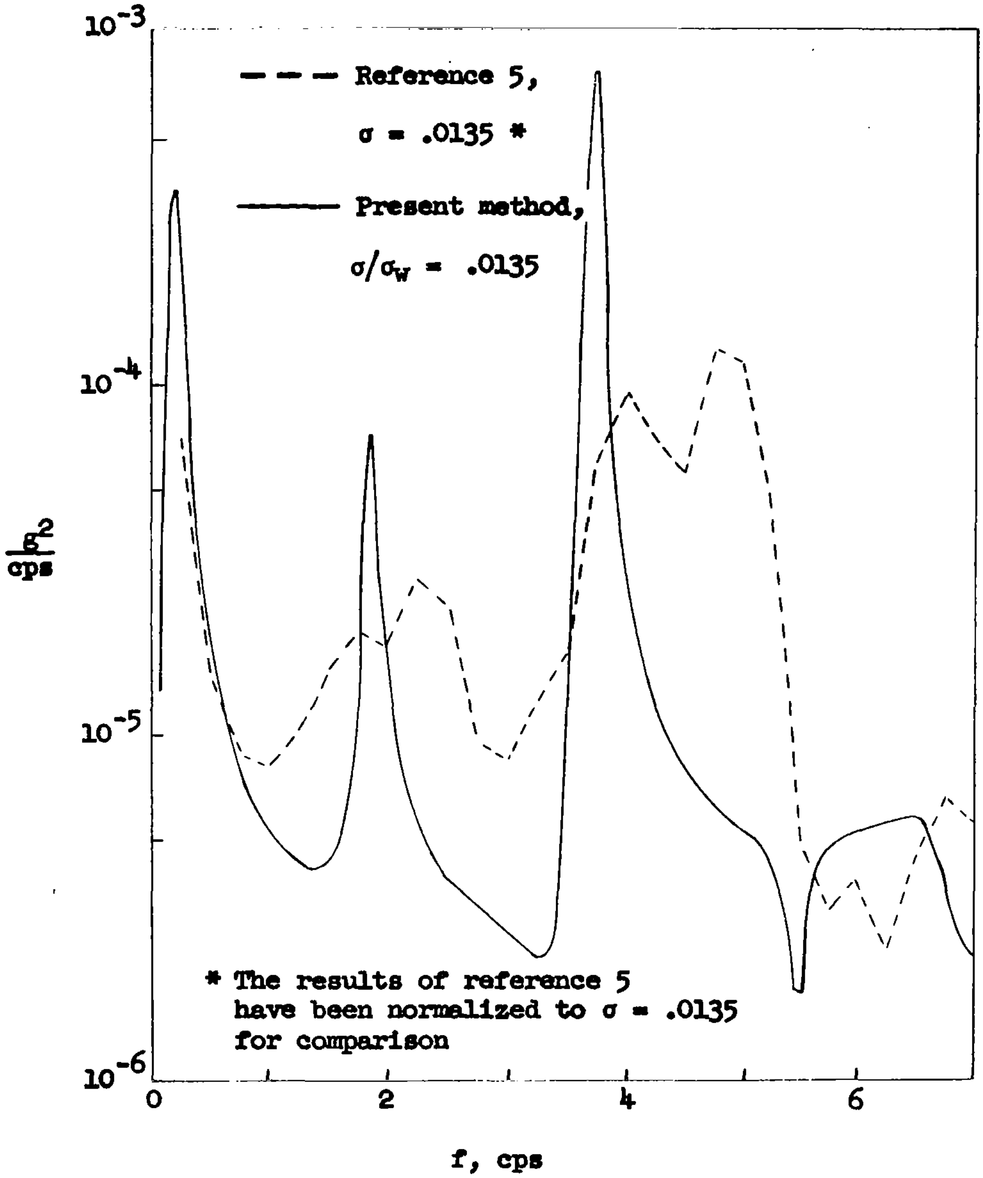

(b) Acceleration at the pilot station compared with reference 5.

Figure 5.- Concluded.

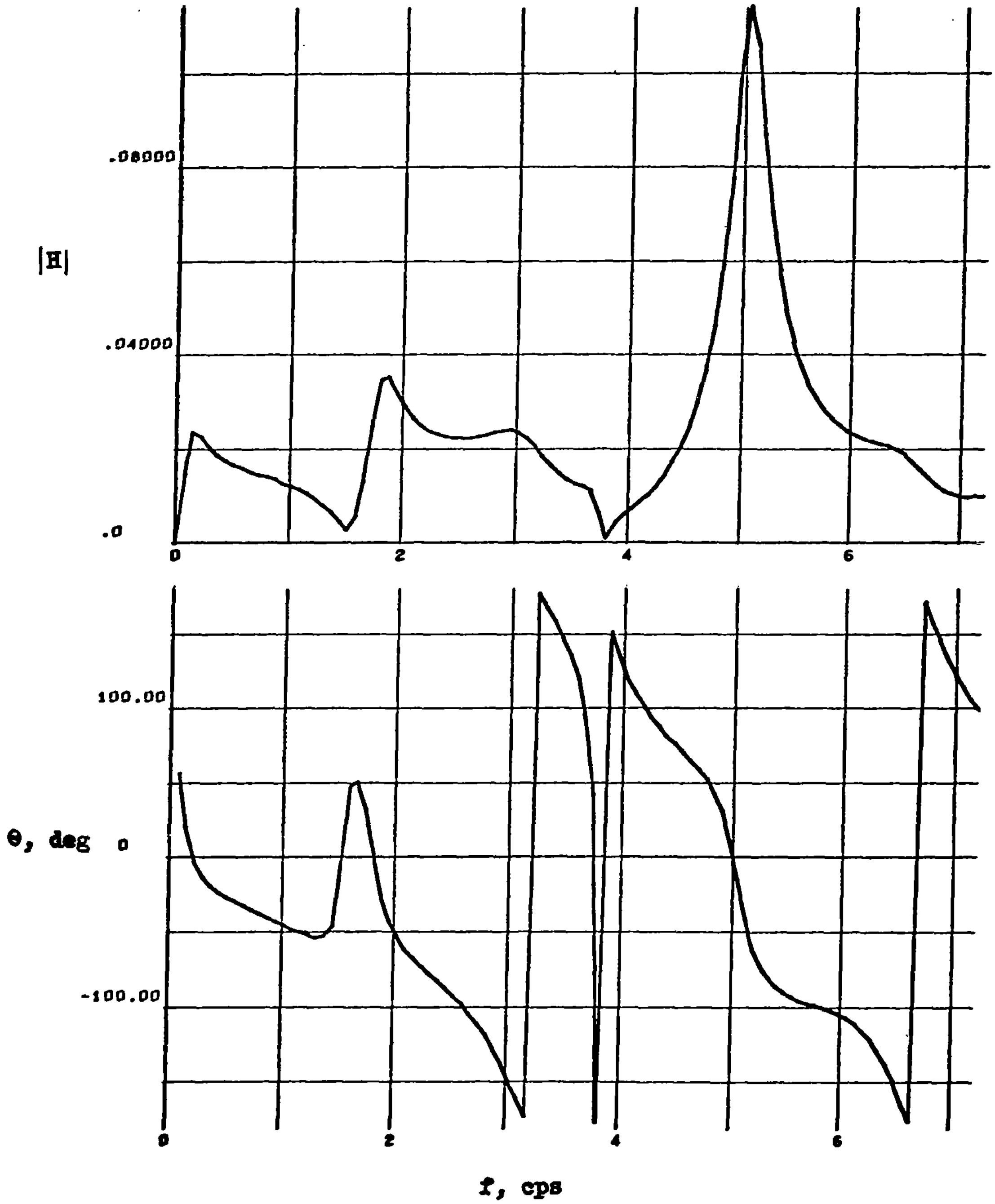

(a) Acceleration at the center of gravity station.

Figure 6.- System response functions for Condition 2-1.

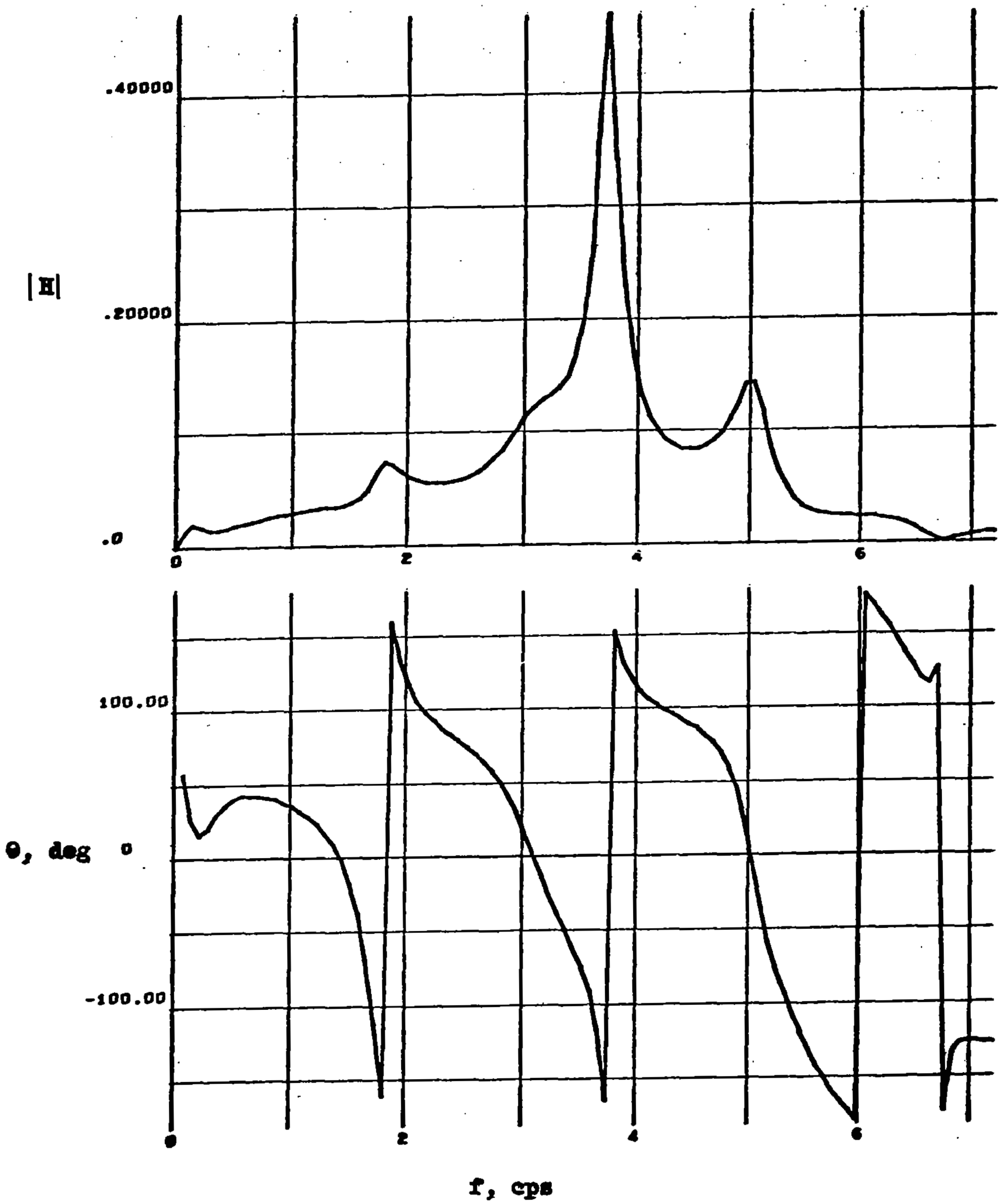

(b) Acceleration at the pilot station.

Figure 6.- Concluded.

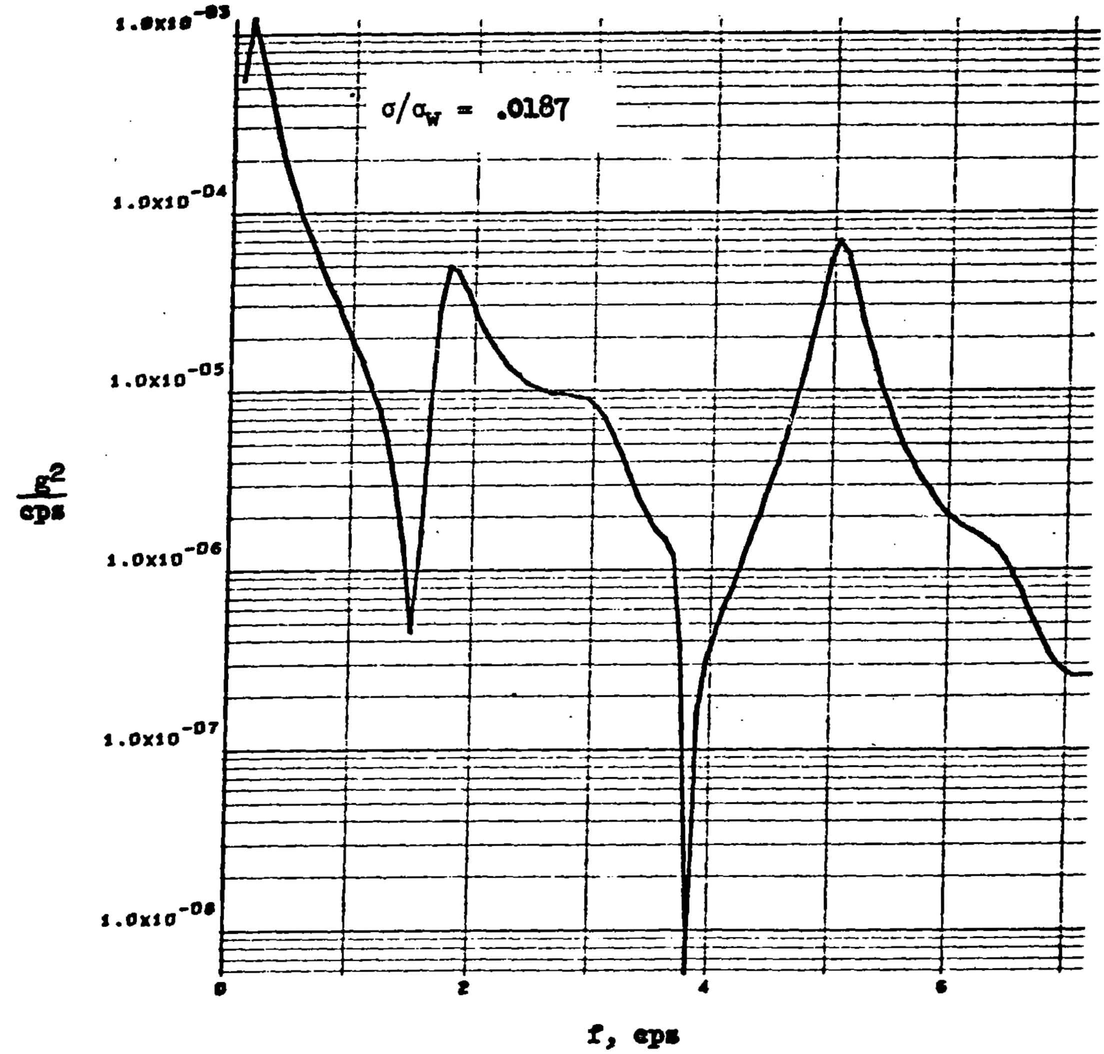

(a) Acceleration at the center of gravity station.

Figure 7.- Power spectra for Condition 2-1.

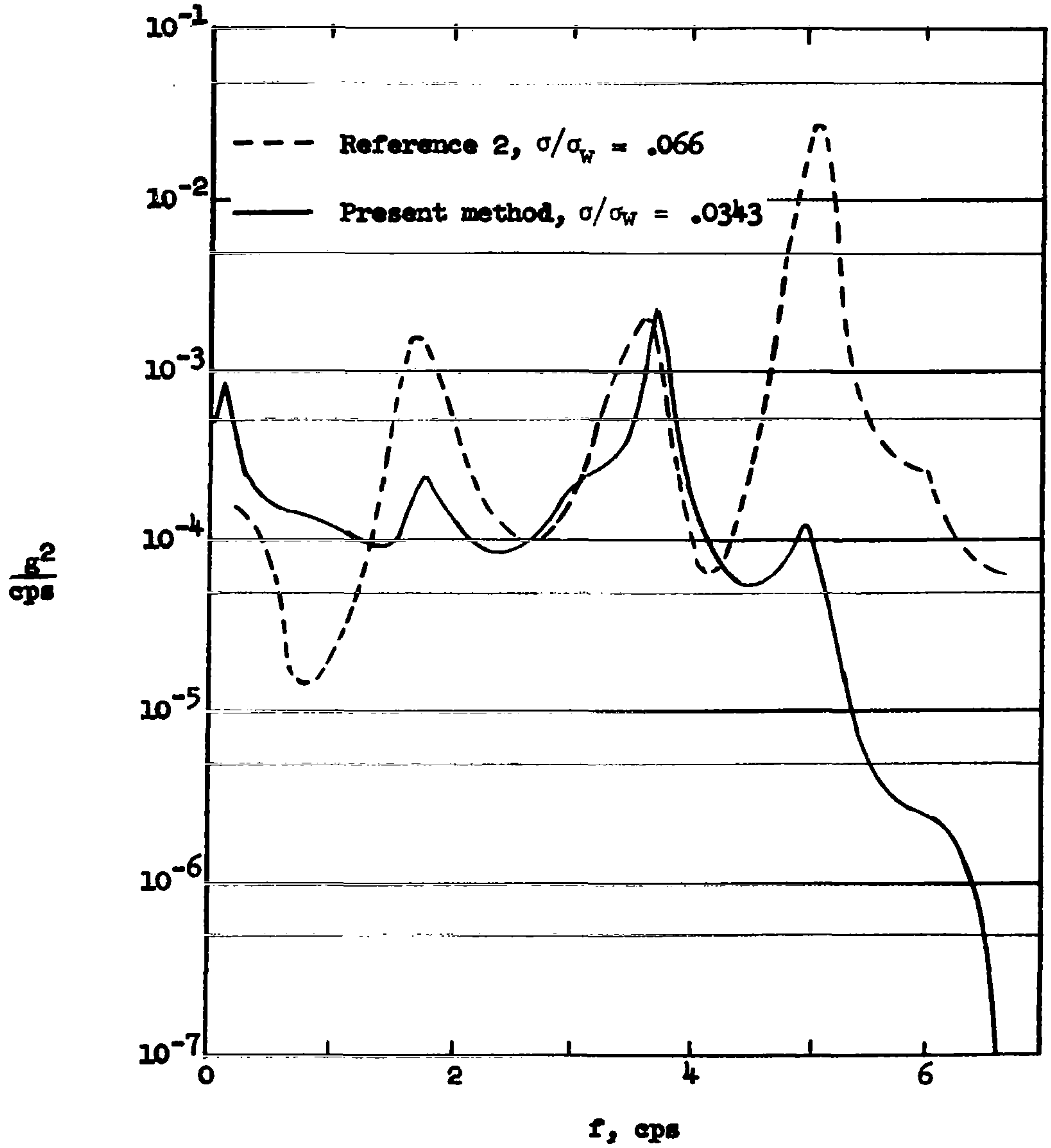

(b) Acceleration at the pilot station compared with reference 2.

Figure 7.- Concluded.

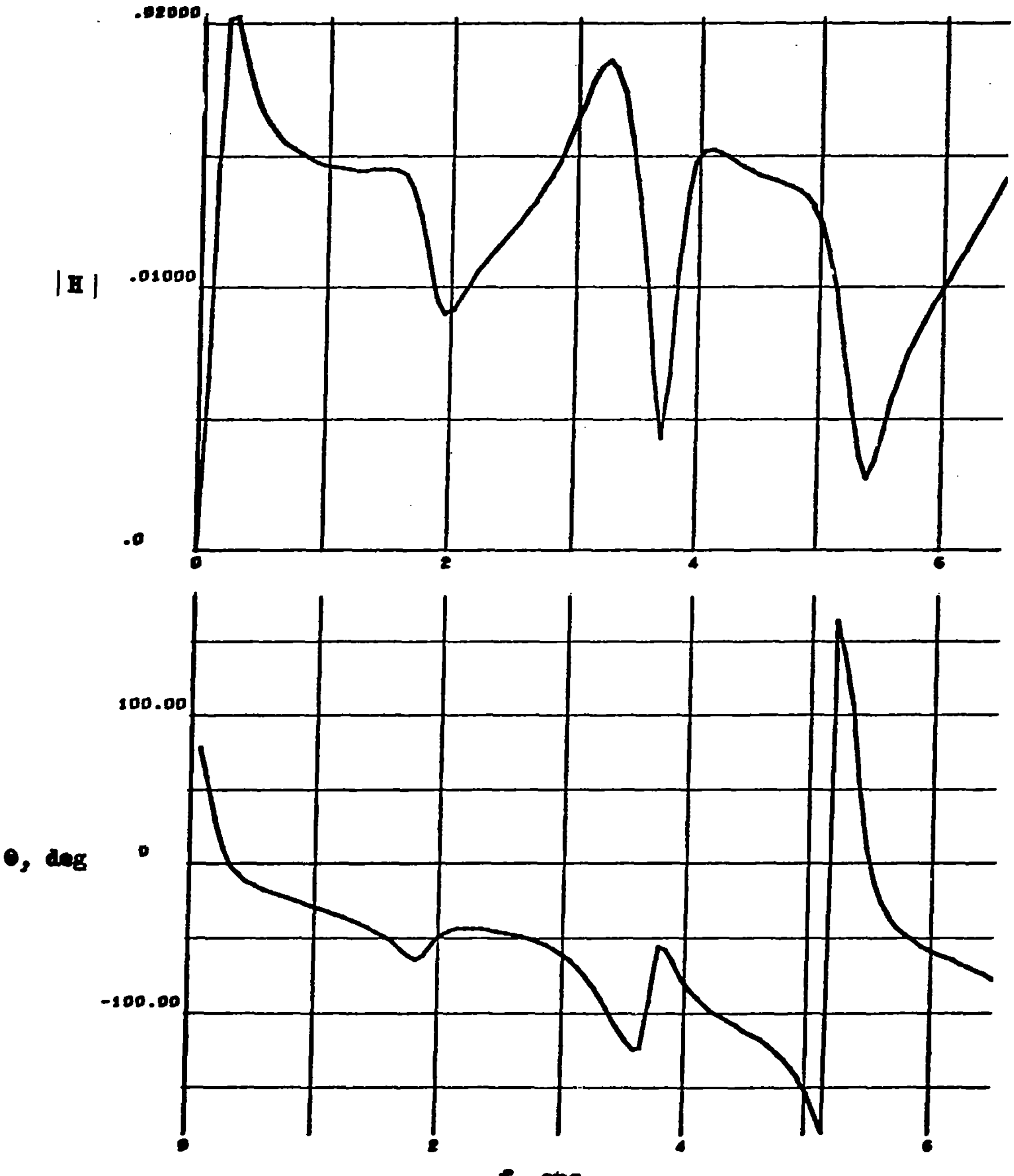

(a) Acceleration at the center of gravity station.

Figure 8.- System response functions for Condition 2-2.

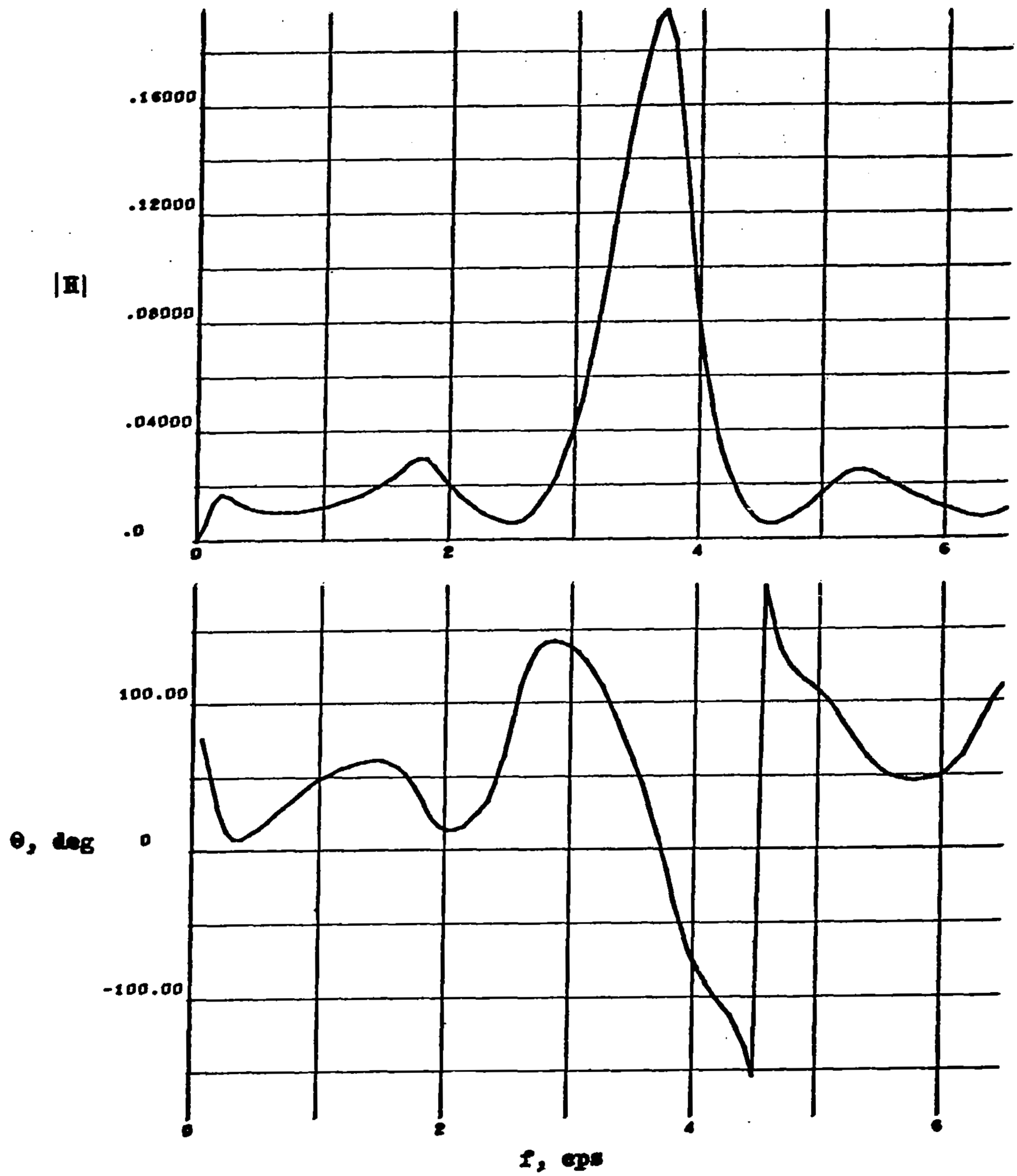

(b) Acceleration at the pilot station.

Figure 8.- Concluded.

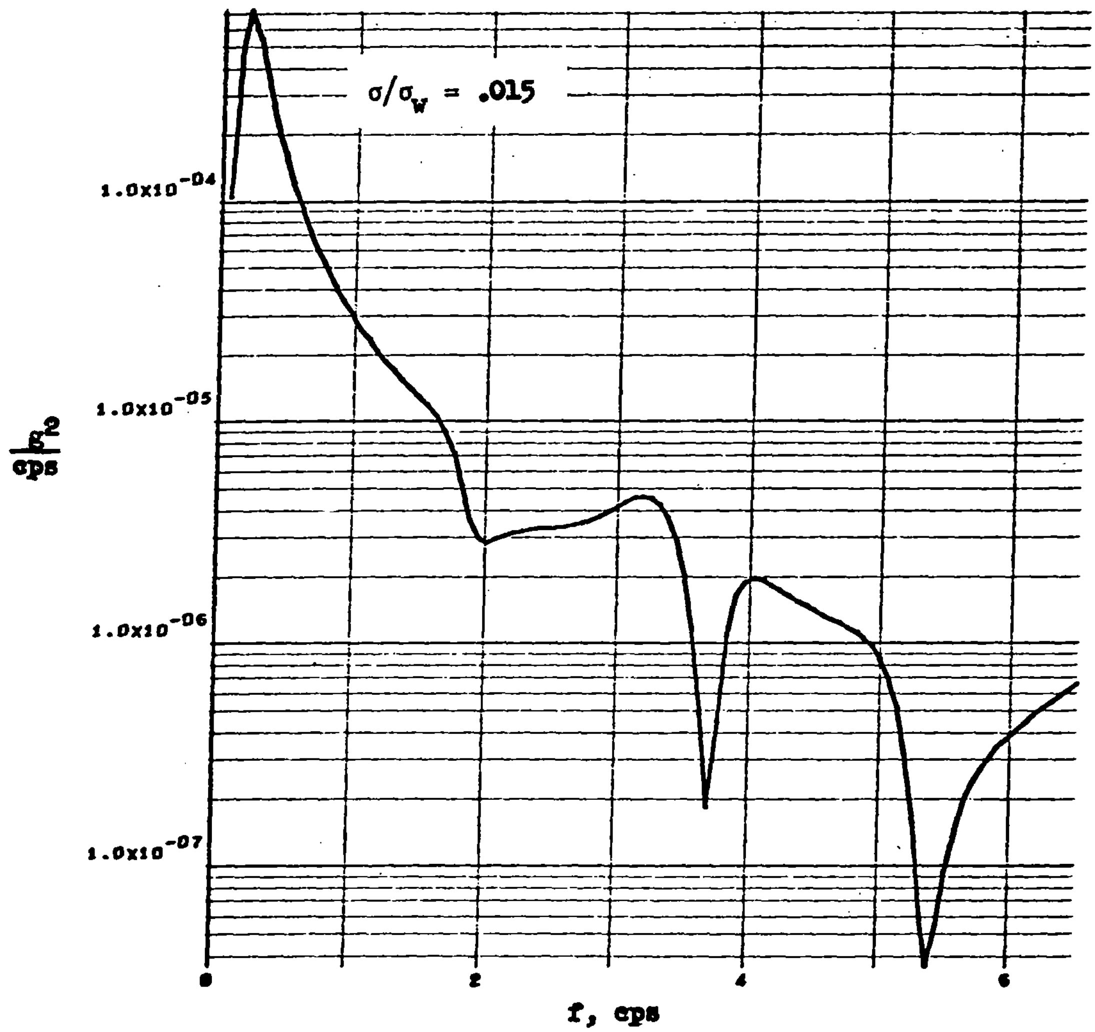

(a) Acceleration at the center of gravity station.

Figure 9.- Power spectra for Condition 2-2.

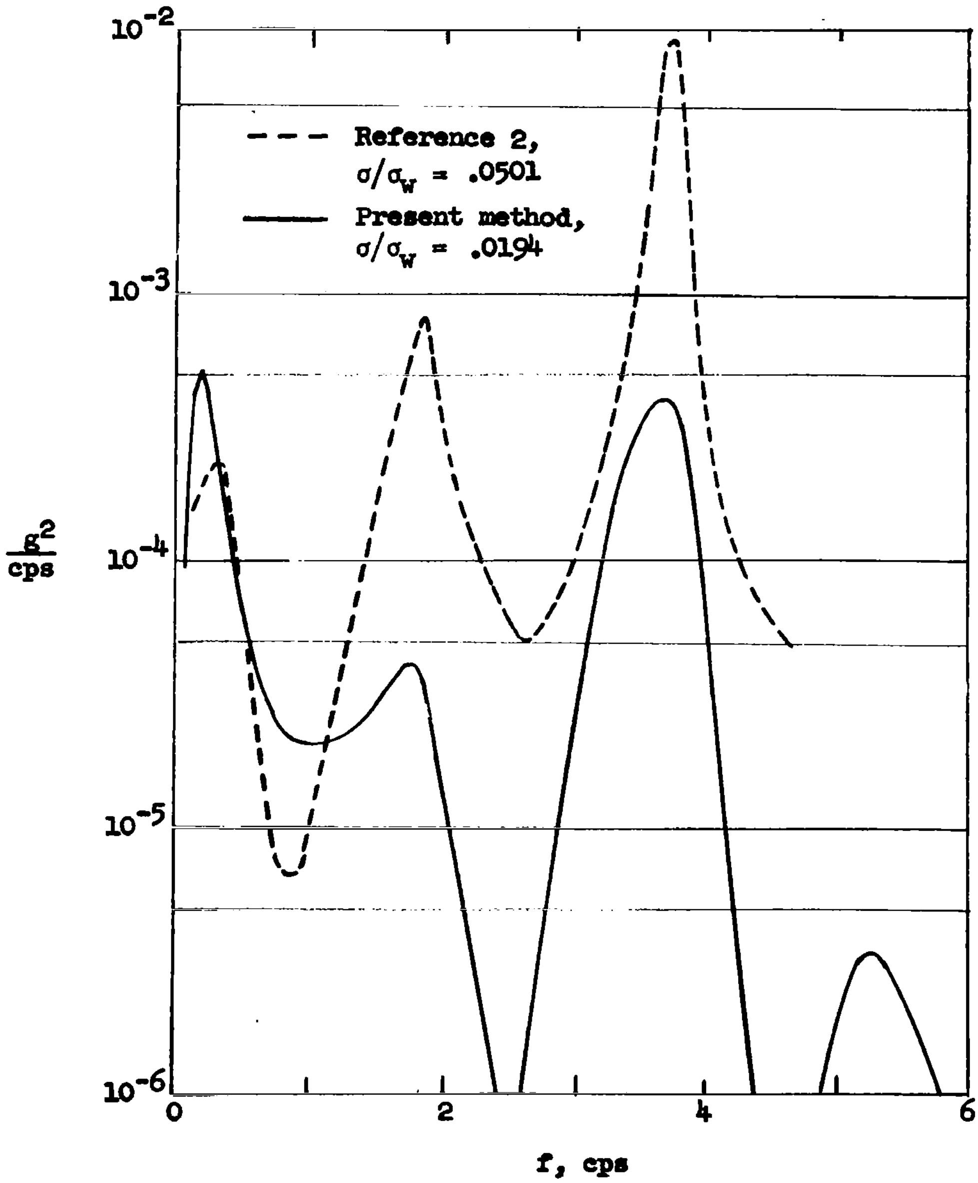

(b) Acceleration at the pilot station compared with reference 2.

Figure 9.- Concluded.

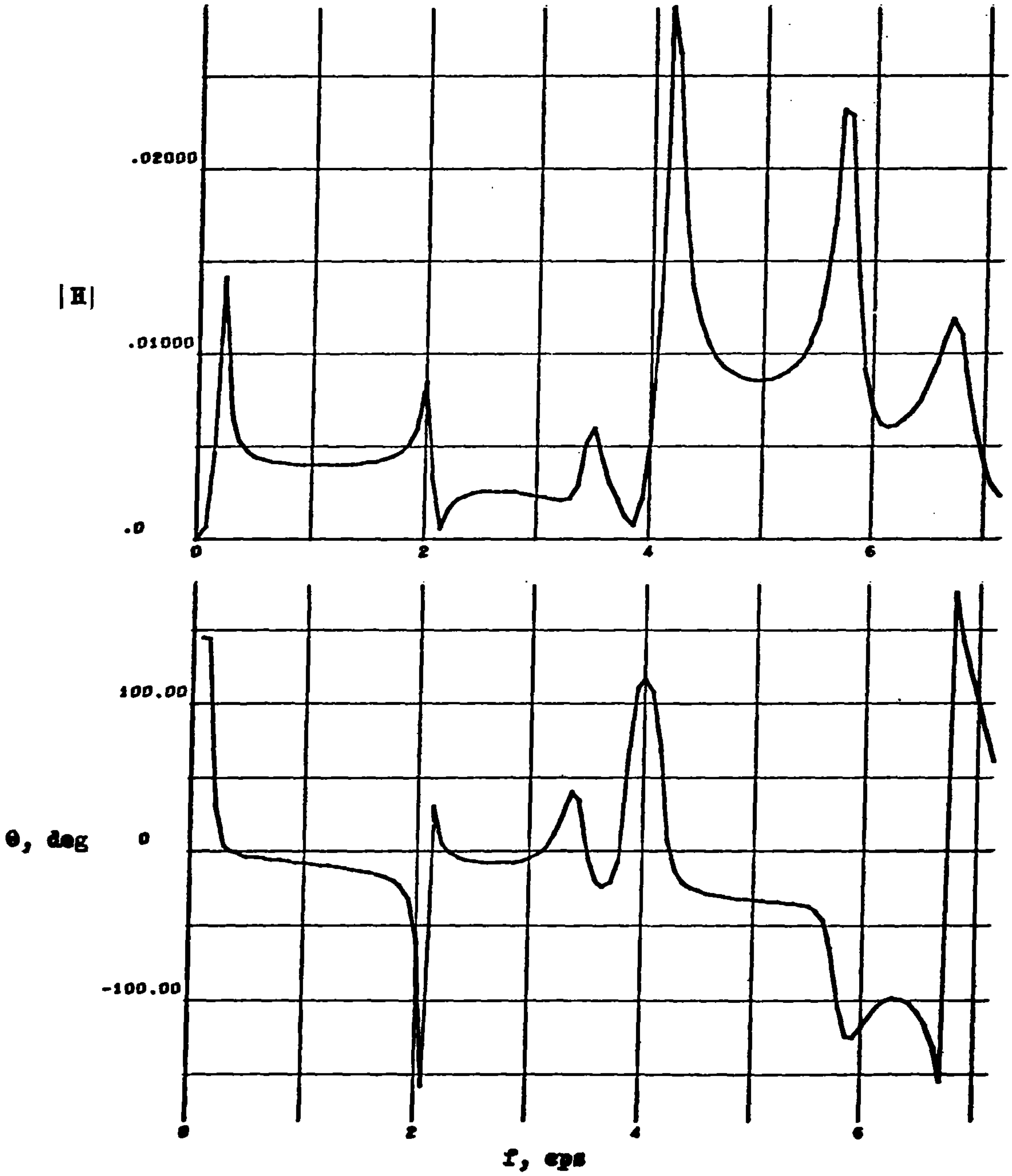

(a) Acceleration at the center of gravity station.

Figure 10.- System response functions for Condition 2-3.

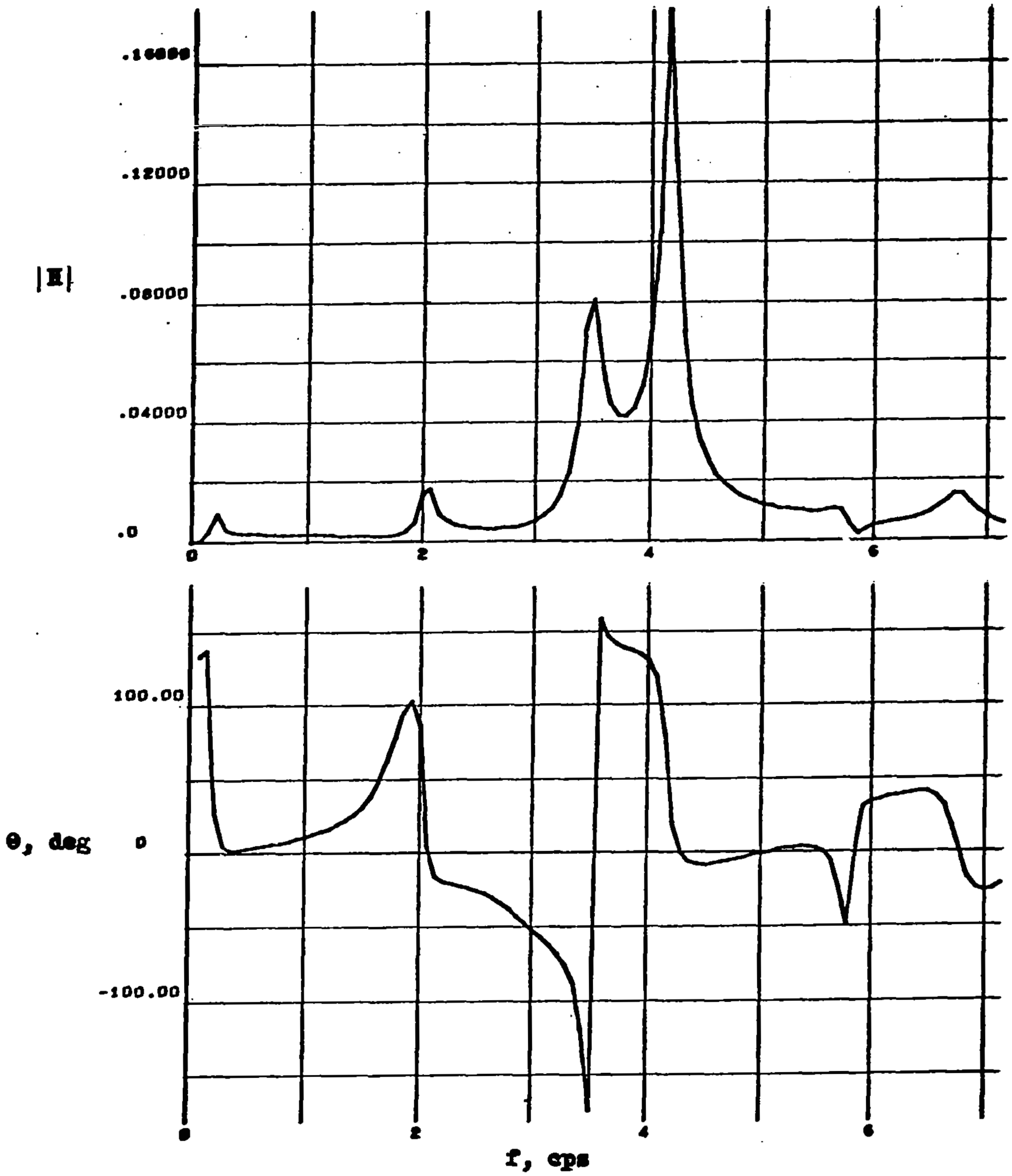

(b) Acceleration at the pilot station.

Figure 10.- Concluded.

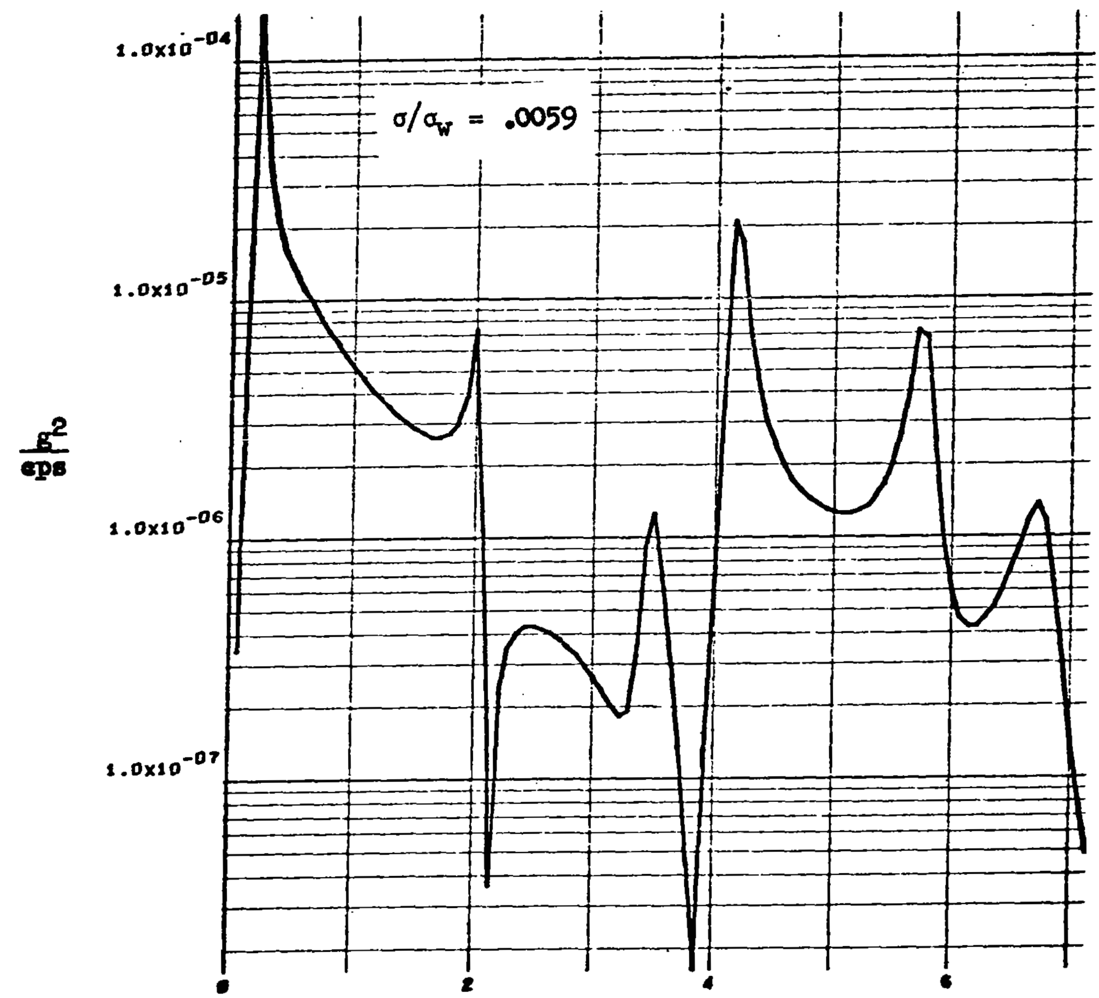

(a) Acceleration at the center of gravity station.

Figure 11.- Power spectra for Condition 2-3.

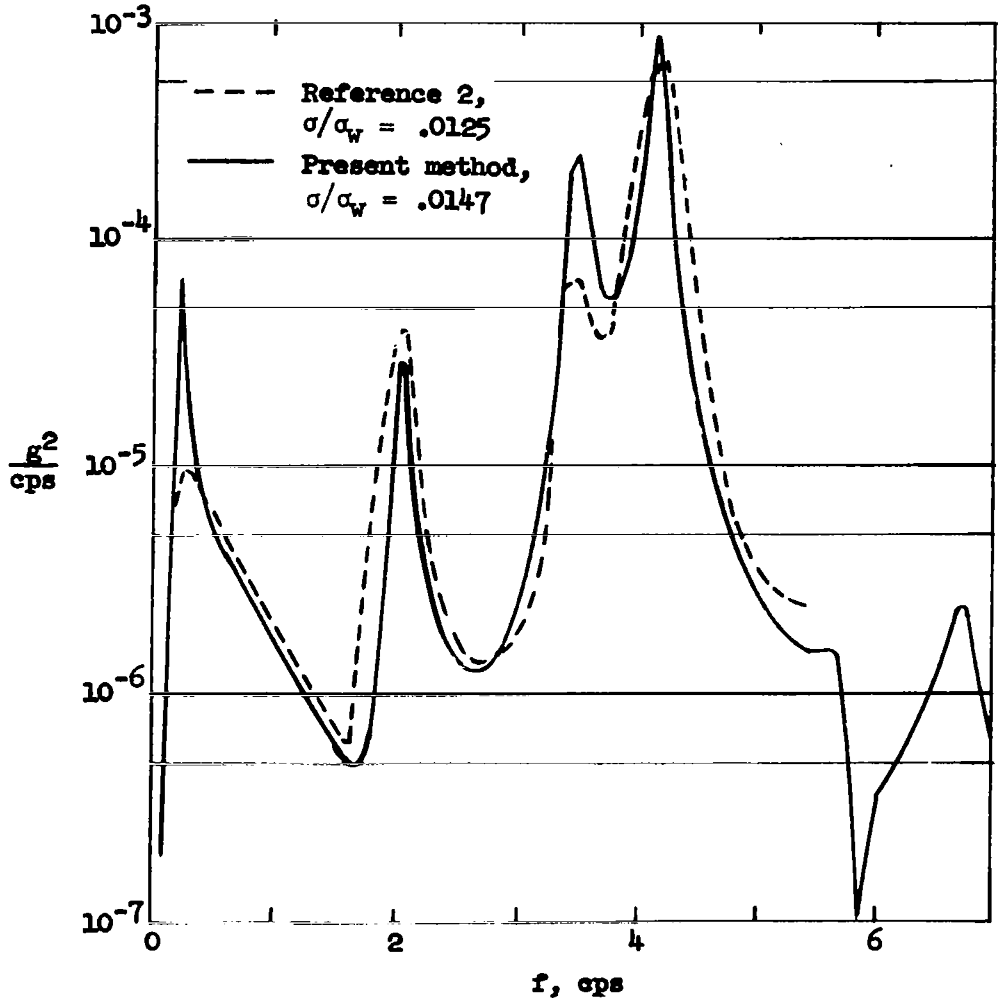

(b) Acceleration at the pilot station compared with reference 2.

Figure 11.- Concluded.

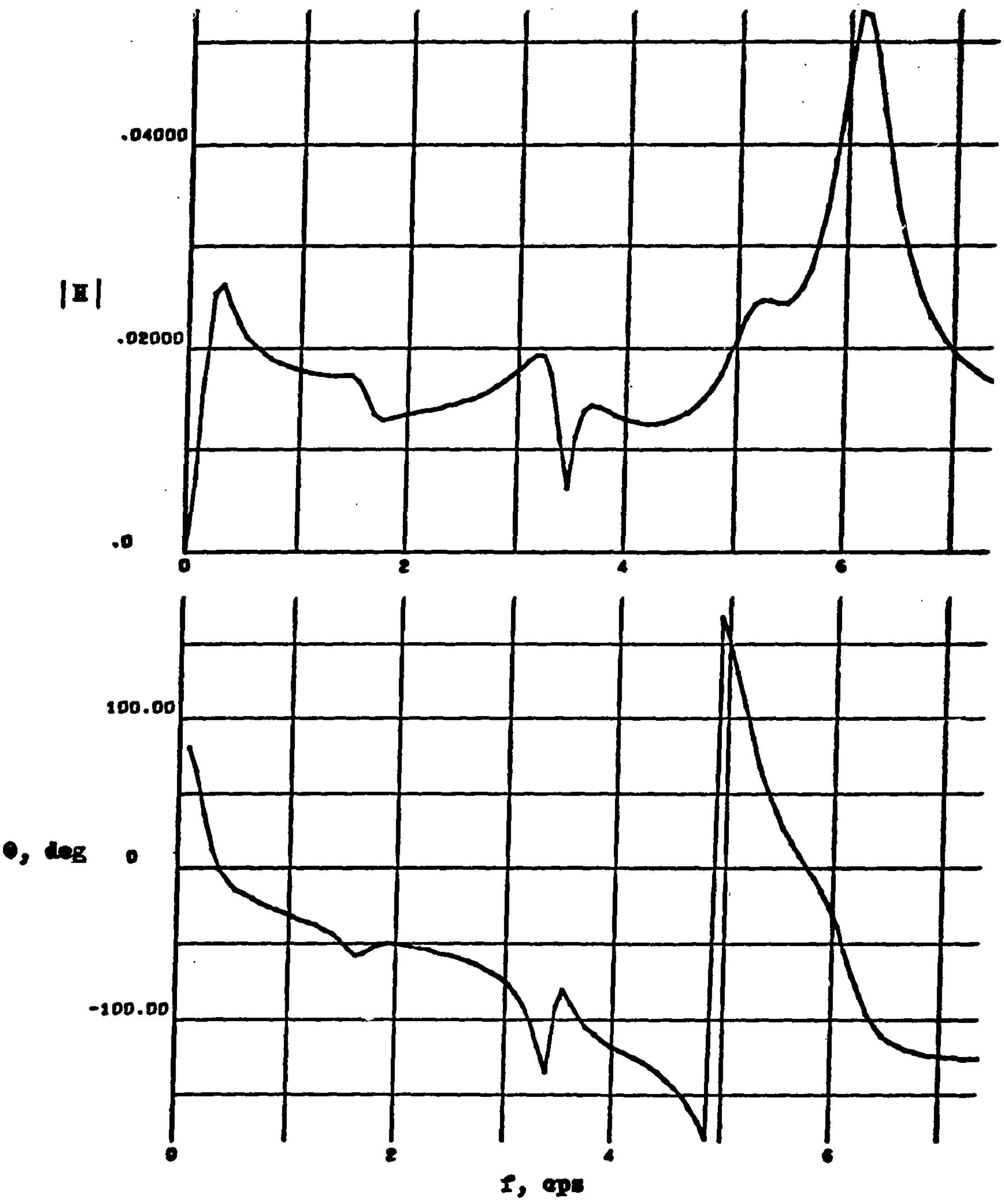

(a) Acceleration at the center of gravity station.

Figure 12.- System response functions for Condition 3-1.

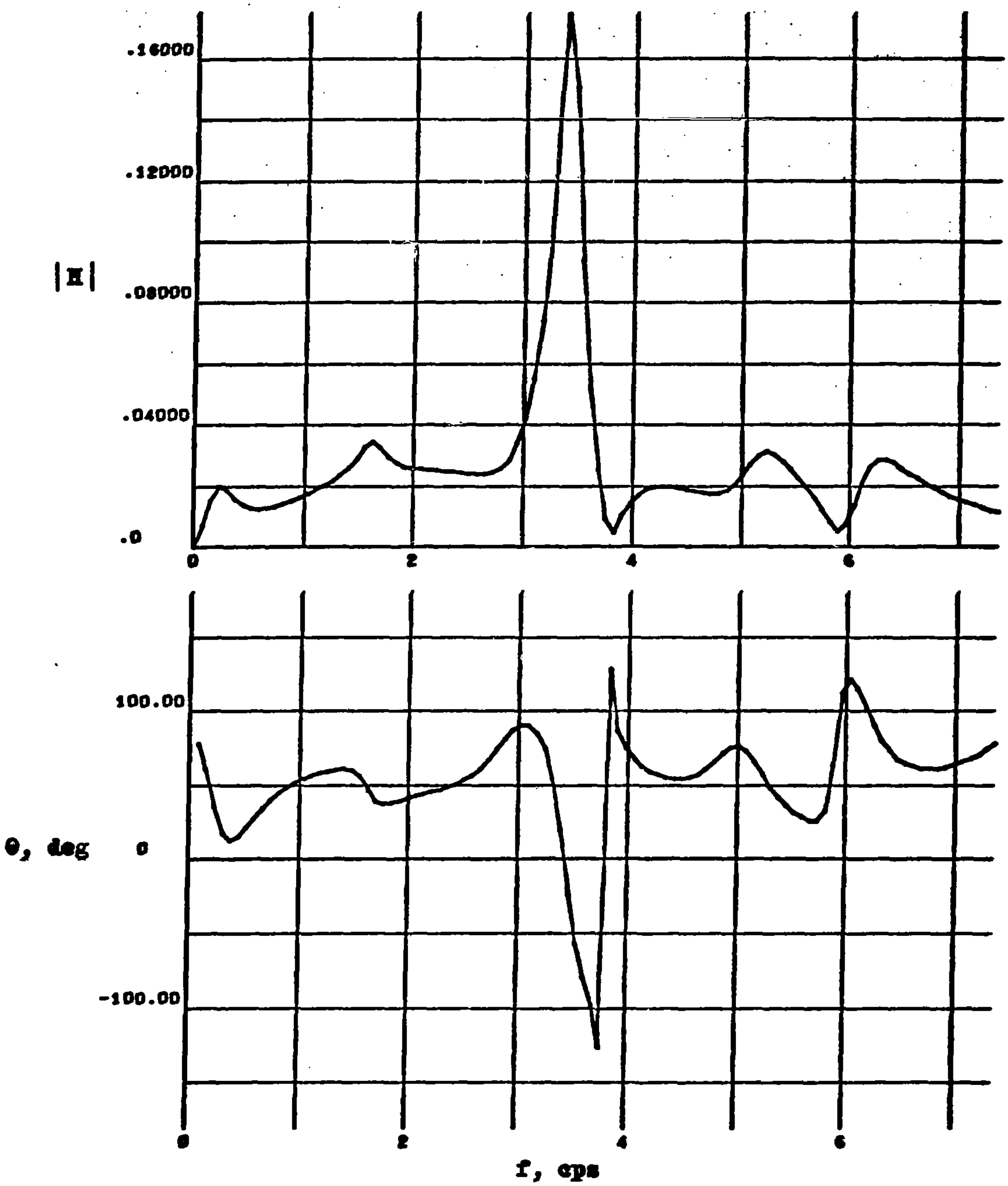

(b) Acceleration at the pilot station.

Figure 12.- Continued.

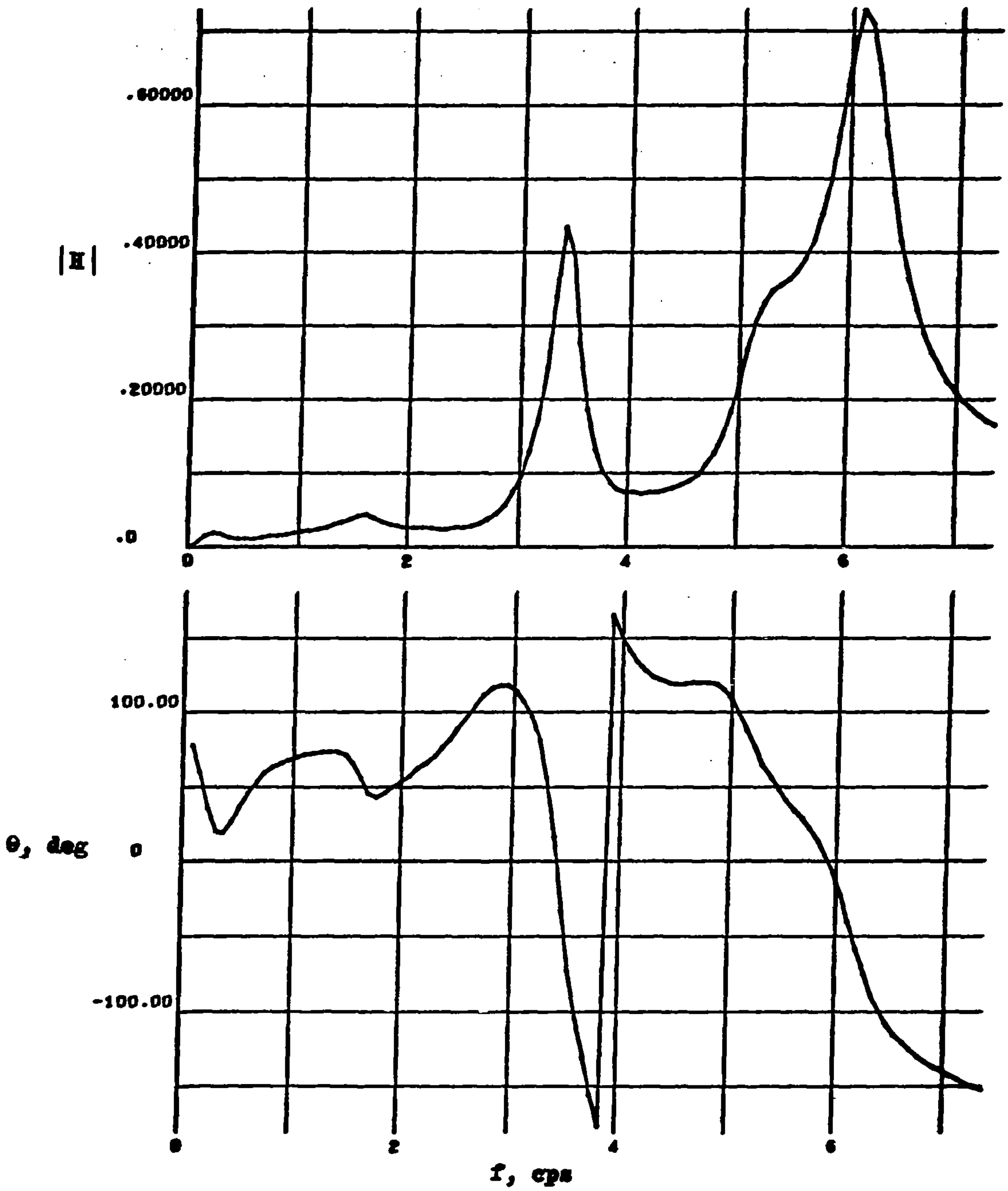

(c) Acceleration at the nose instrumentation package station.

Figure 12.- Continued.

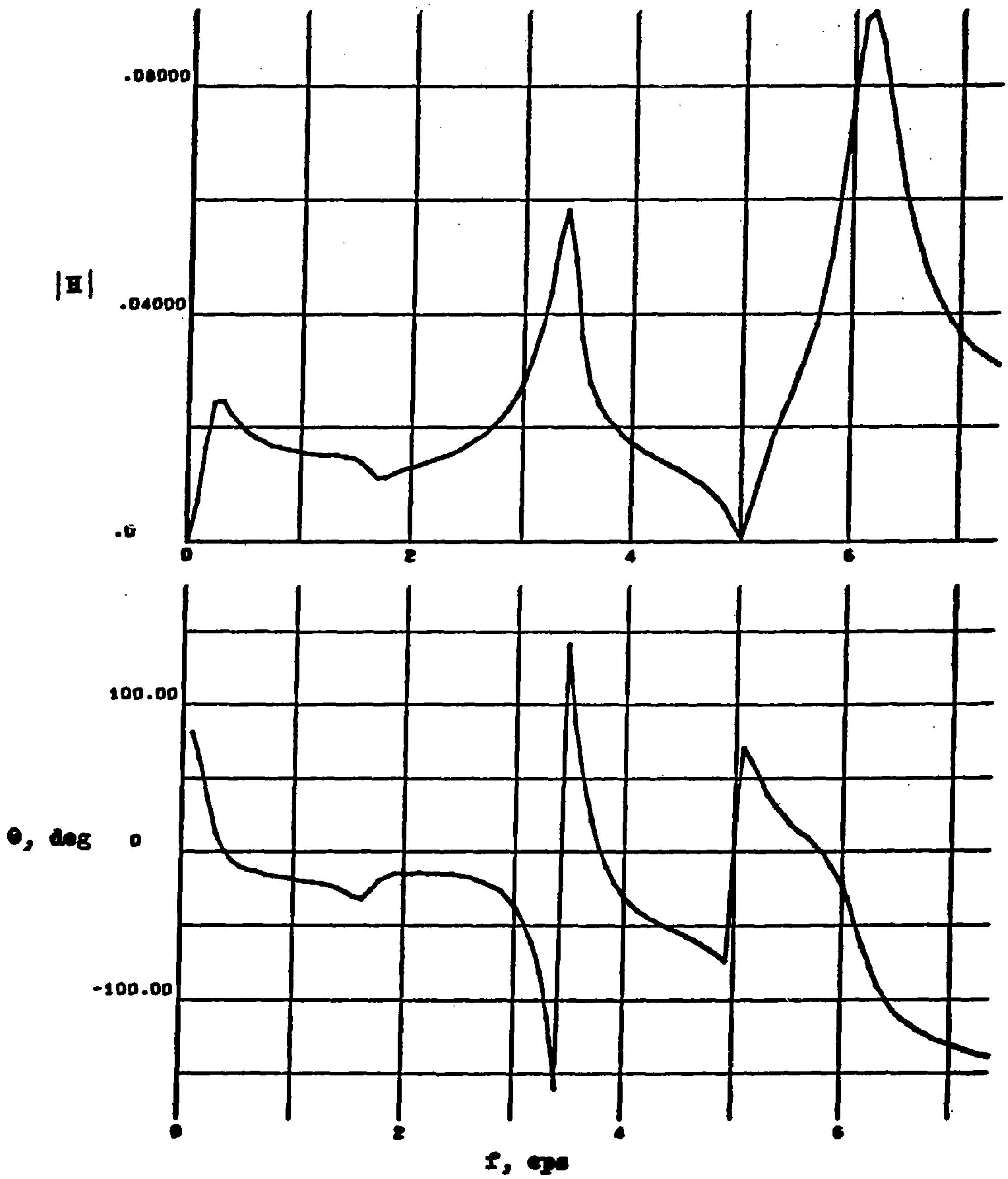

(d) Acceleration at the wing apex station.

Figure 12.- Continued.

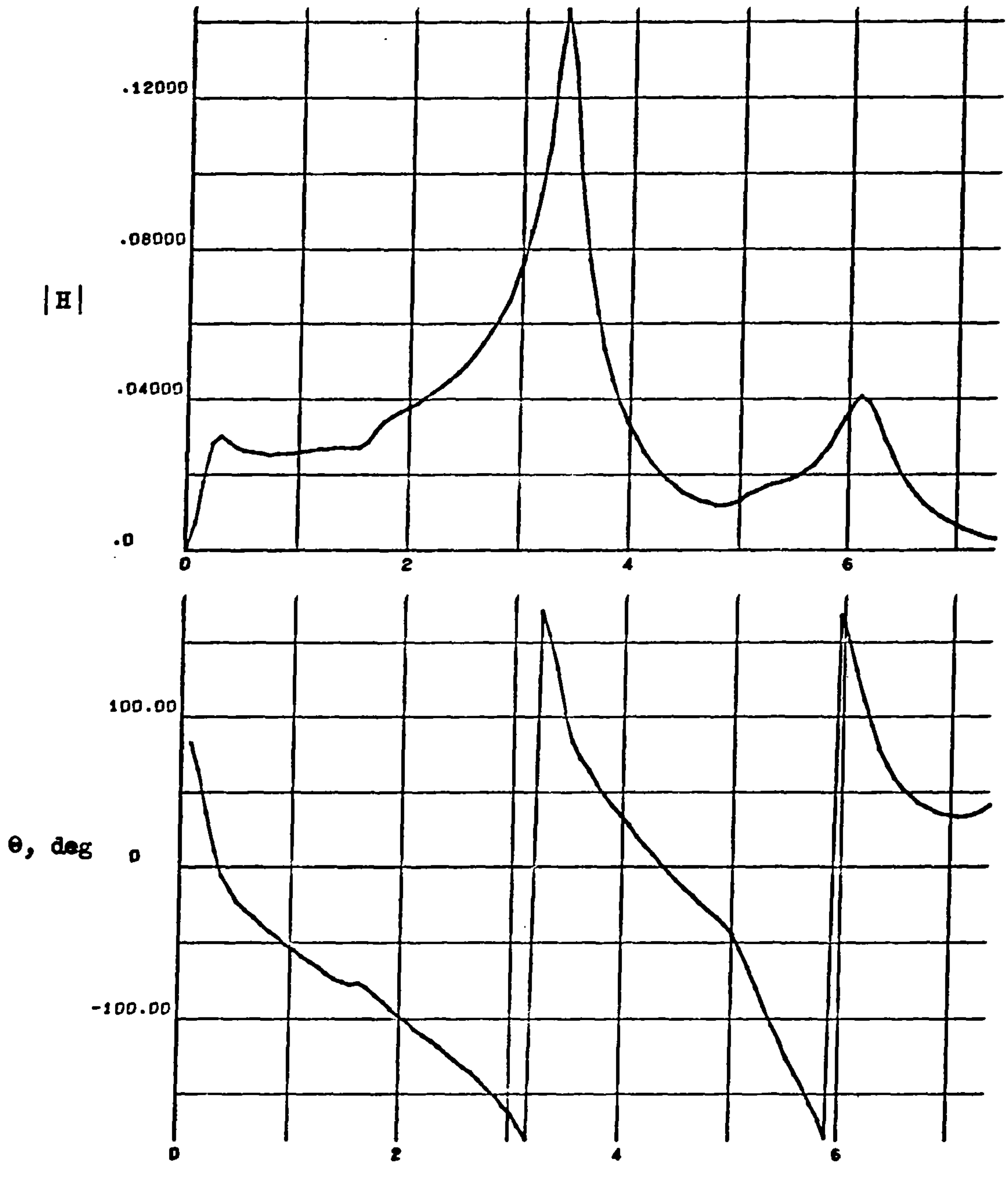

(e) Acceleration at the aft fuselage station.

Figure 12.- Continued.

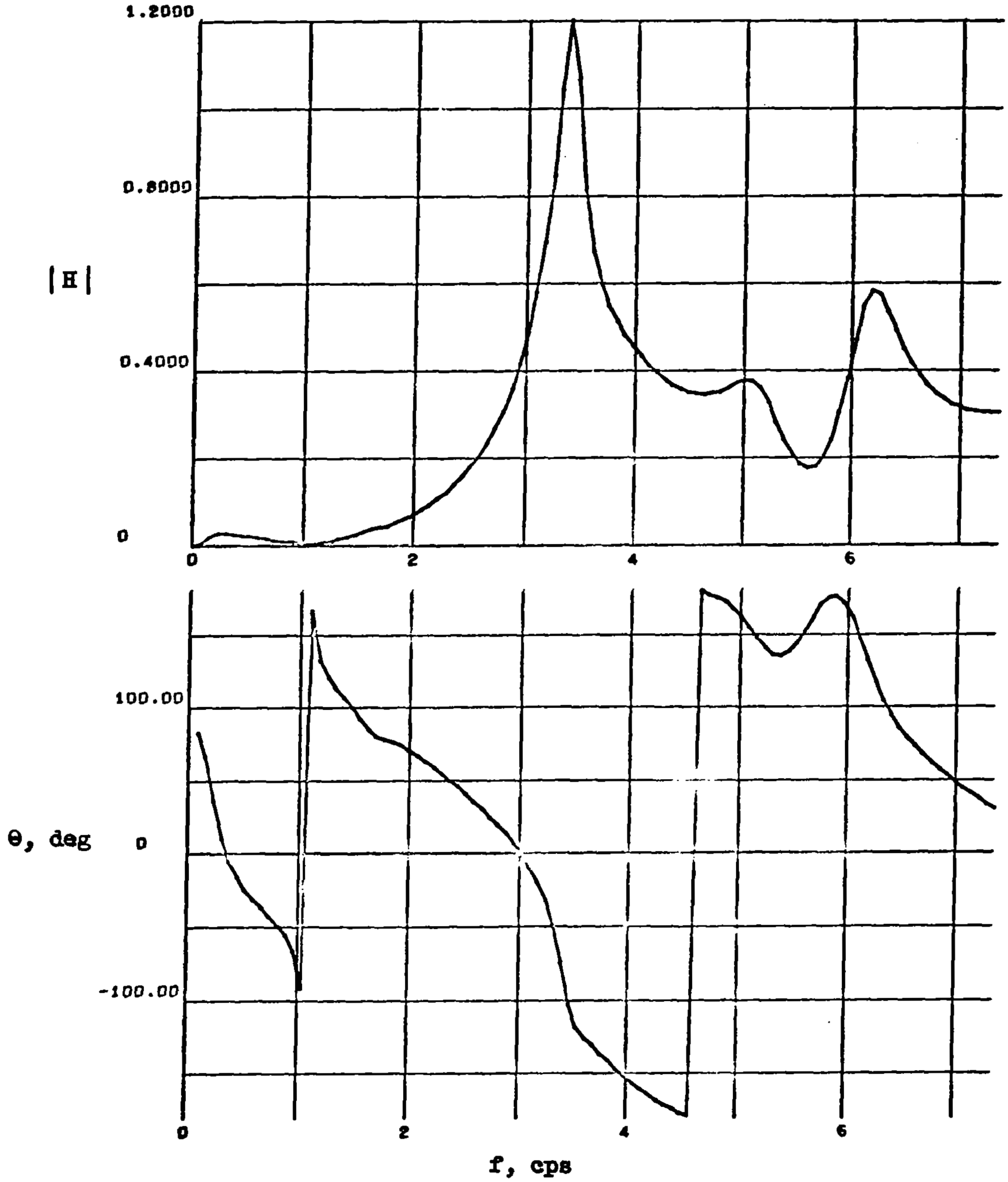

(f) Acceleration at the wing tip station.

Figure 12.- Continued.

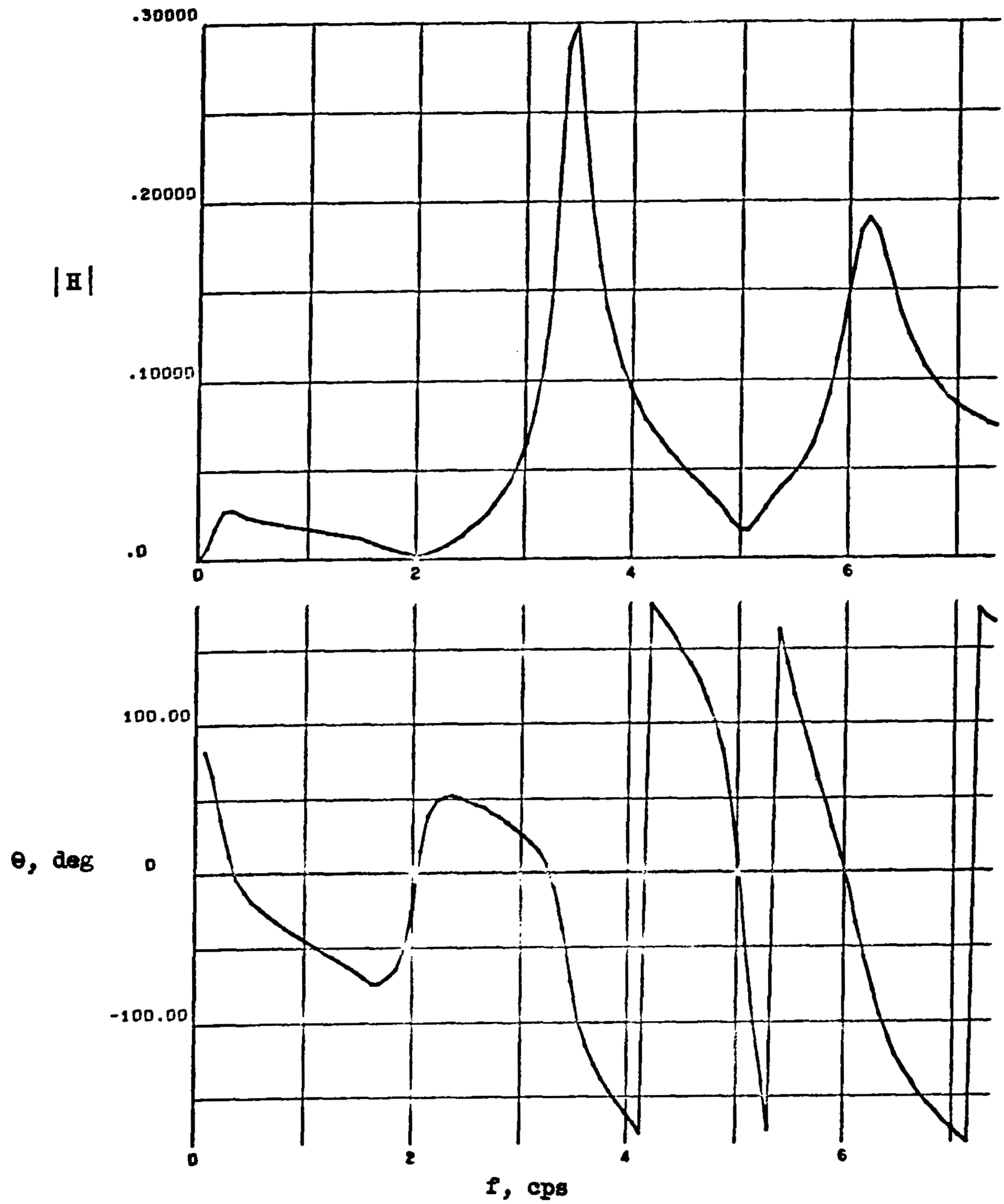

(g) Acceleration at the forward wing tip hinge line station.

Figure 12.- Continued.

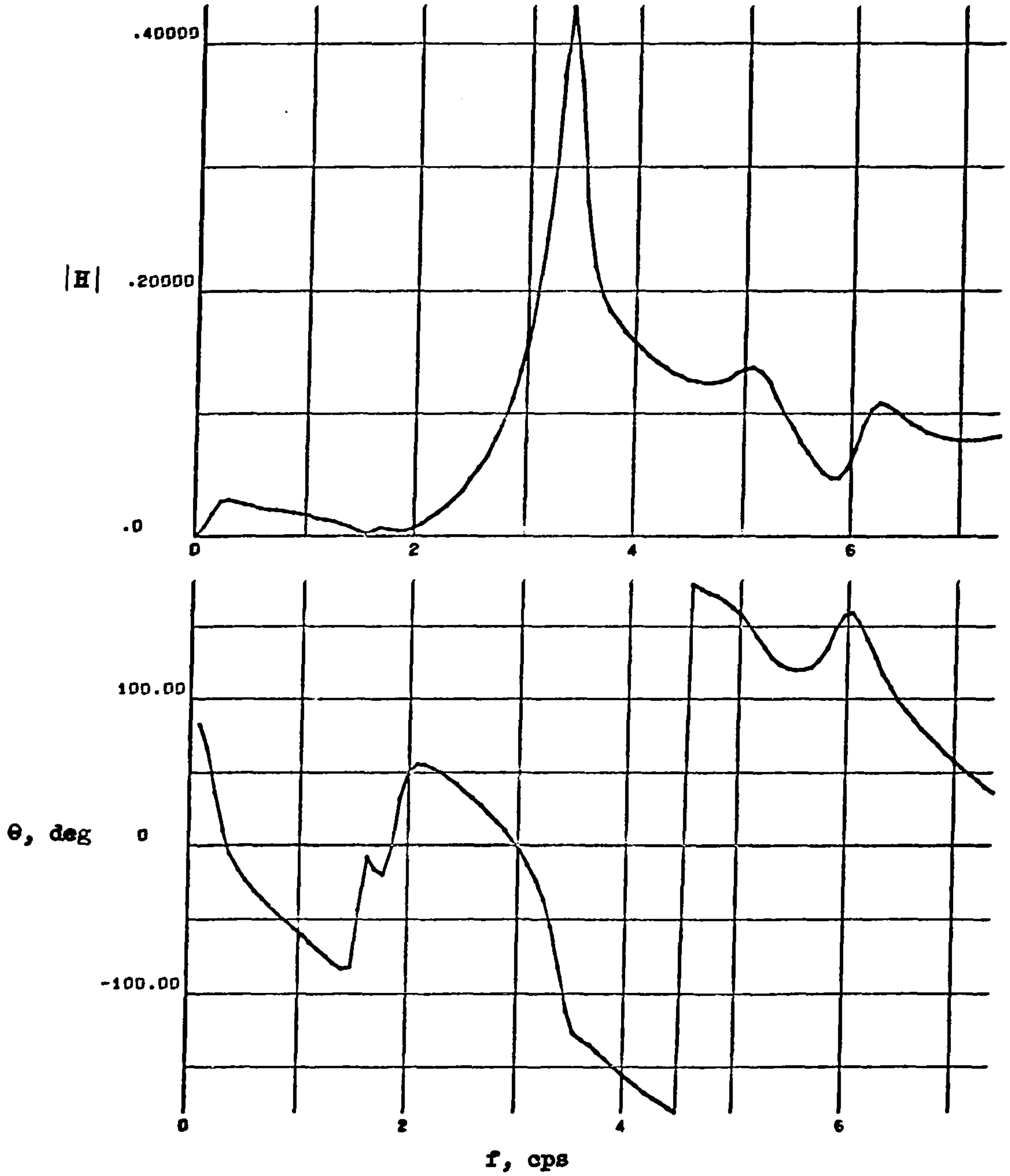

(h) Acceleration at the aft wing tip hinge line station.

Figure 12.- Continued.

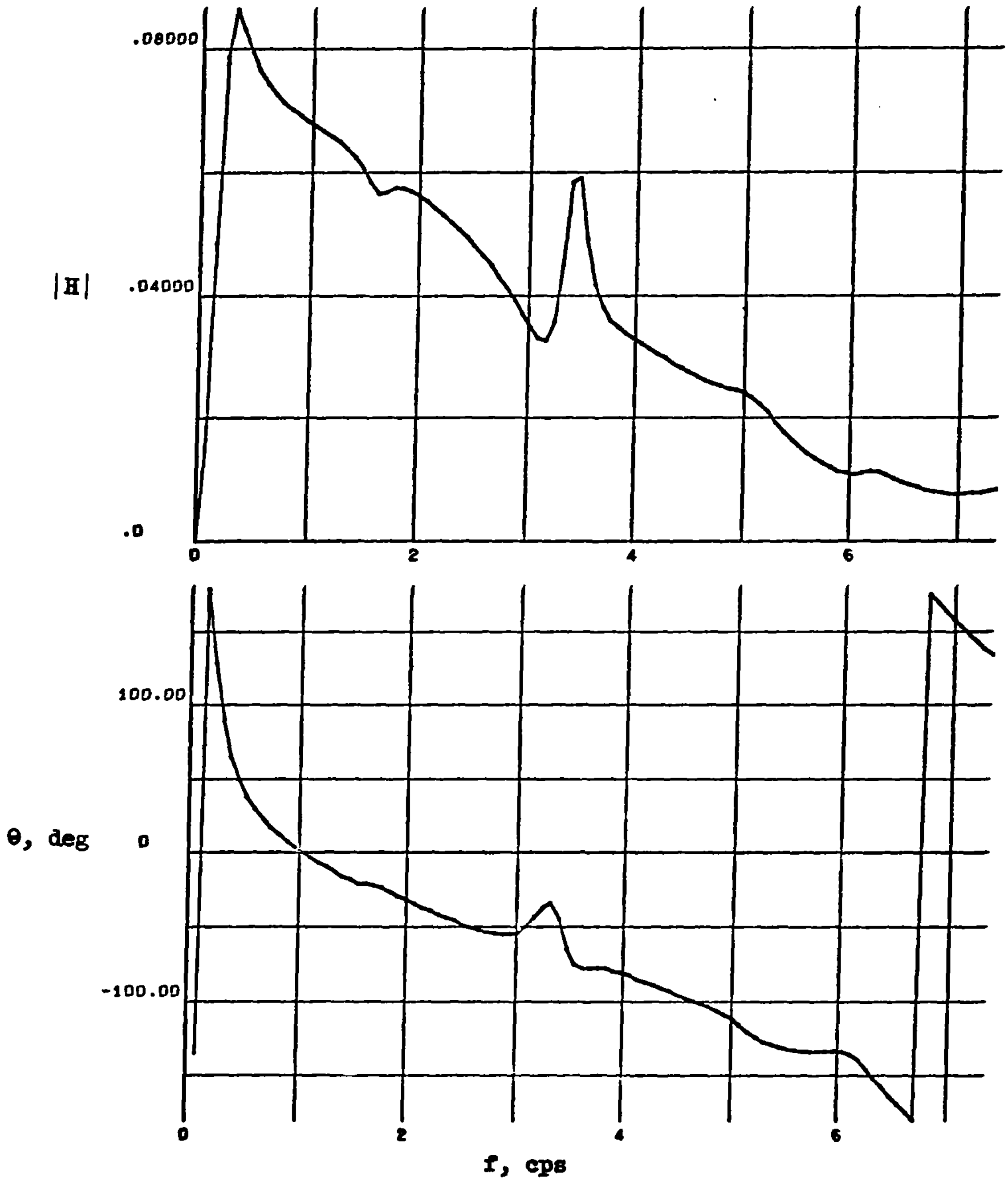

(i) Rate of pitch.

Figure 12.- Continued.

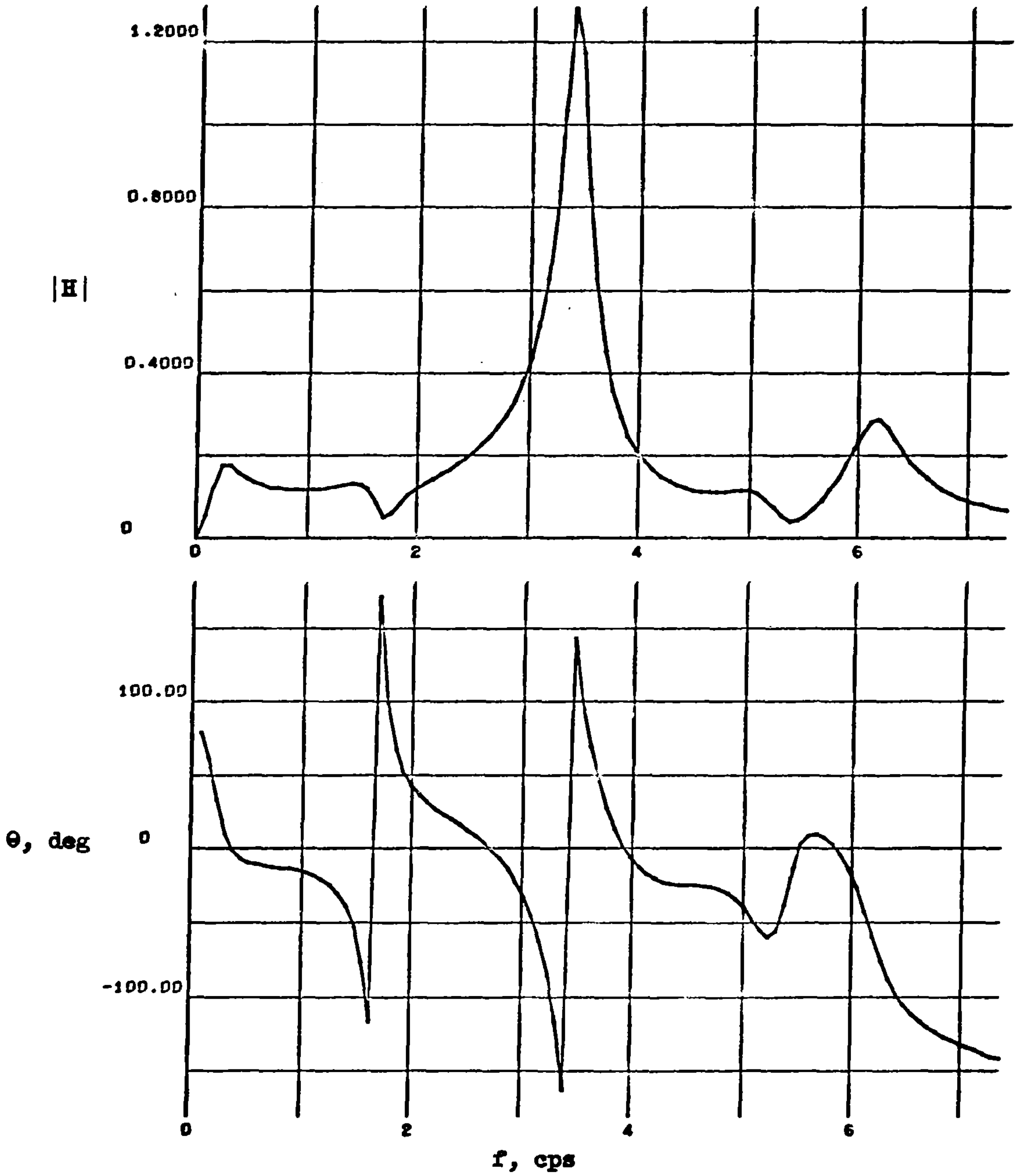

(j) Fuselage bending moment at station 1040, 10^6 in-lb.

Figure 12.- Continued.

(k) Wing tip hinge moment, 10^6 in-lb.

Figure 12.- Concluded.

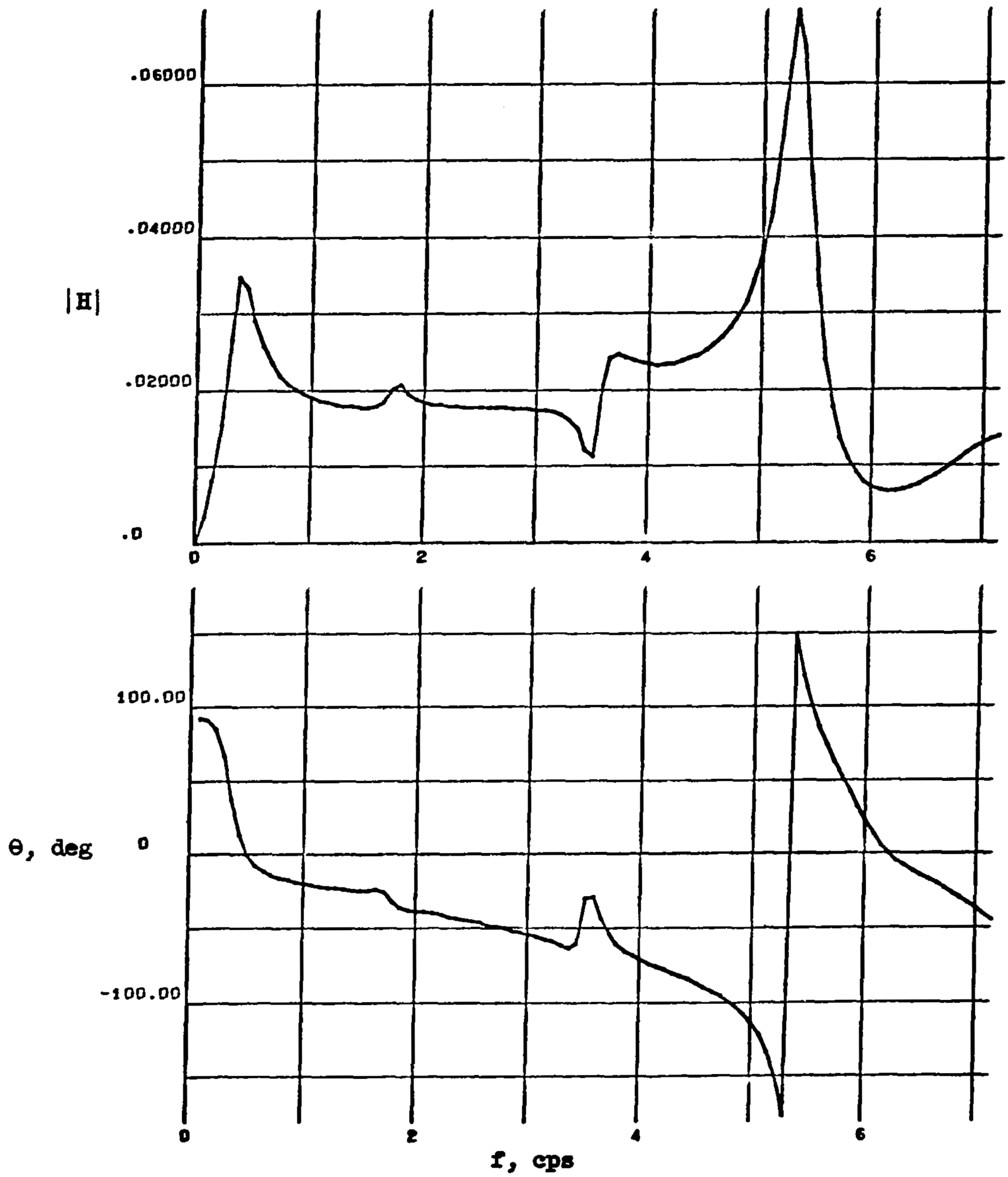

(a) Acceleration at the center of gravity station.

Figure 13.- System response functions for Condition 3-2.

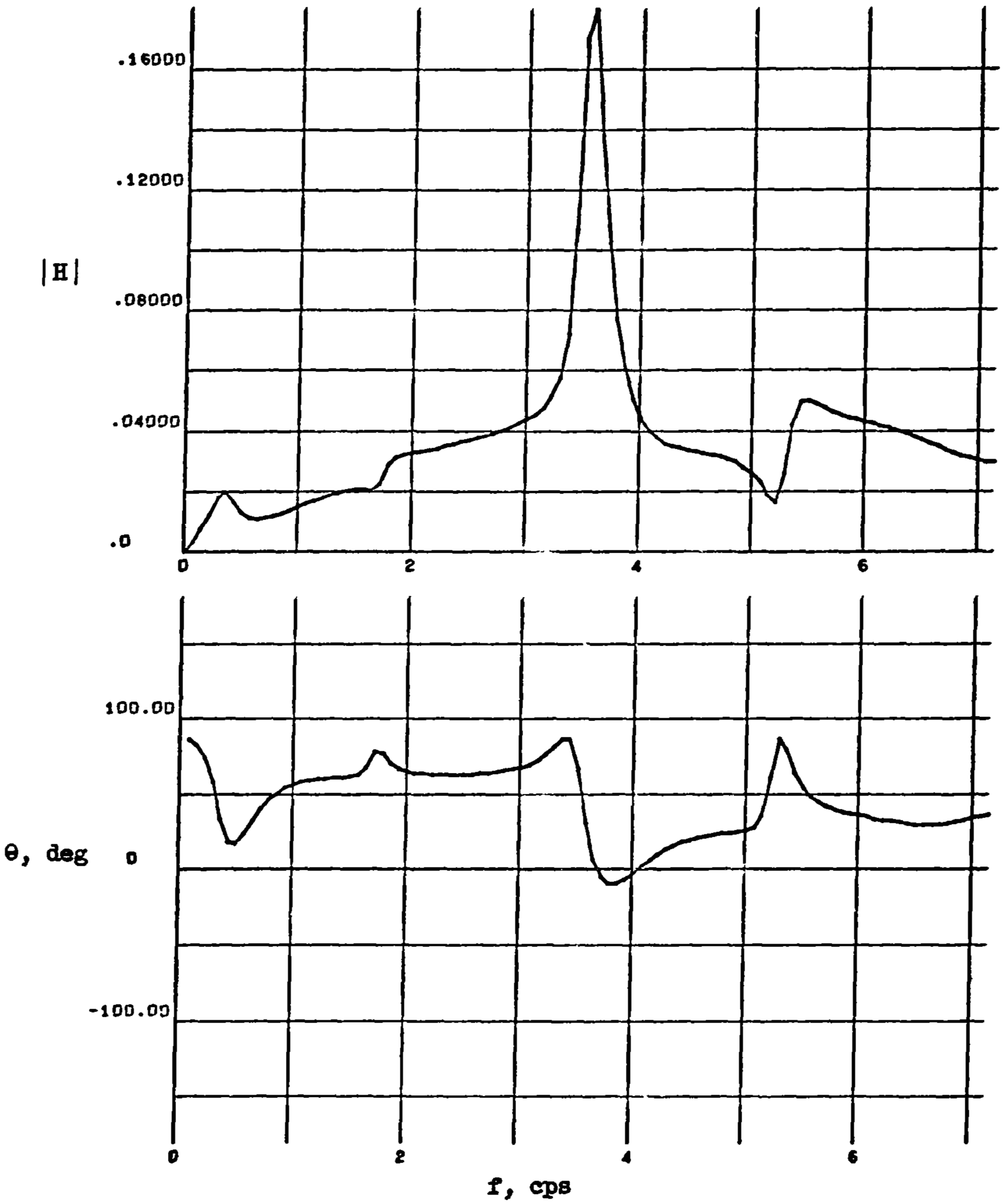

(b) Acceleration at the pilot station.

Figure 13.- Continued.

(c) Acceleration at the nose instrumentation package station.

Figure 13.- Continued.

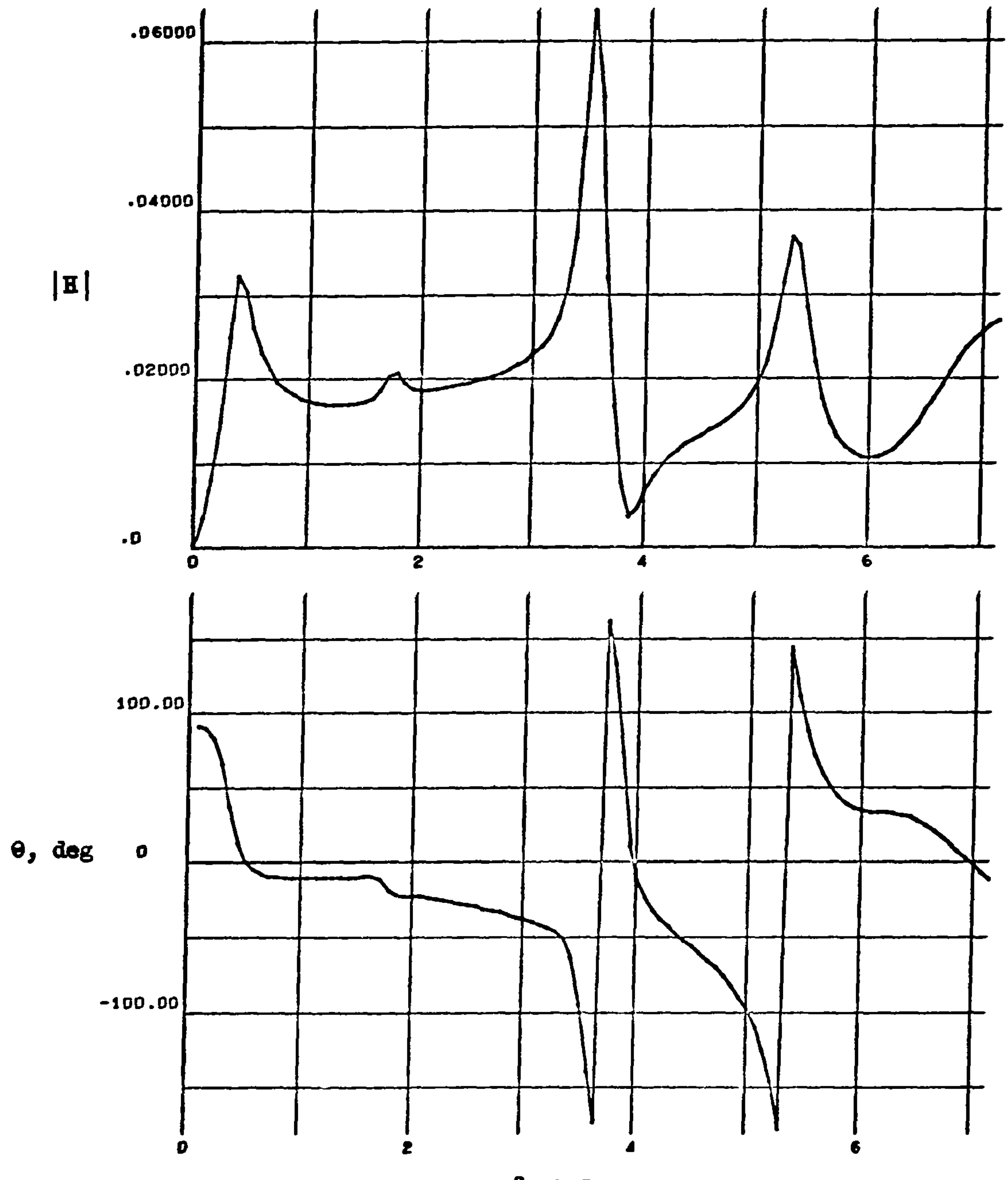

(d) Acceleration at the wing apex station.

Figure 13.- Continued.

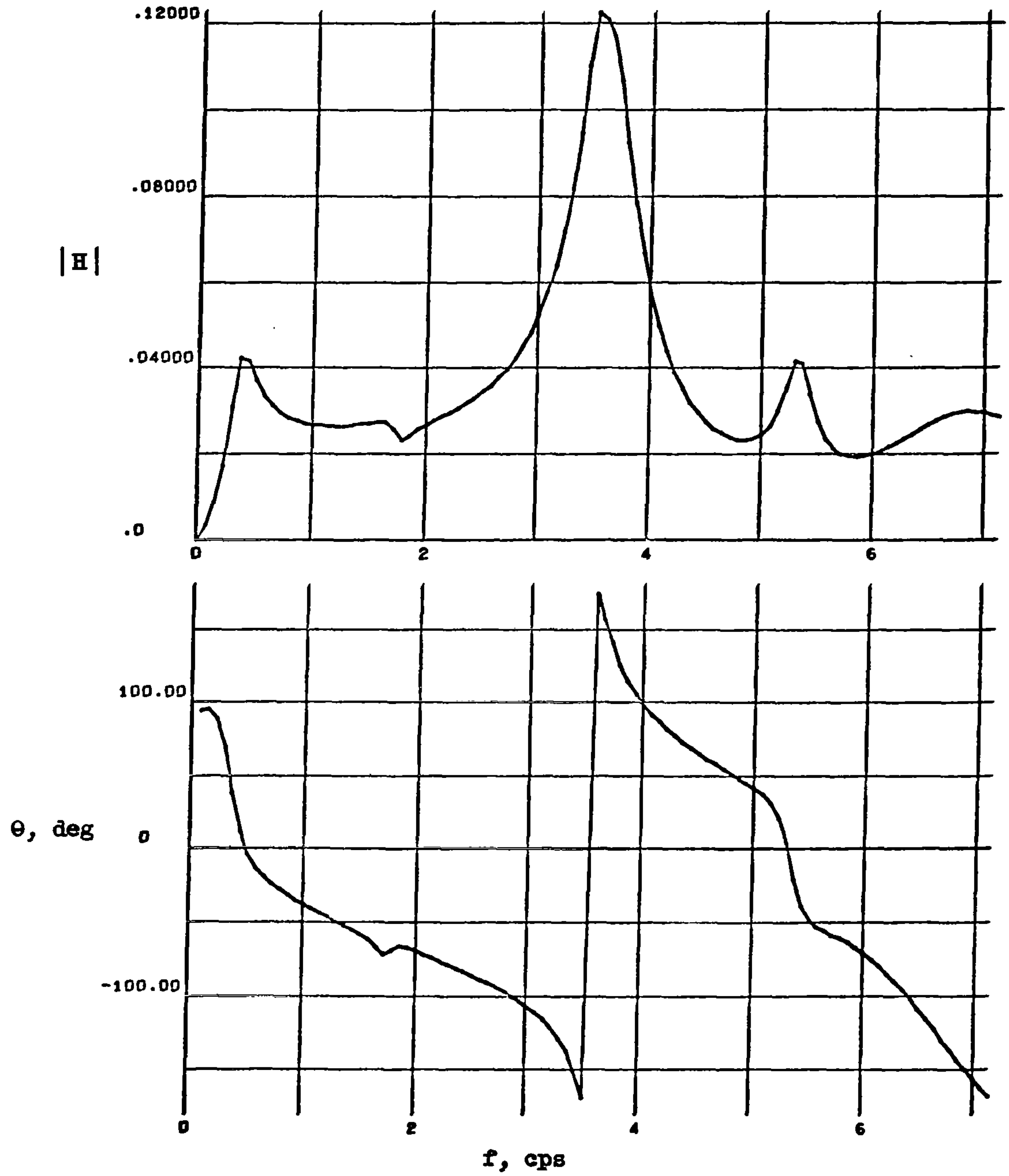

(e) Acceleration at the aft fuselage station.

Figure 13.- Continued.

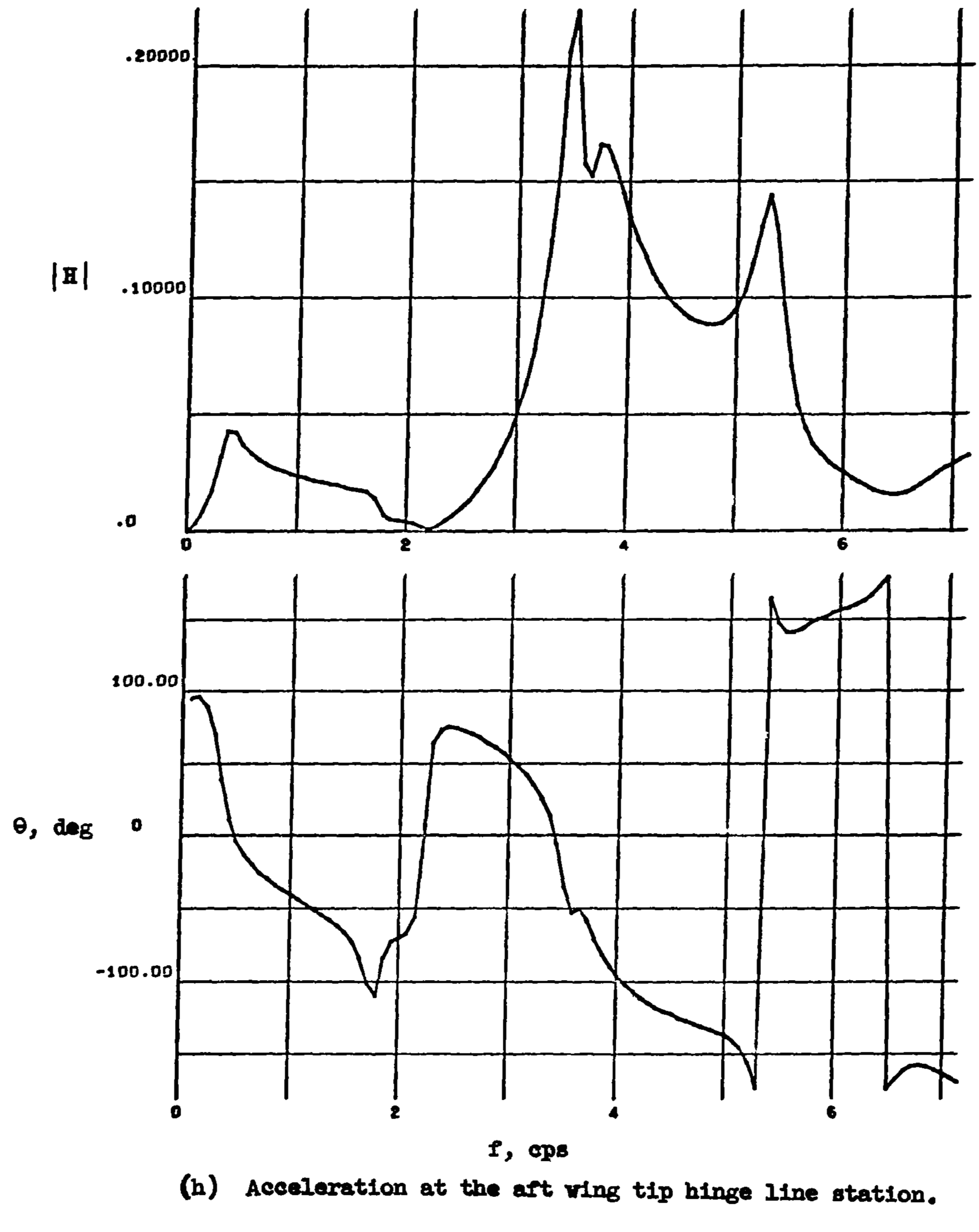

(h) Acceleration at the aft wing tip hinge line station.

Figure 13.- Continued.

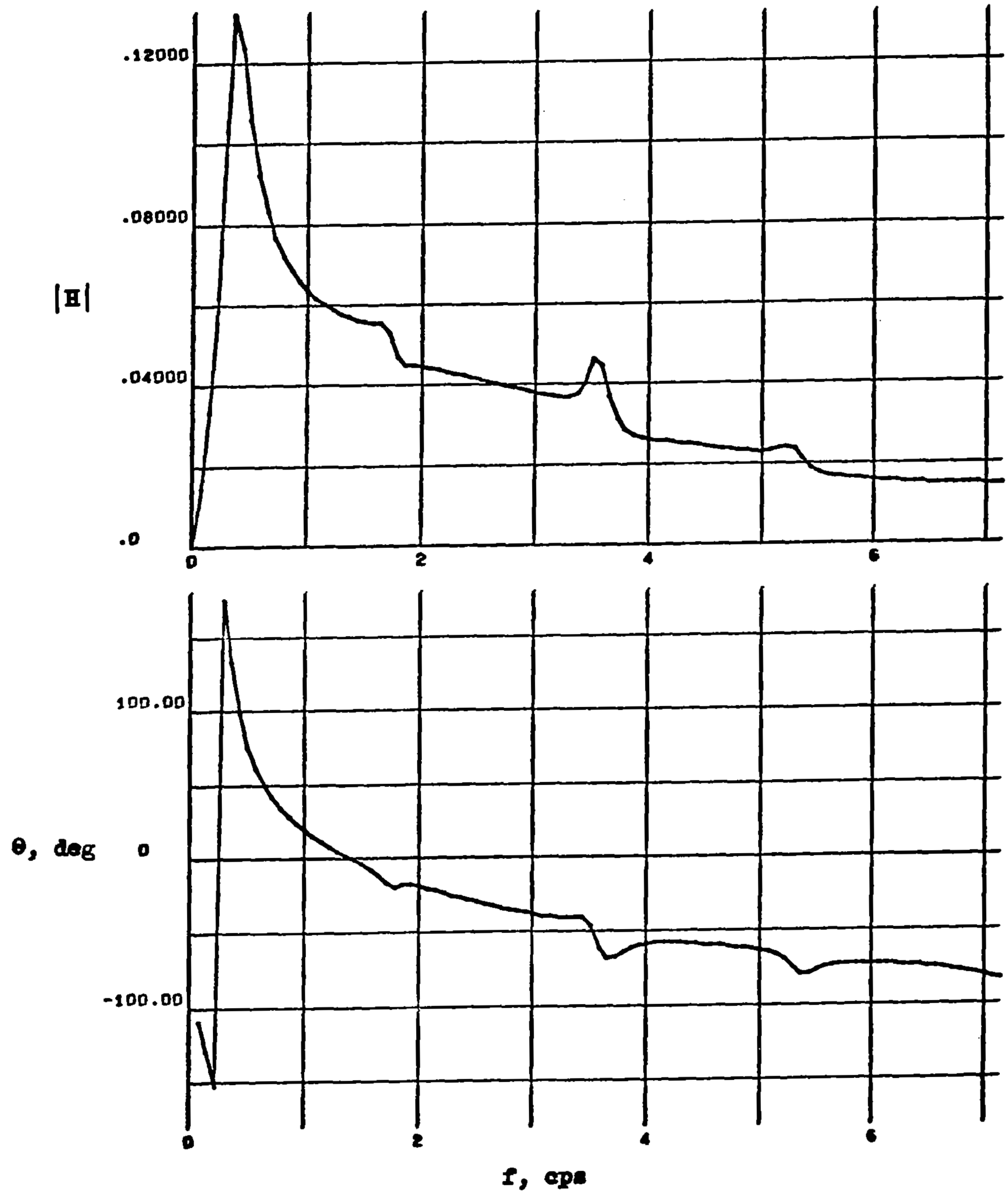

(i) Rate of pitch.

Figure 13.- Continued.

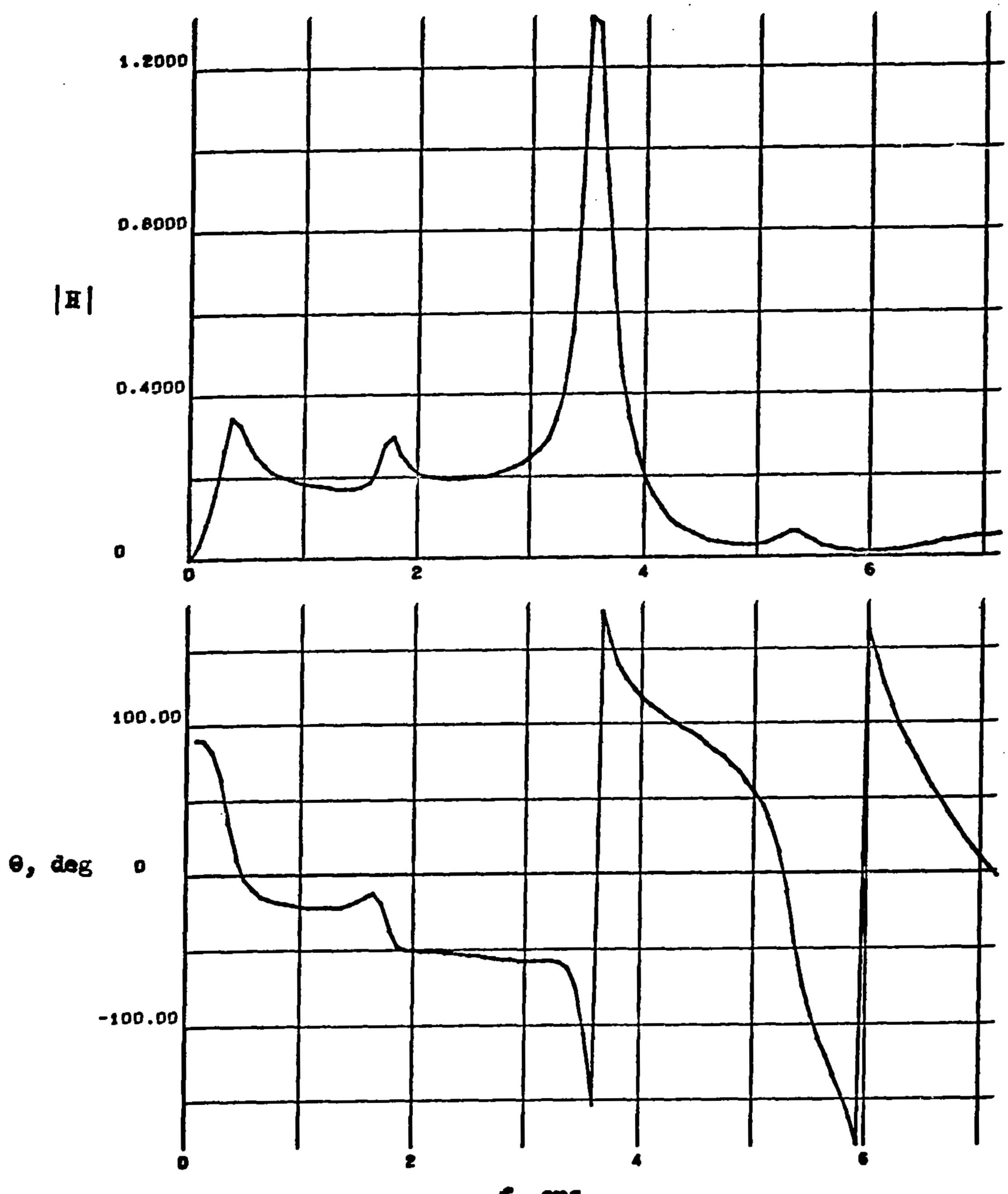

(j) Fuselage bending moment at station 1040, 10^6 in-lb.

Figure 13.- Continued.

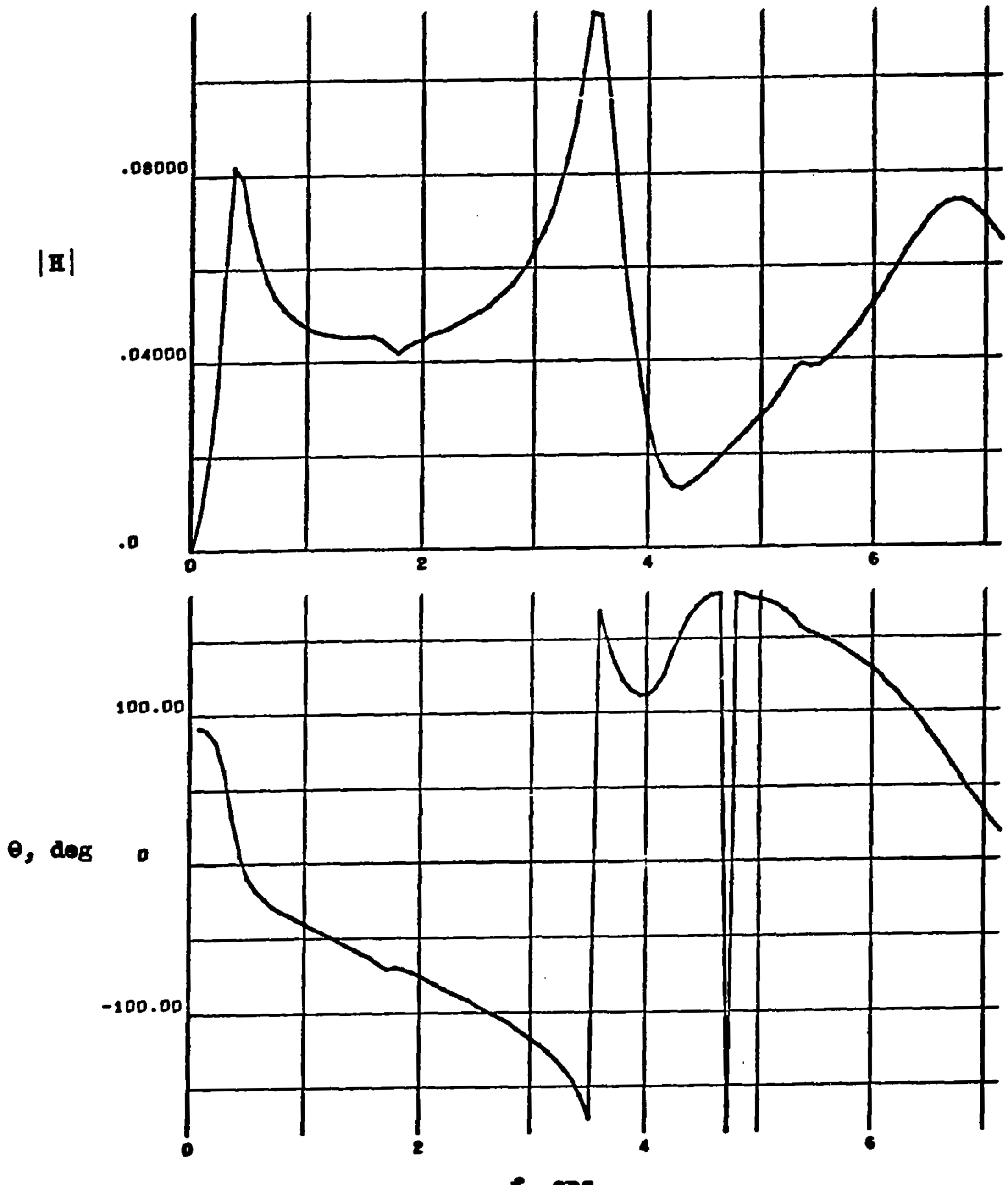

(k) Wing tip hinge moment, 10^6 in-lb.

Figure 13.- Concluded.

(a) Acceleration at the center of gravity station.

Figure 14.- System response functions for Condition 3-3.

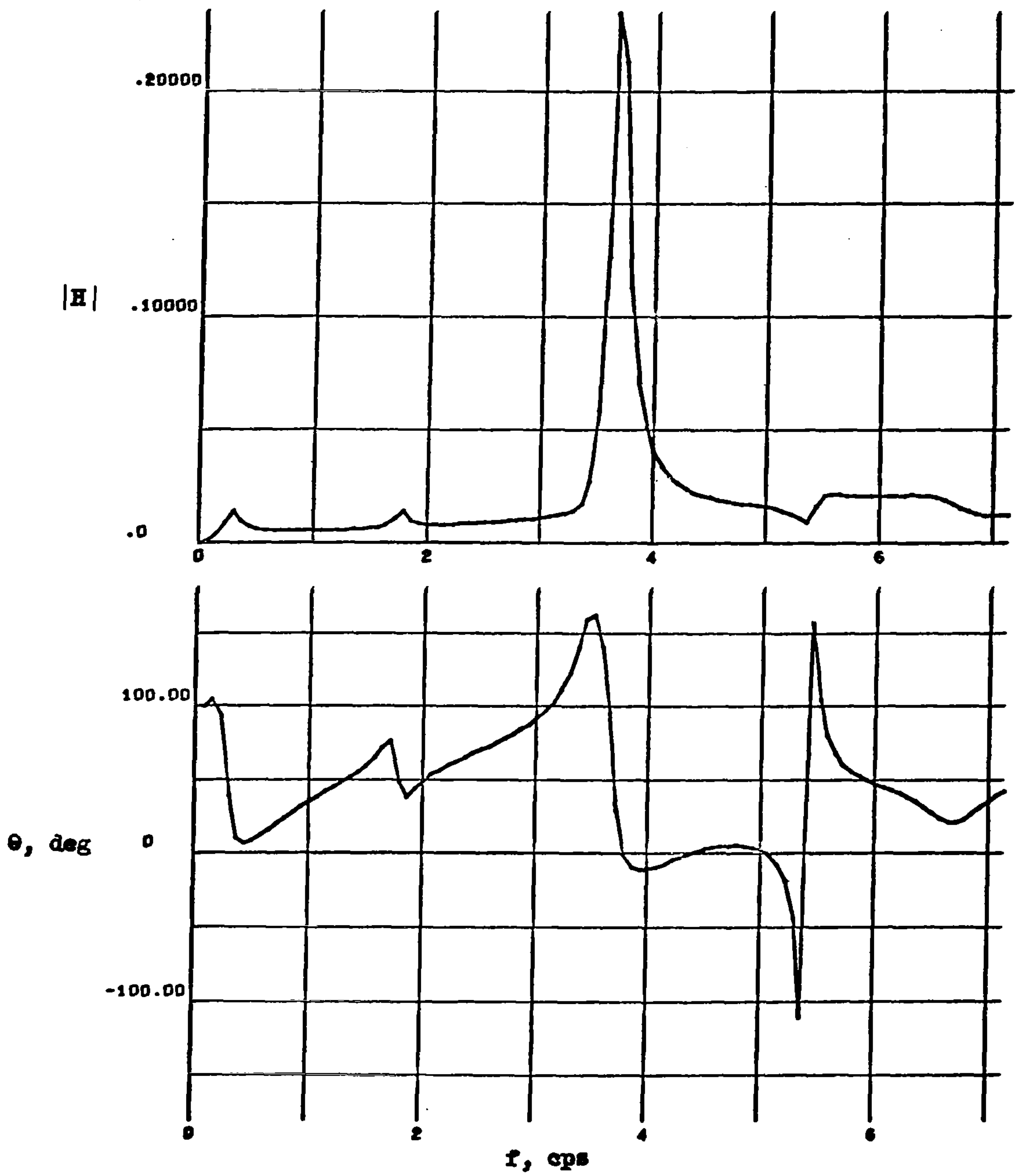

(b) Acceleration at the pilot station.

Figure 14.- Continued.

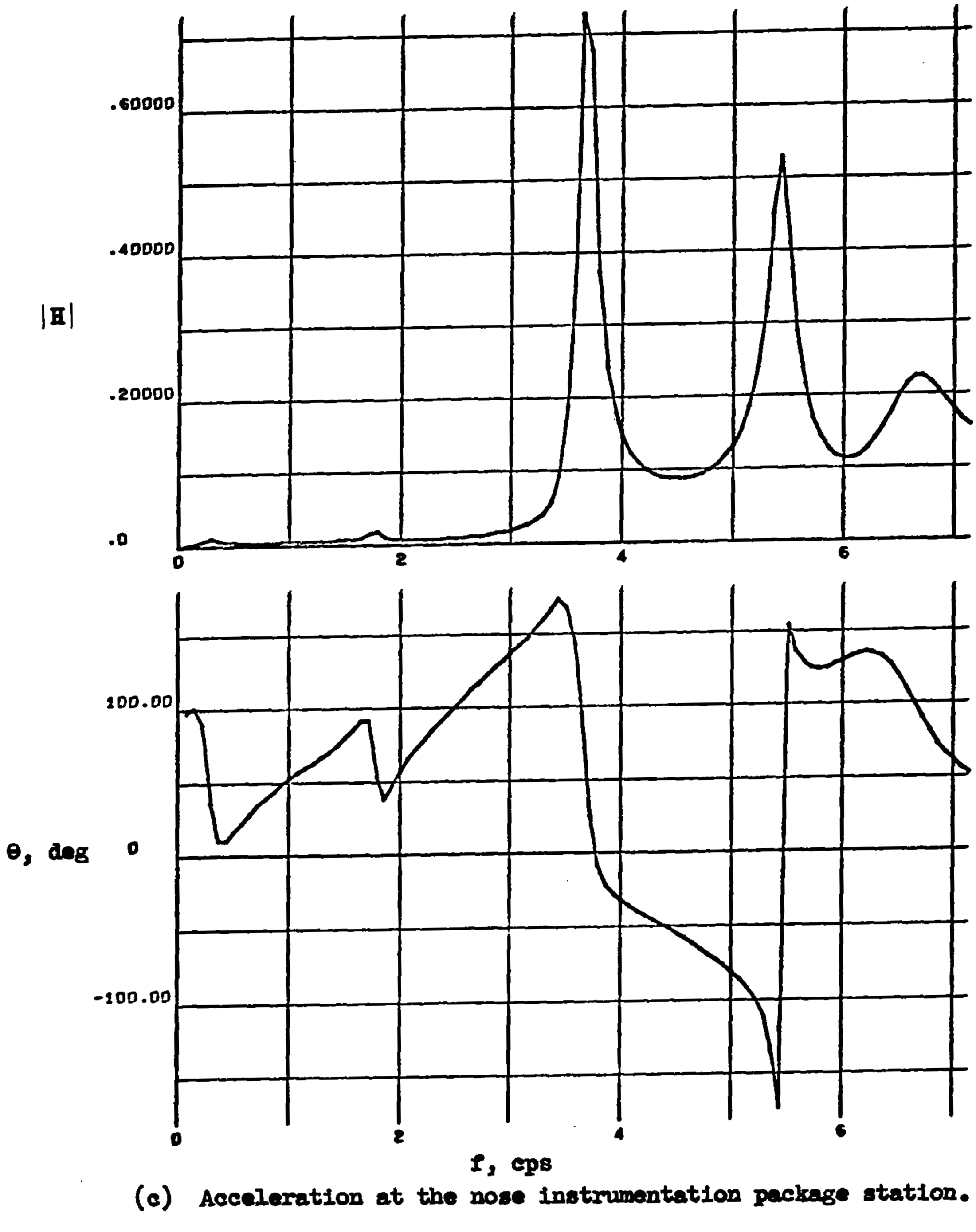

(c) Acceleration at the nose instrumentation package station.

Figure 14.- Continued.

(d) Acceleration at the wing apex station.

Figure 14.- Continued.

(e) Acceleration at the aft fuselage station.

Figure 14.- Continued.

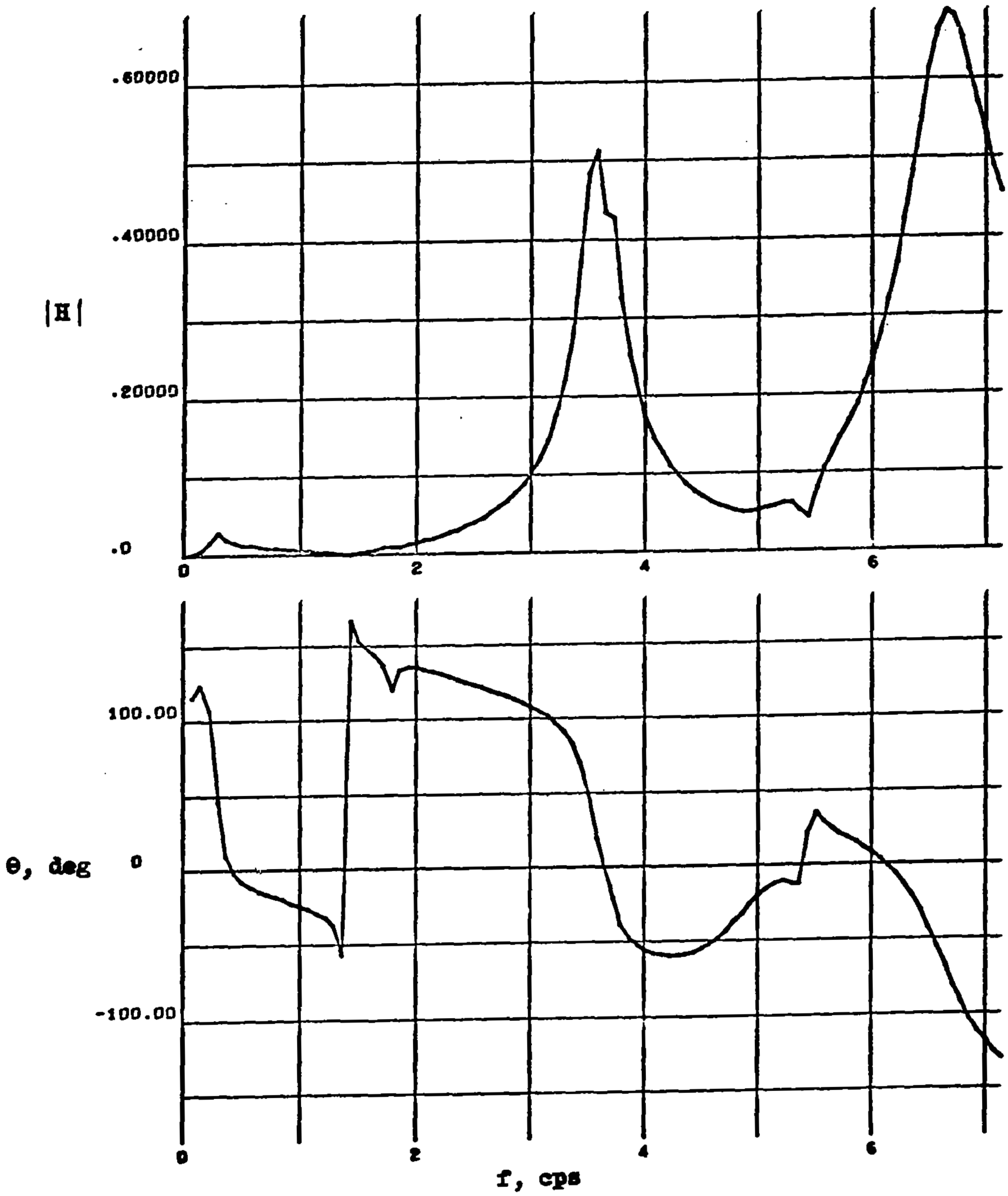

(f) Acceleration at the wing tip station.

Figure 14.- Continued.

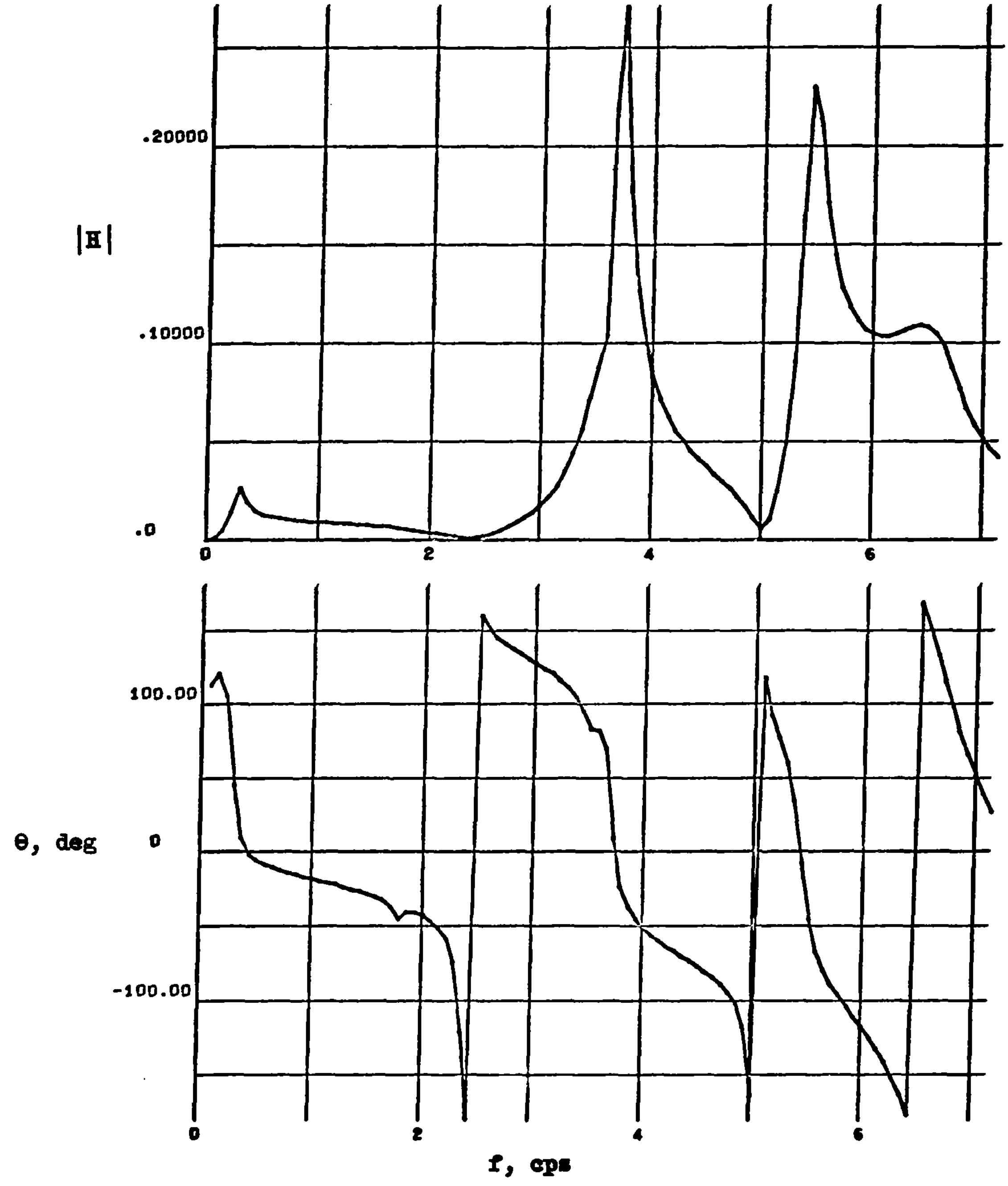

(g) Acceleration at the forward wing tip hinge line station.

Figure 14.- Continued.

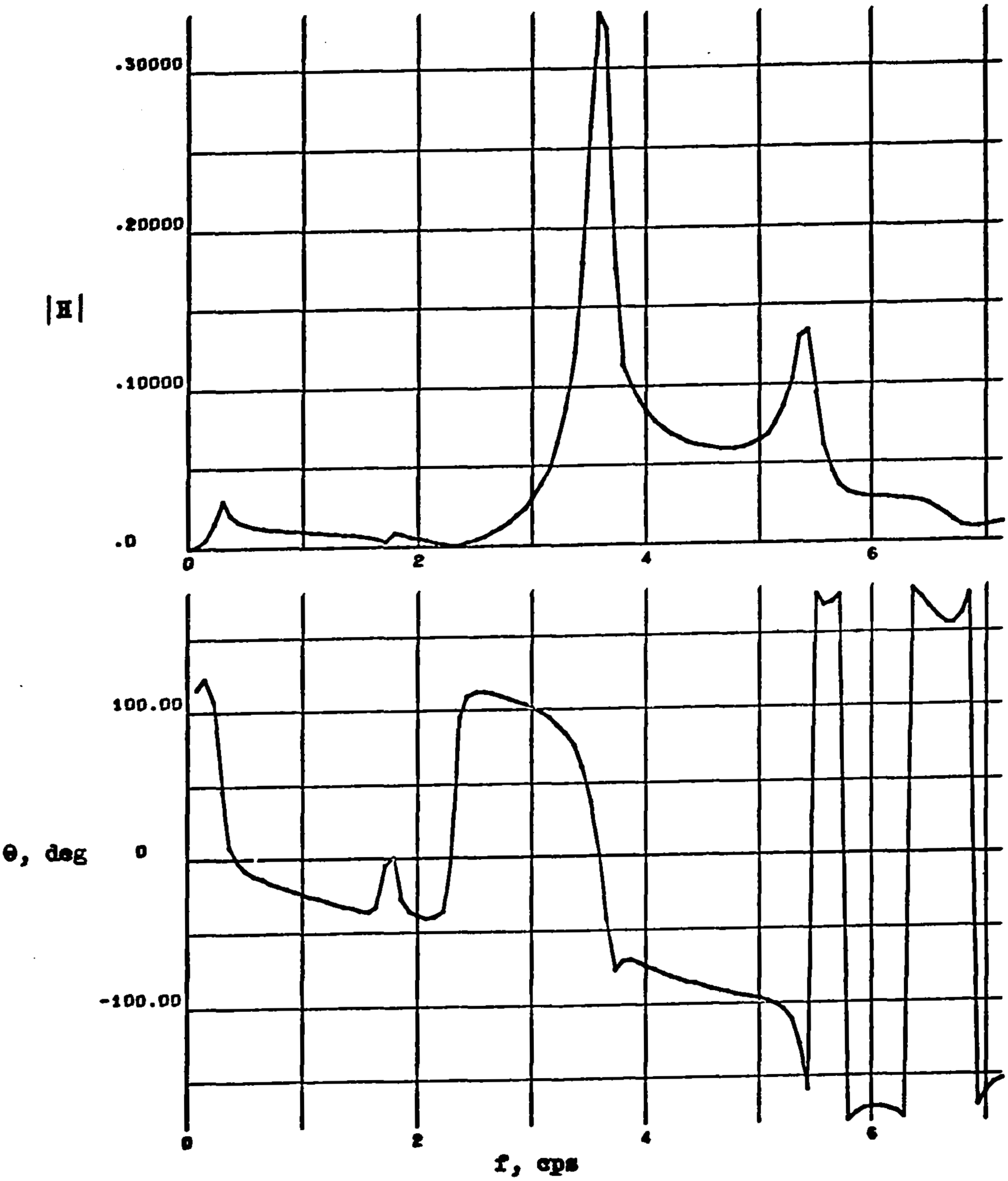

(h) Acceleration at the aft wing tip hinge line station.

Figure 14.- Continued.

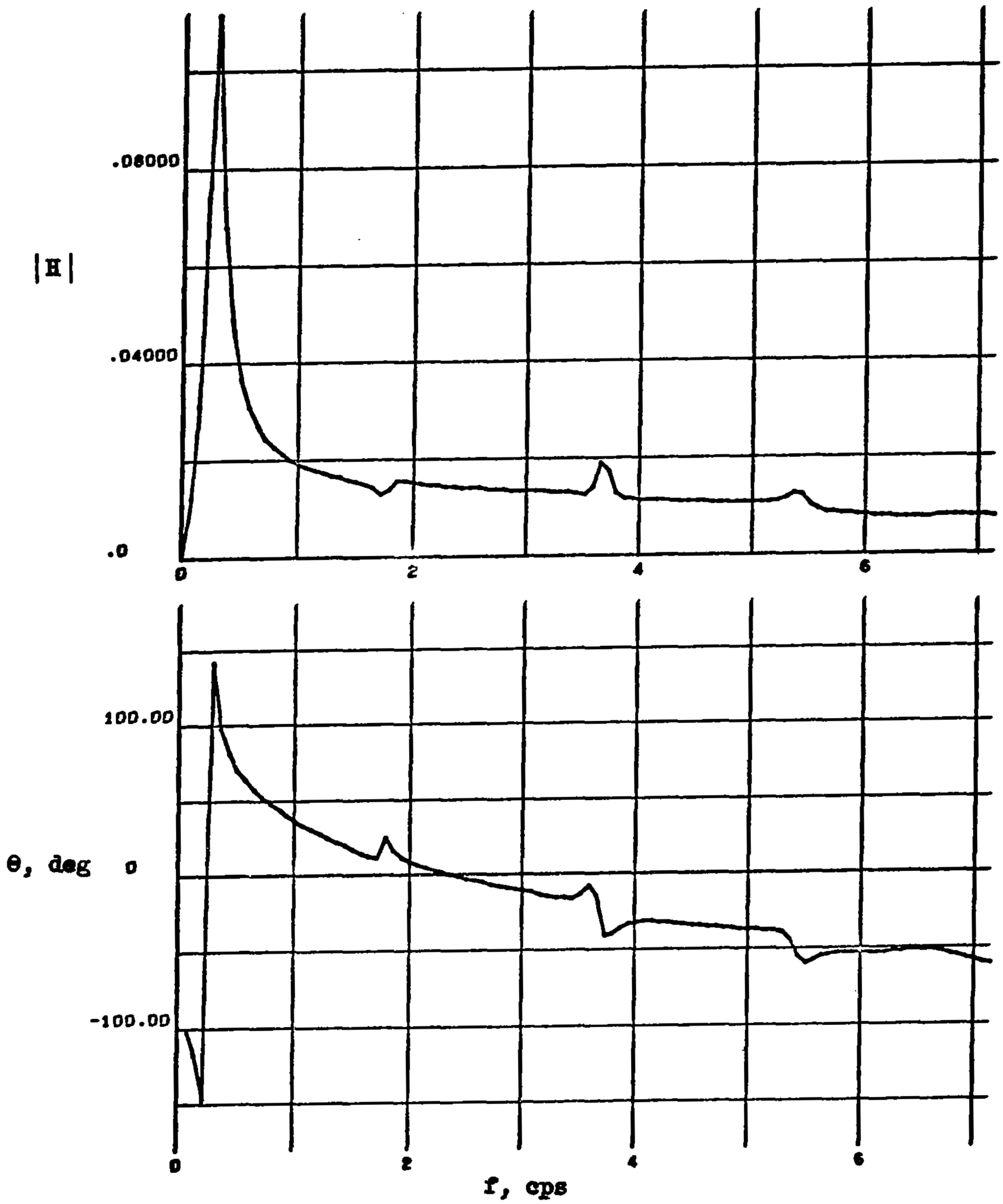

(i) Rate of pitch.

Figure 14.- Continued.

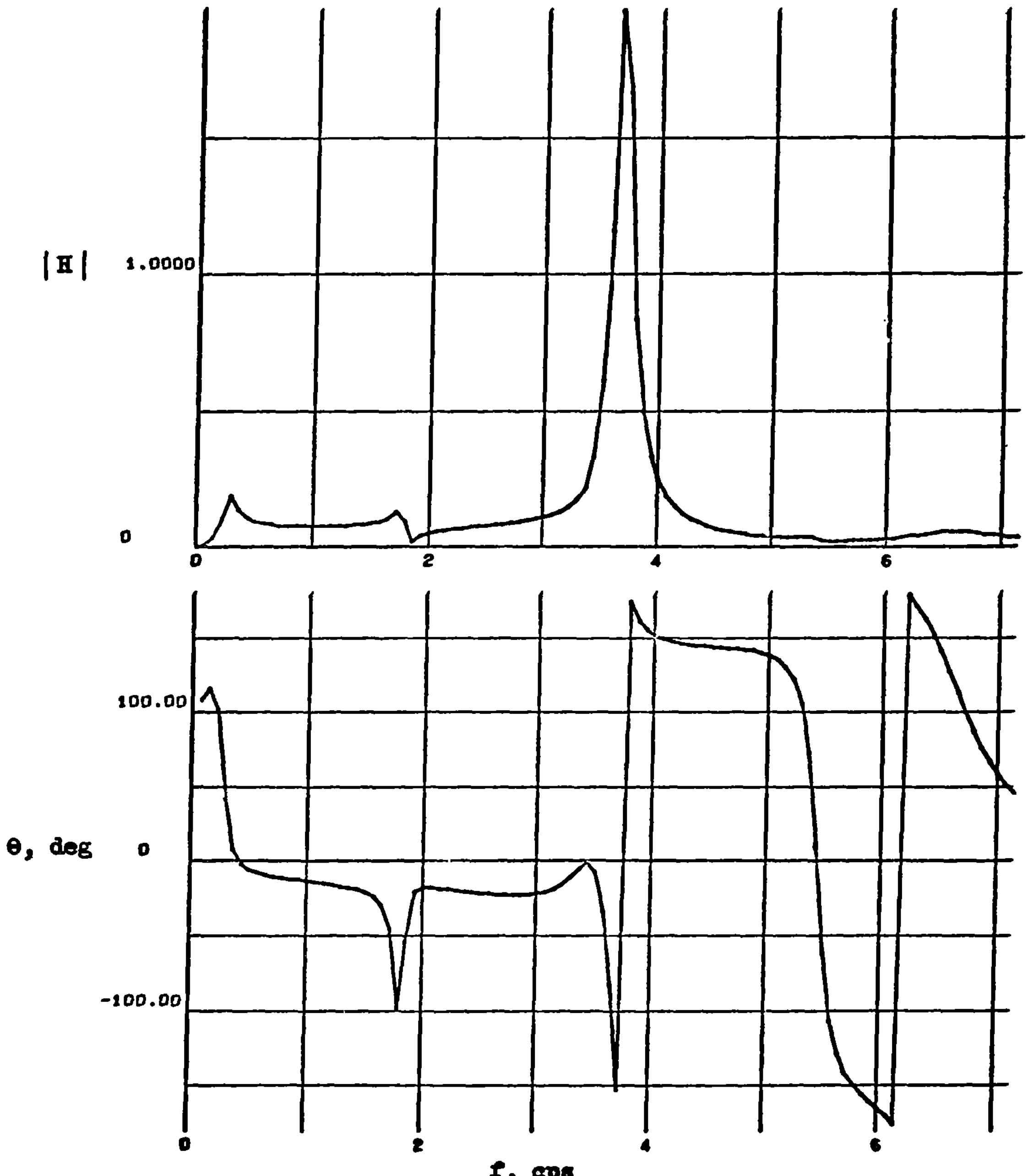

(j) Fuselage bending moment at station 1040, 10^6 in-lb.

Figure 14.- Continued.

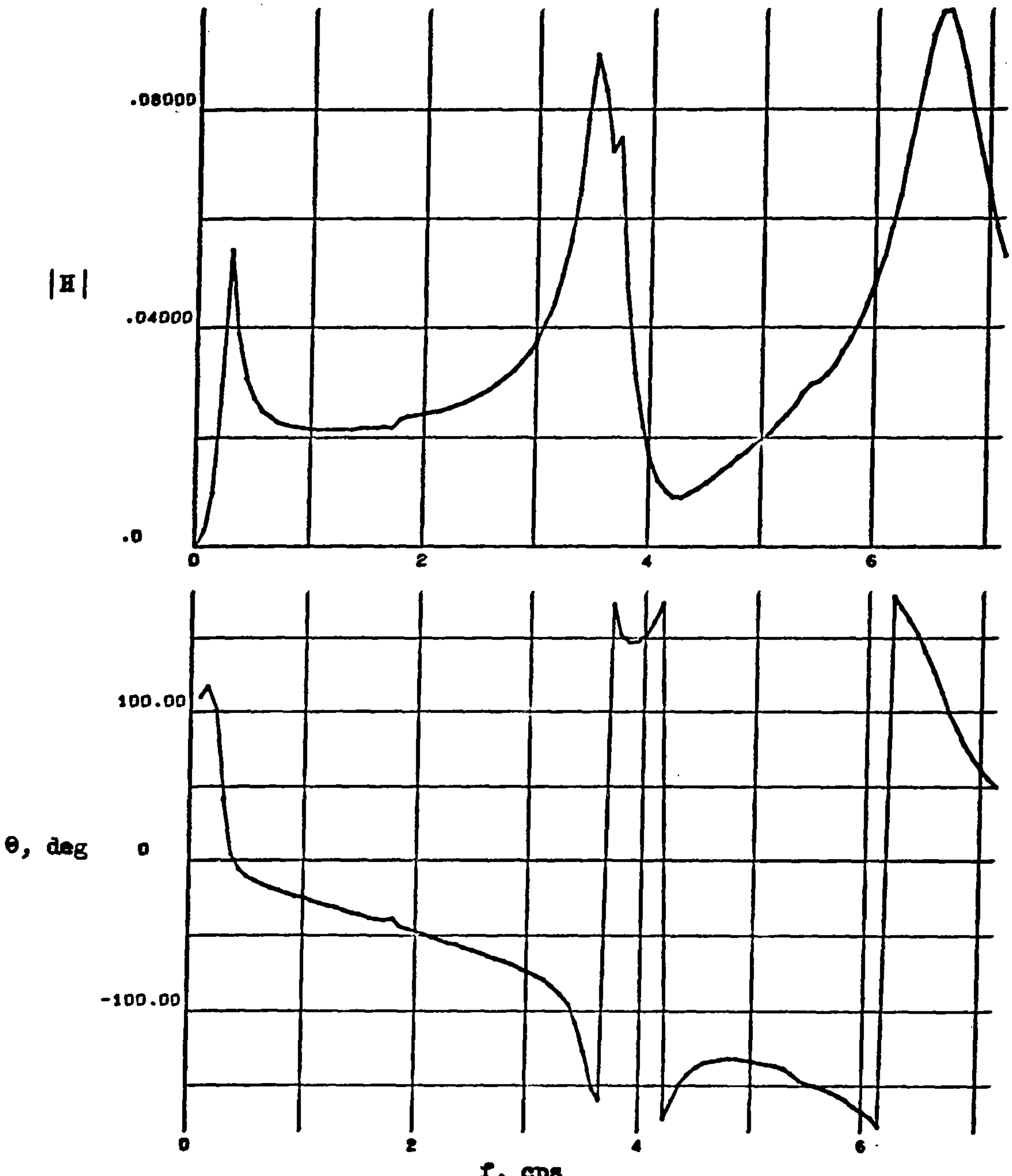

(k) Wing tip hinge moment, 10^6 in-lb.

Figure 14.- Concluded.

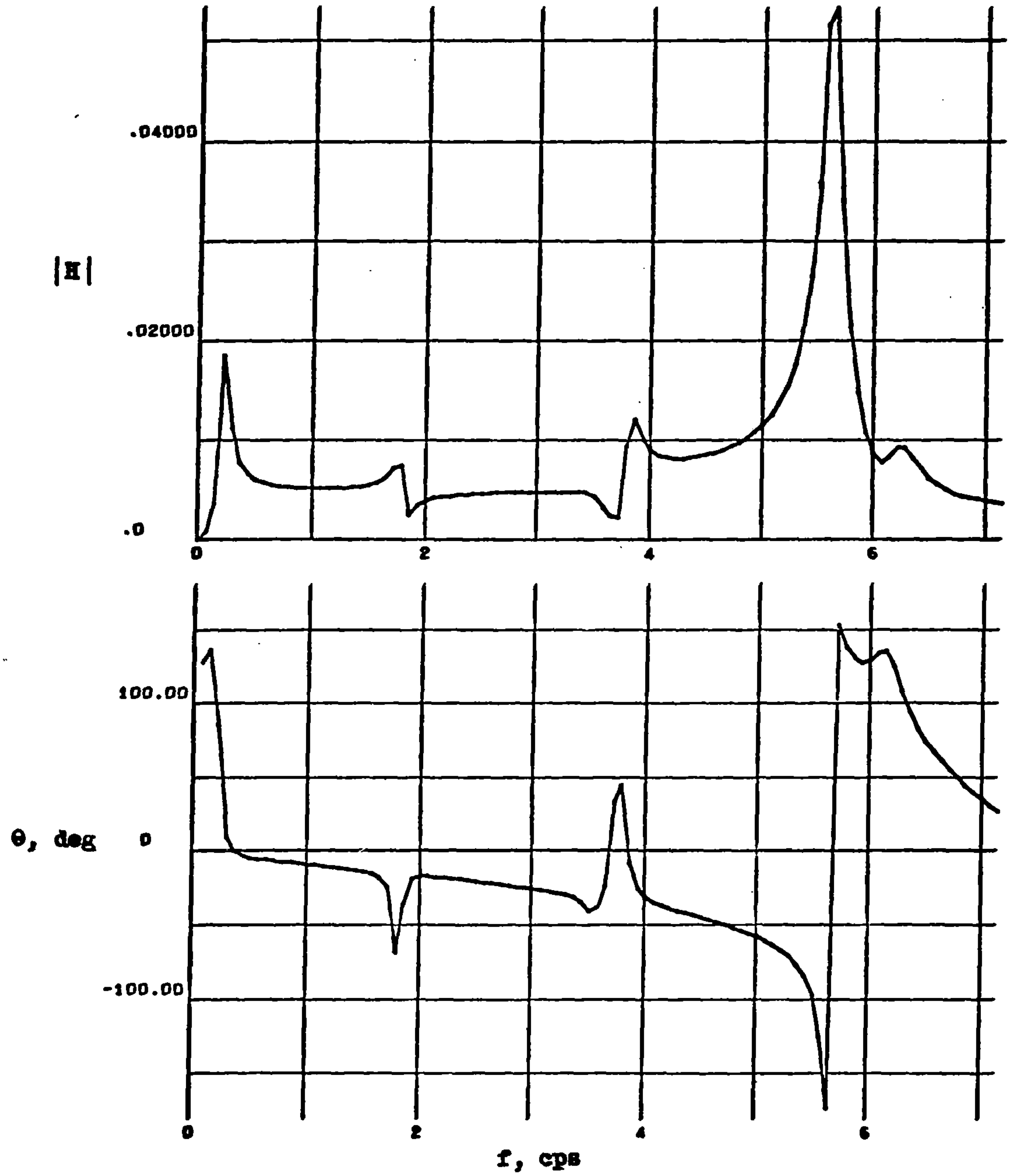

(a) Acceleration at the center of gravity station.

Figure 15.- System response functions for Condition 3-4.

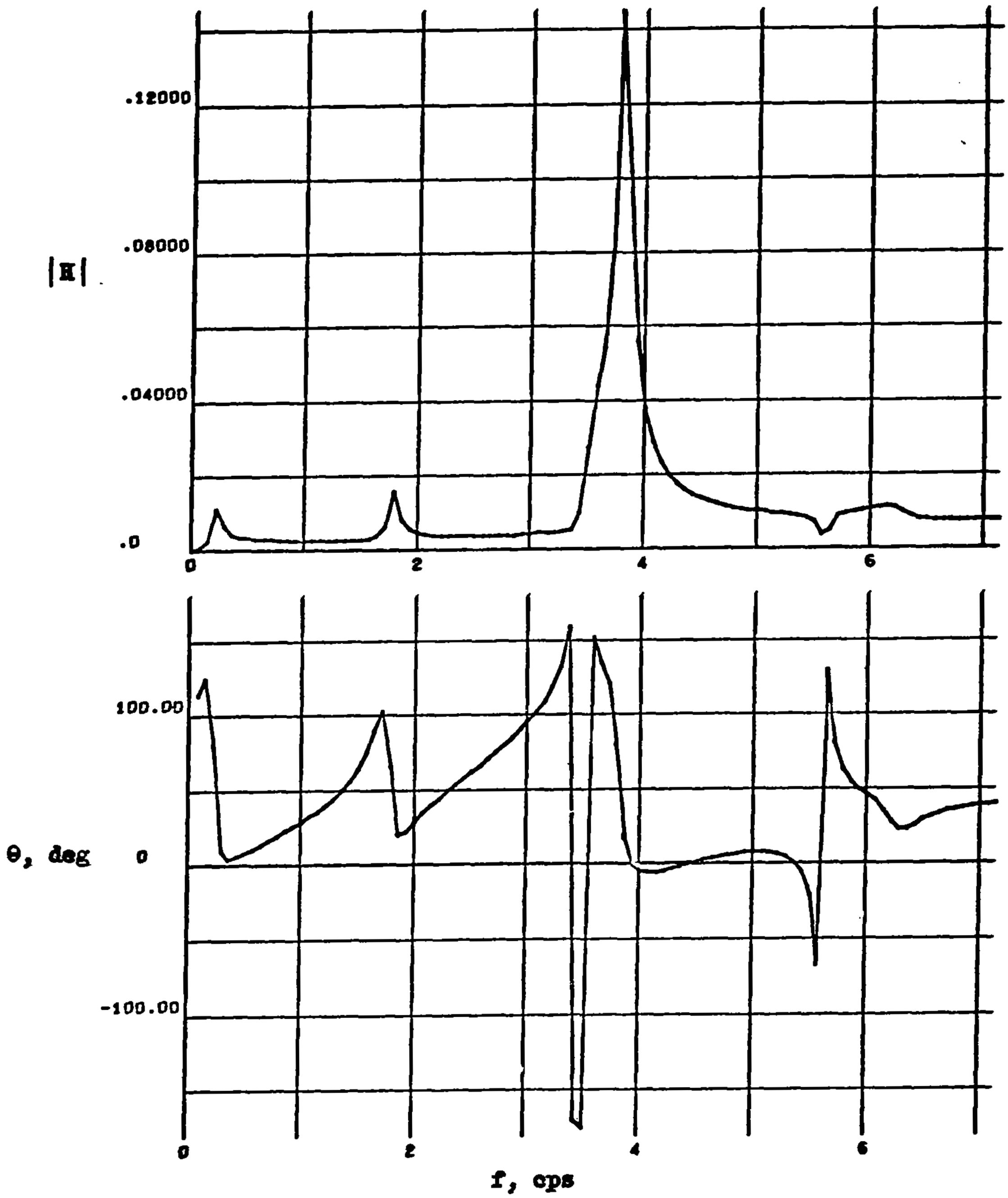

(b) Acceleration at the pilot station.

Figure 15.- Continued.

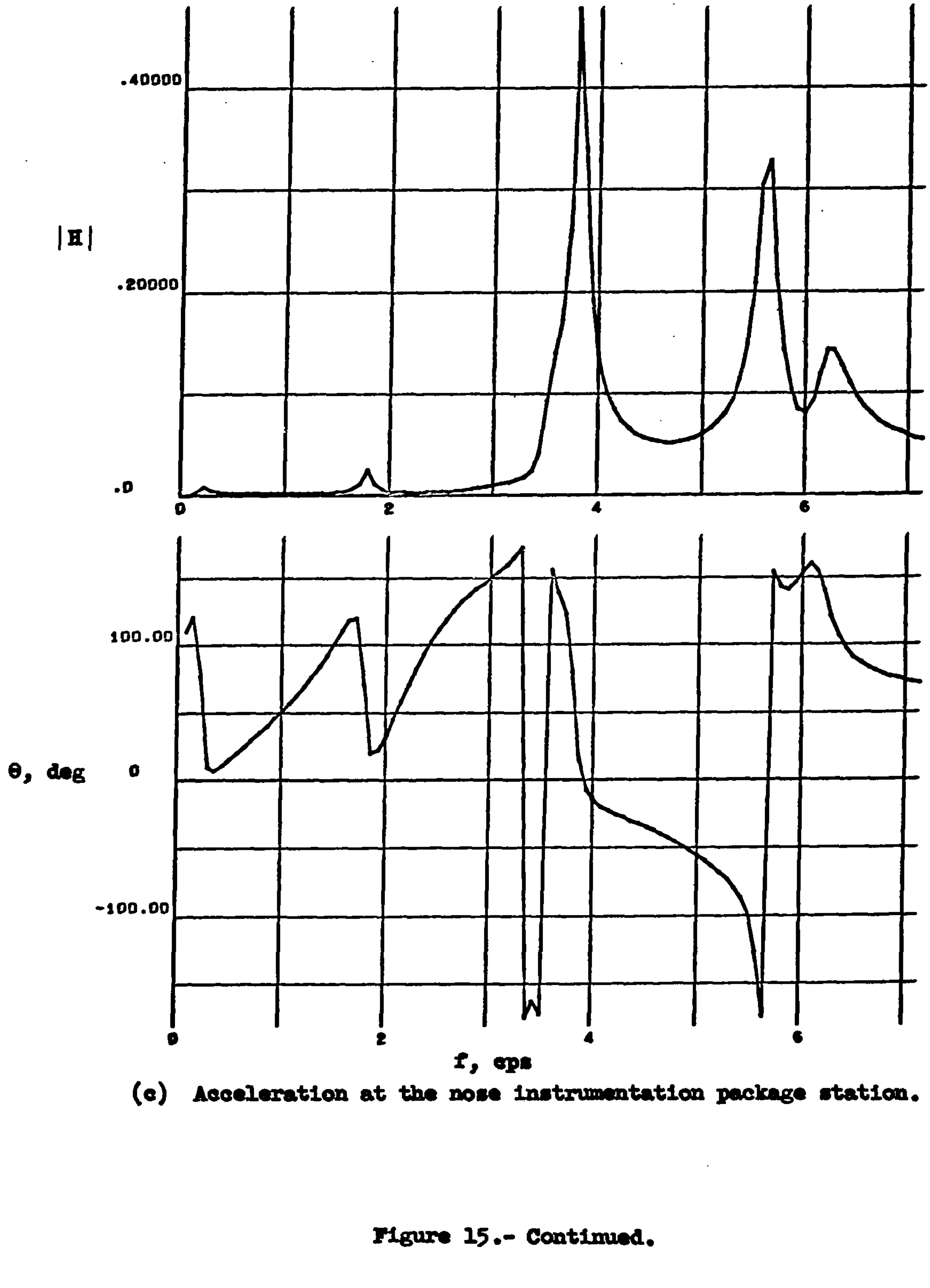

(c) Acceleration at the nose instrumentation package station.

Figure 15.- Continued.

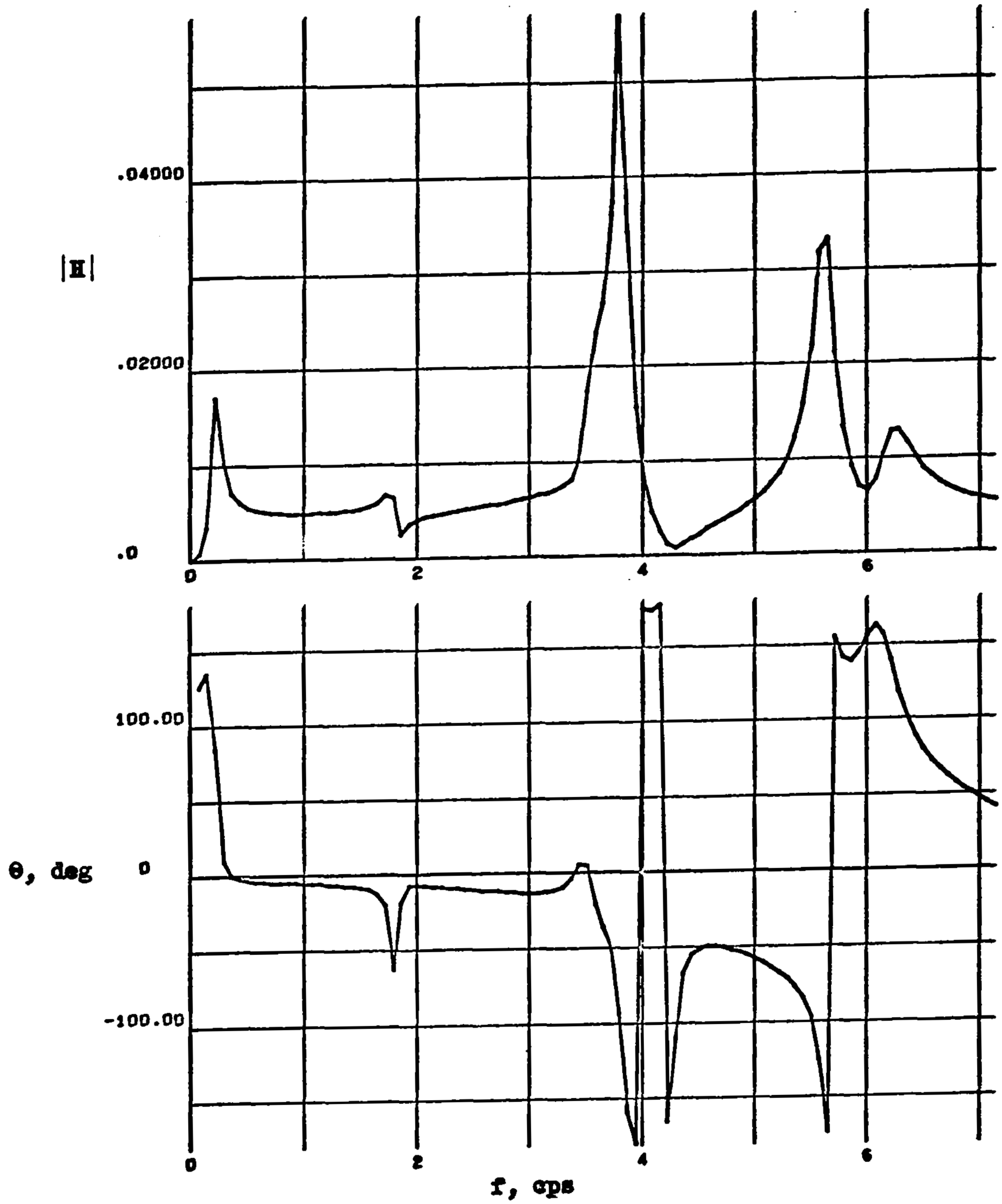

(d) Acceleration at the wing apex station.

Figure 15.- Continued.

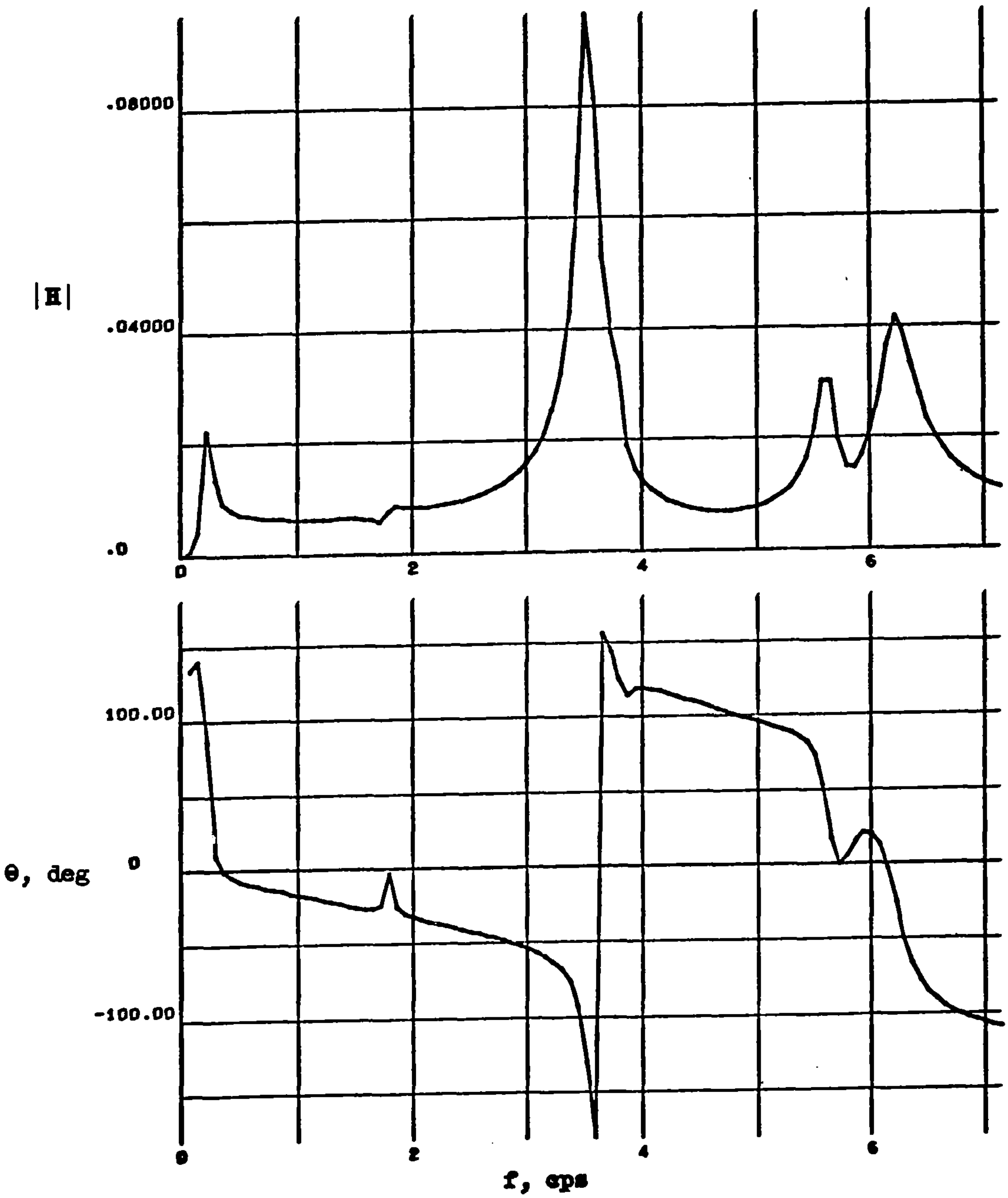

(e) Acceleration at the aft fuselage station.

Figure 15.- Continued.

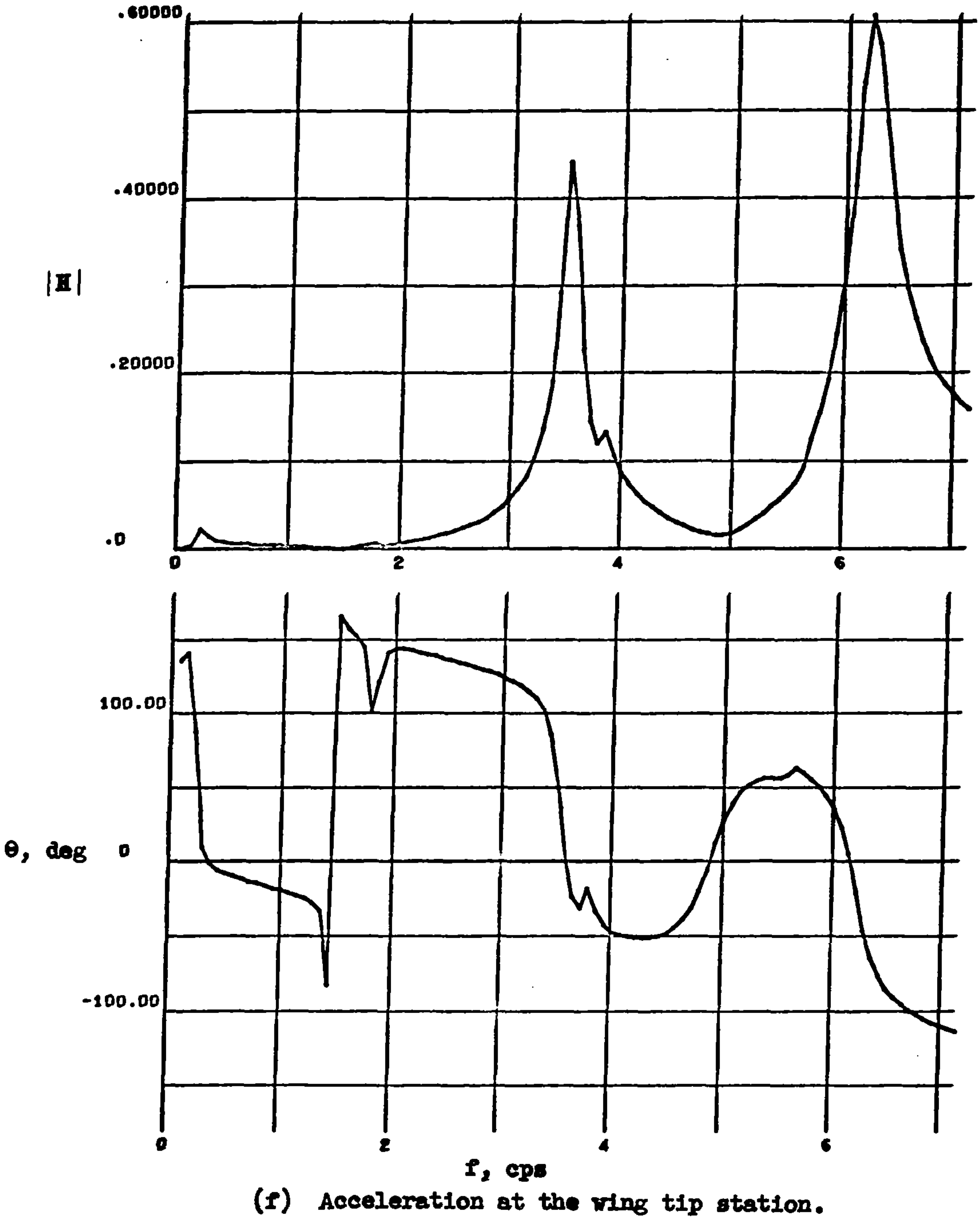

(f) Acceleration at the wing tip station.

Figure 15.- Continued.

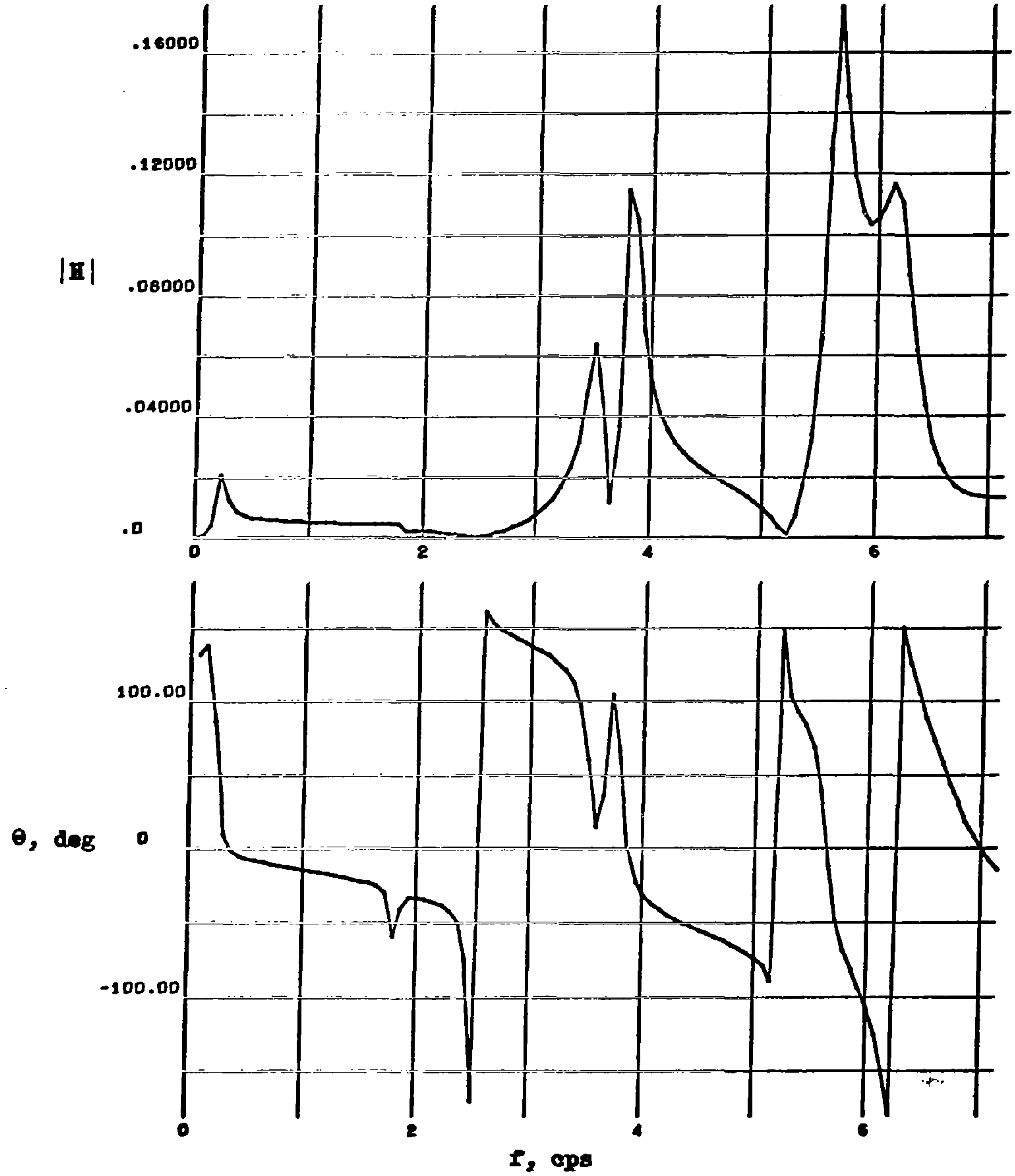

(g) Acceleration at the forward wing tip hinge line station.

Figure 15.- Continued.

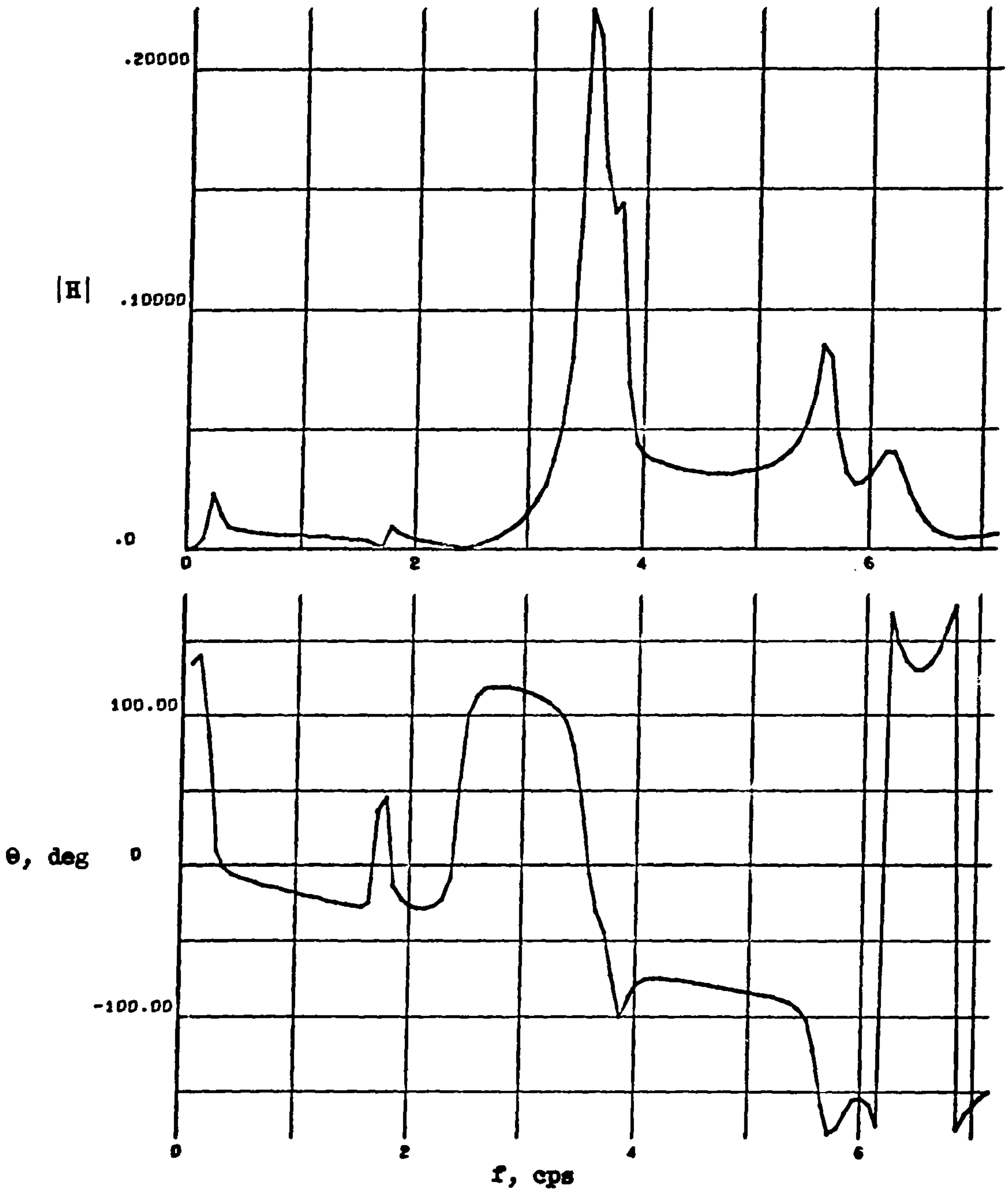

(h) Acceleration at the aft wing tip hinge line station.

Figure 15.- Continued.

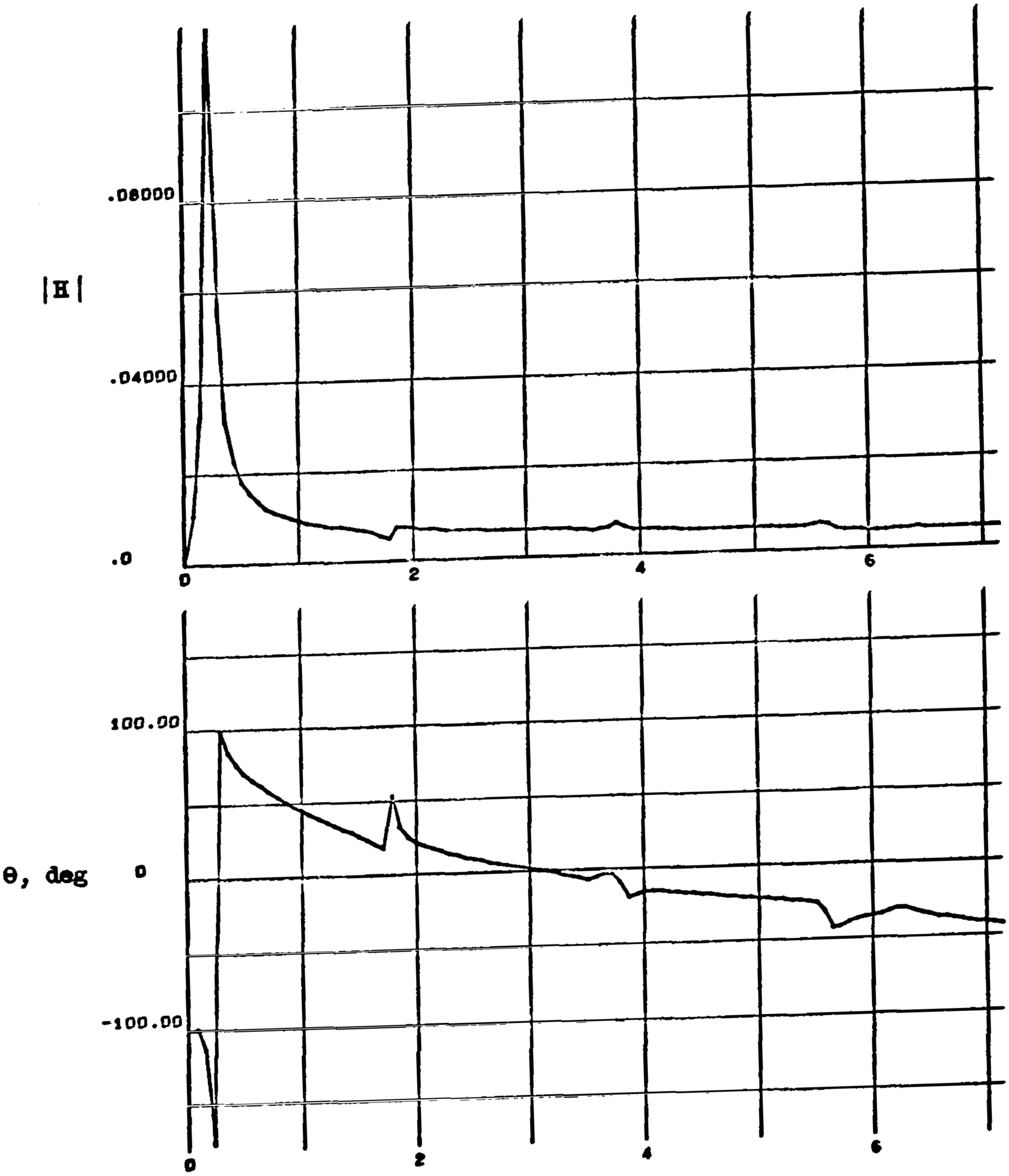

(i) Rate of pitch.

Figure 15.- Continued.

(j) Fuselage bending moment at station 1040, 10^6 in-lb.

Figure 15.- Continued.

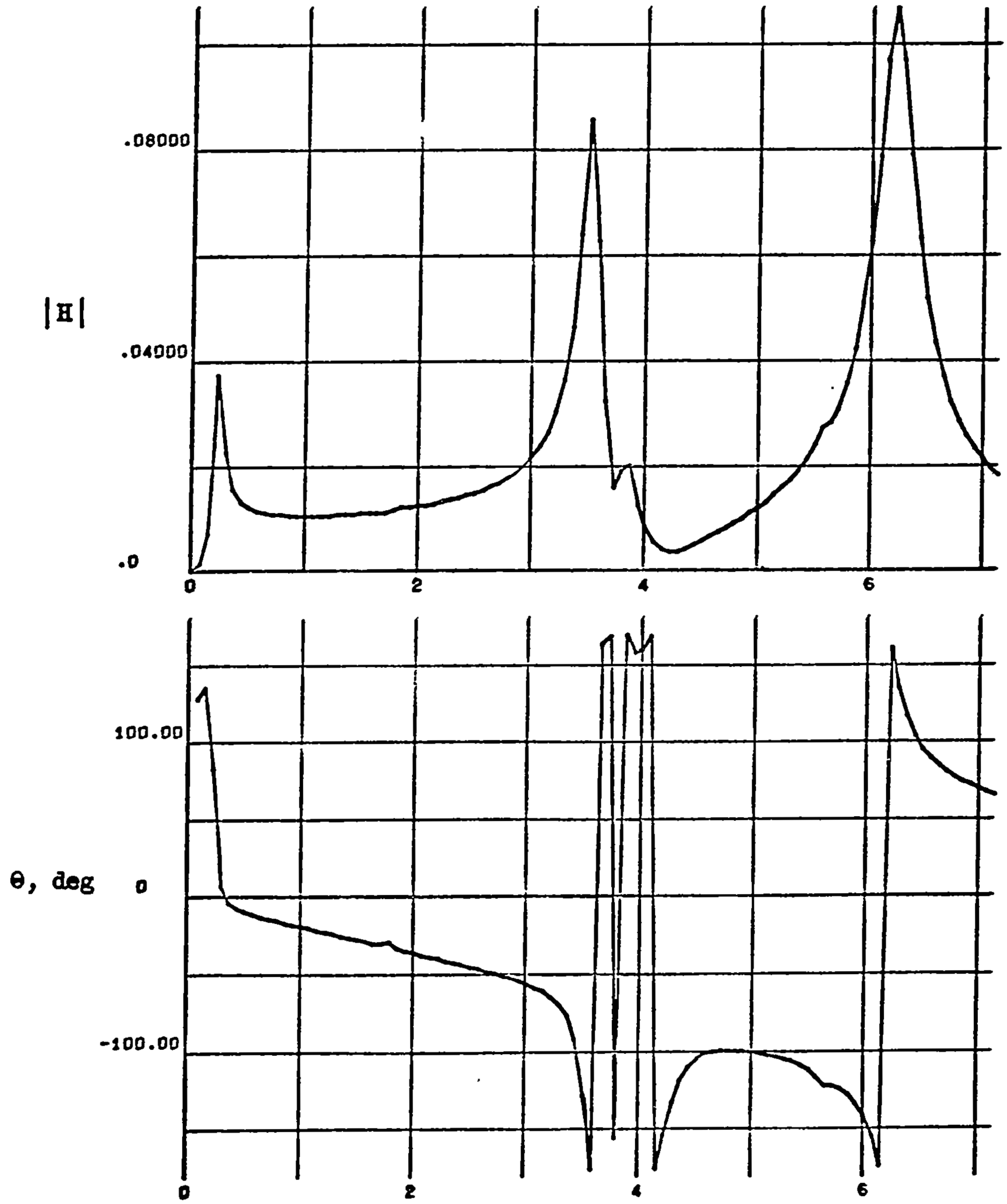

(k) Wing tip hinge moment, 10^6 in-lb.

Figure 15.- Concluded.

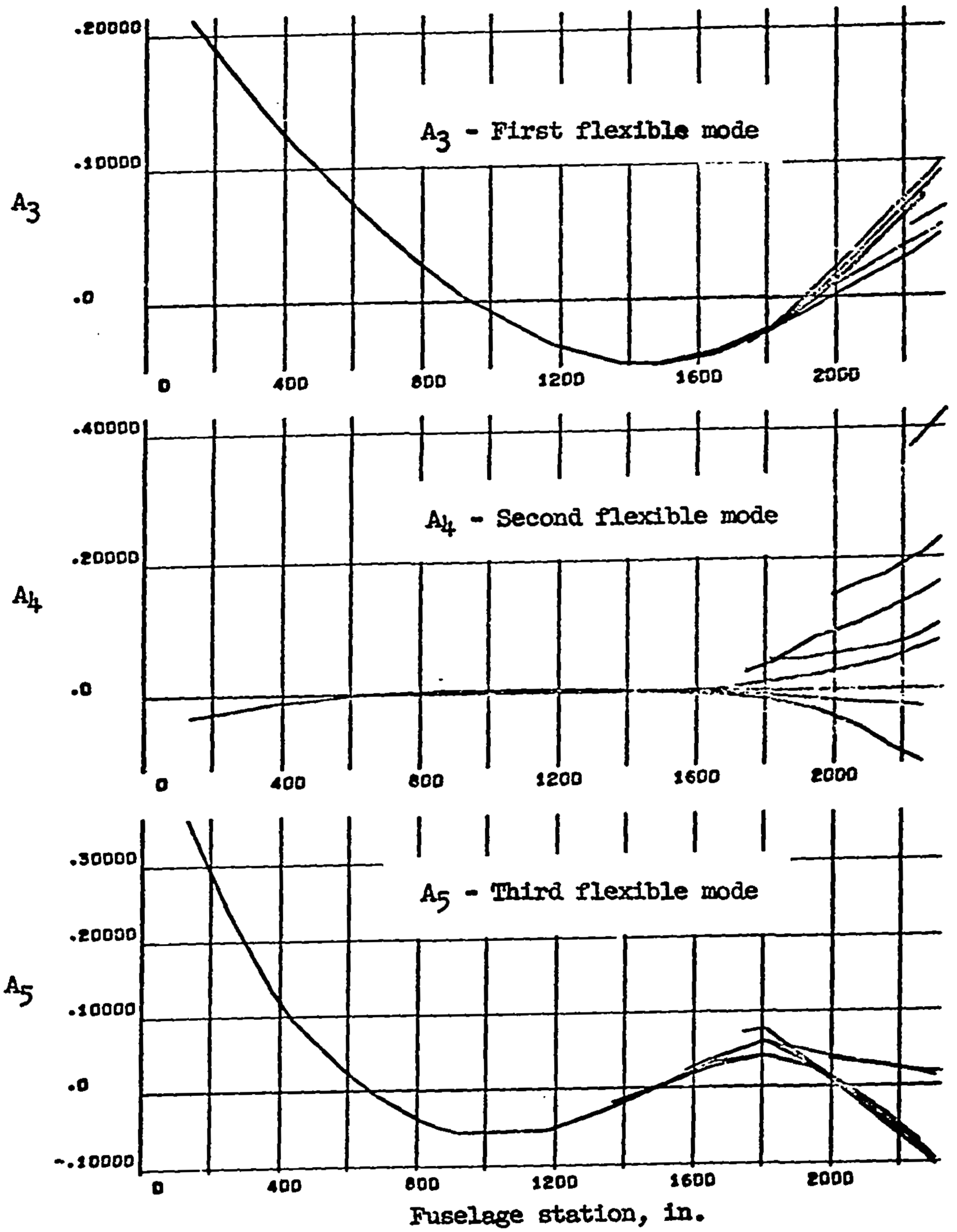

Figure 16.- Flexible mode shapes for Condition 1-1.

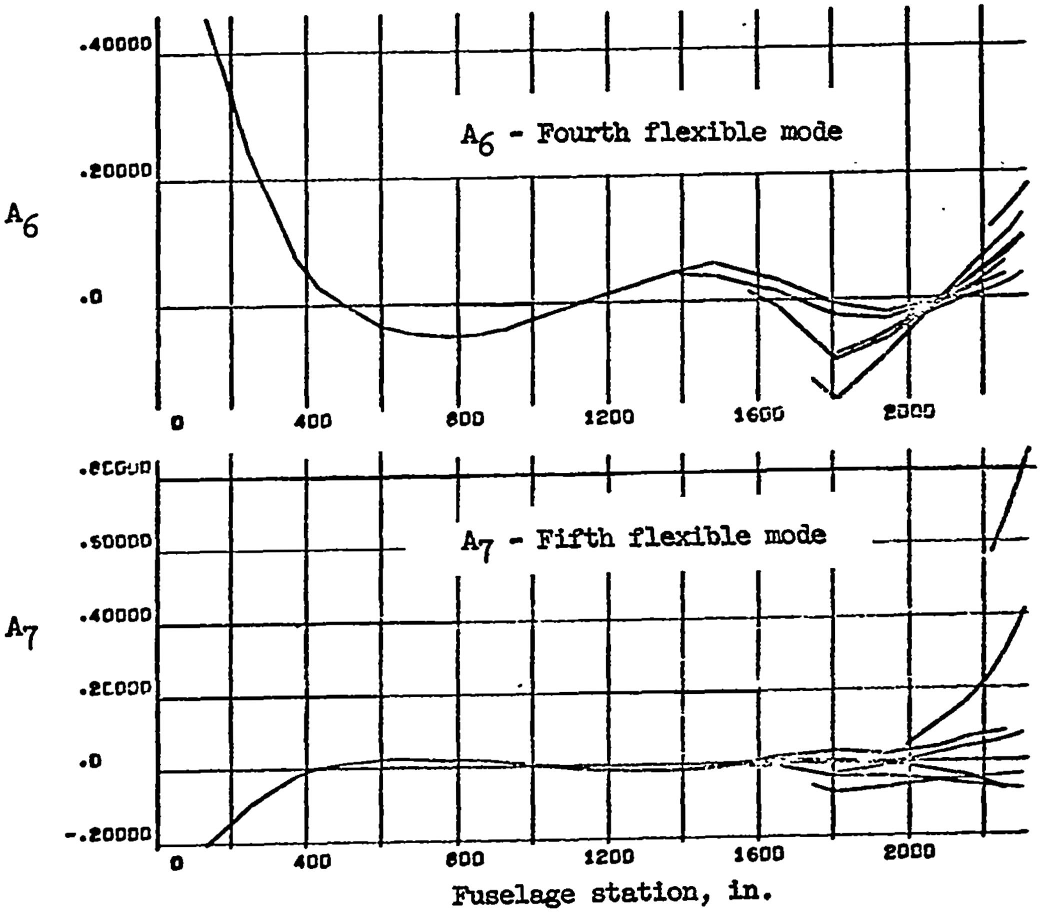

Figure 16.- Concluded.

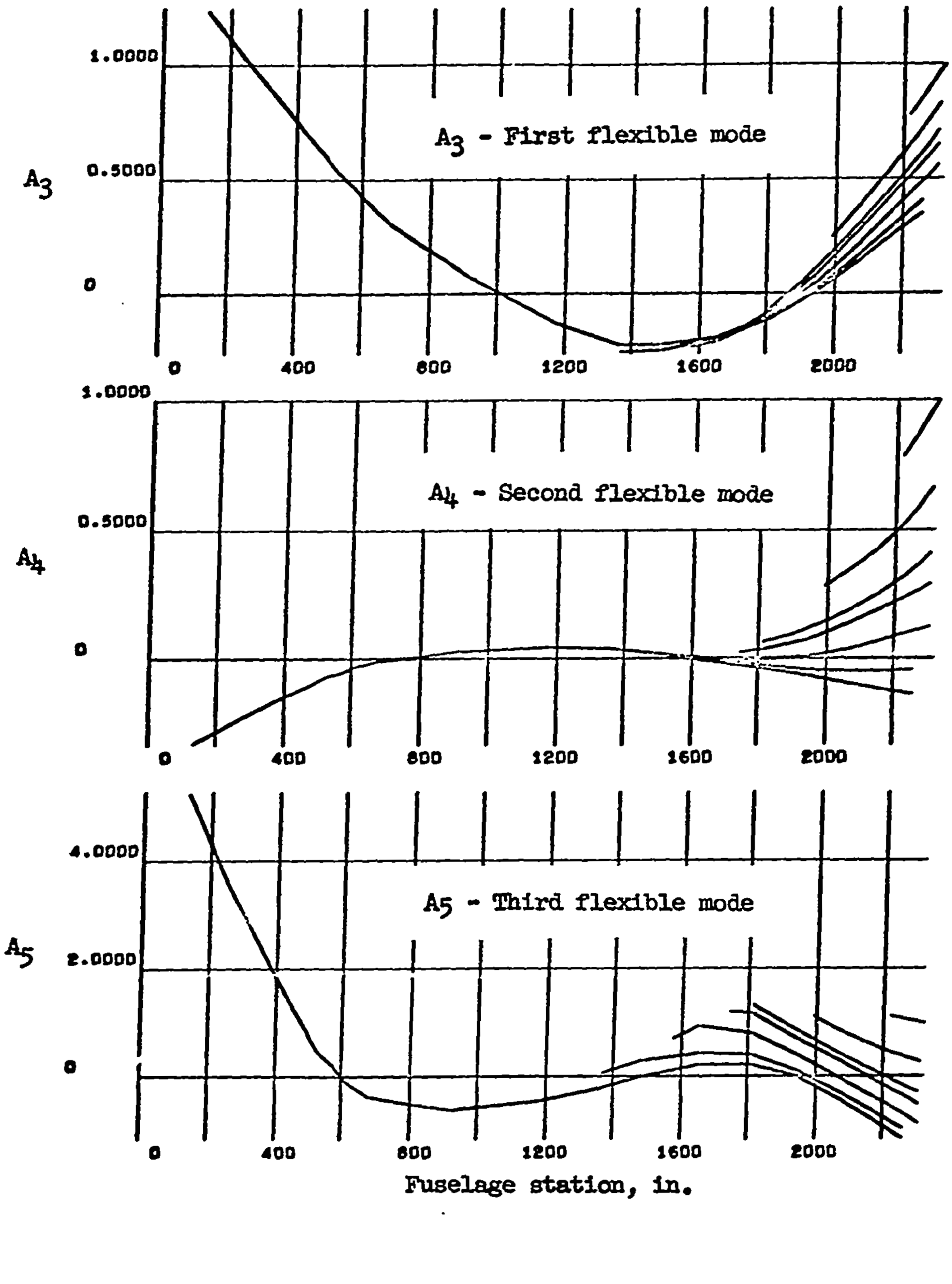

Figure 17.- Flexible mode shapes for Conditions 2-1 and 2-2.

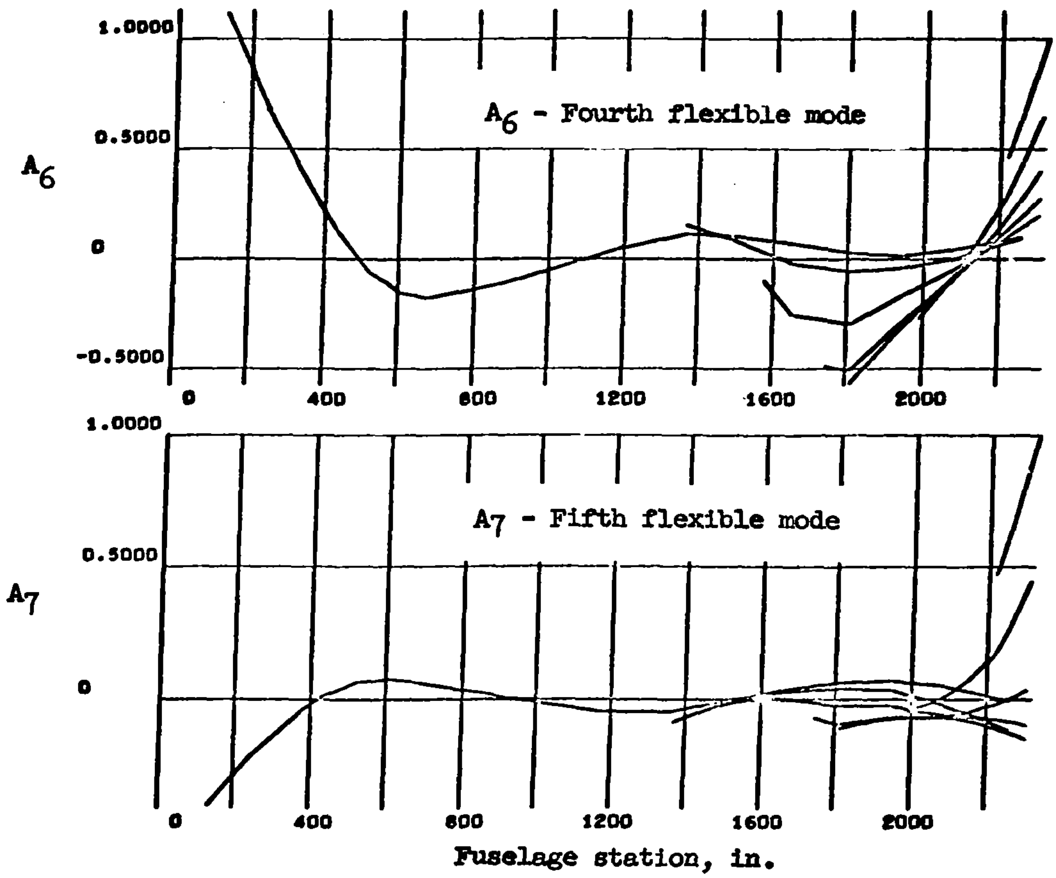

Figure 17.- Concluded.

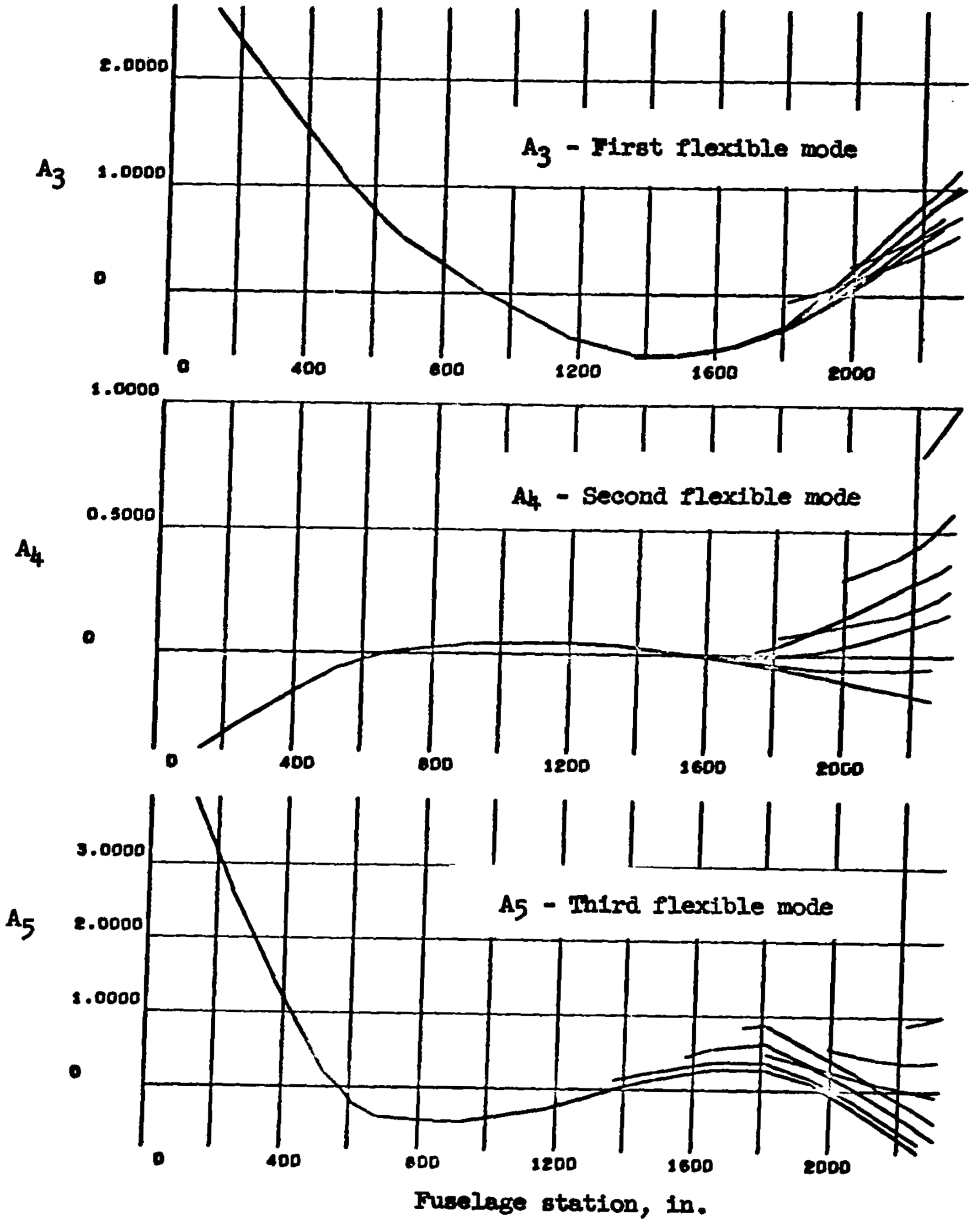

Figure 18.- Flexible mode shapes for Condition 2-3.

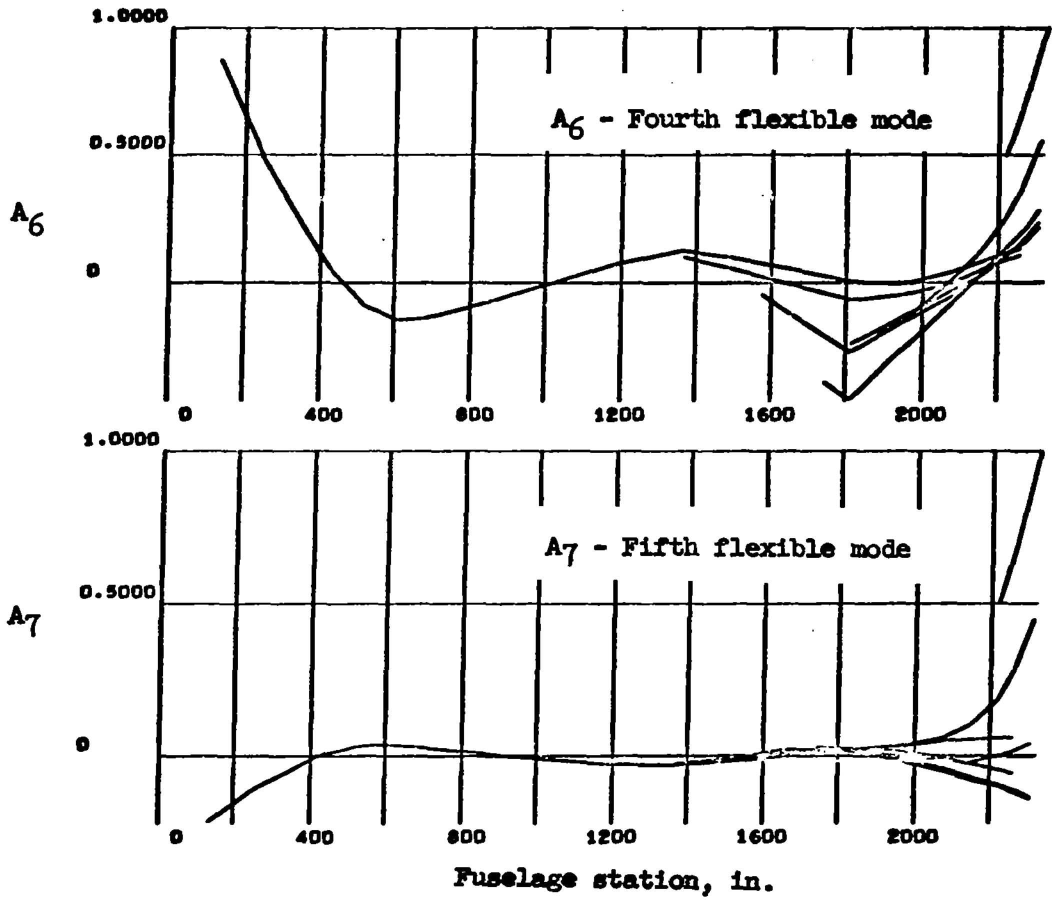

Figure 18.- Concluded.

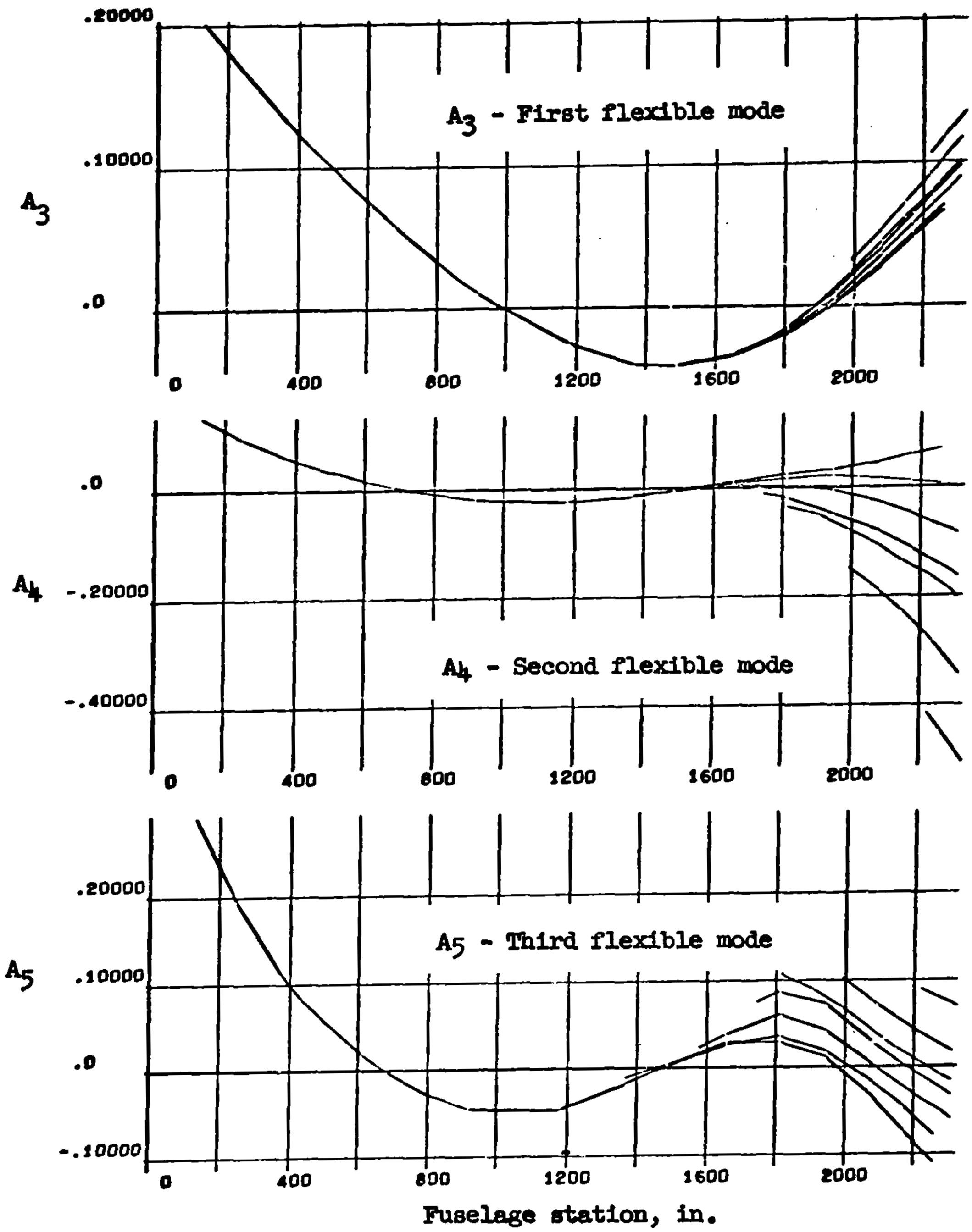

Figure 19.- Flexible mode shapes for Condition 3-1.

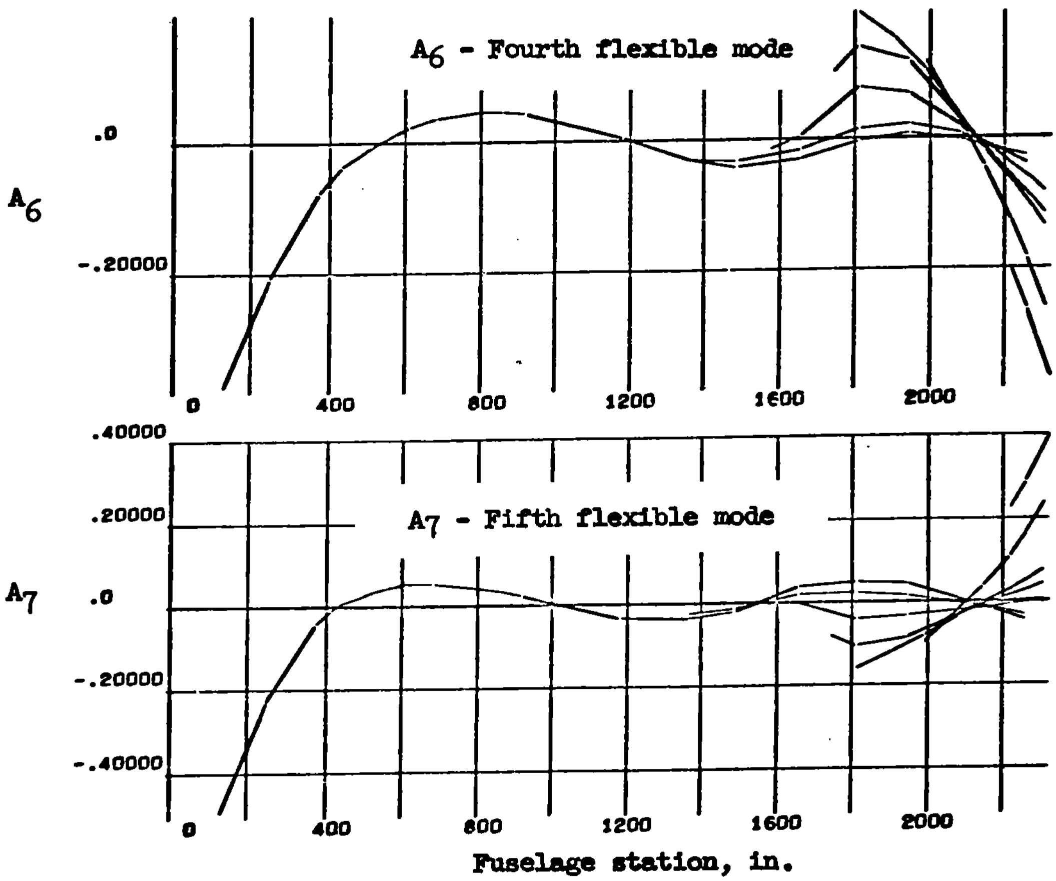

Figure 19.- Concluded.

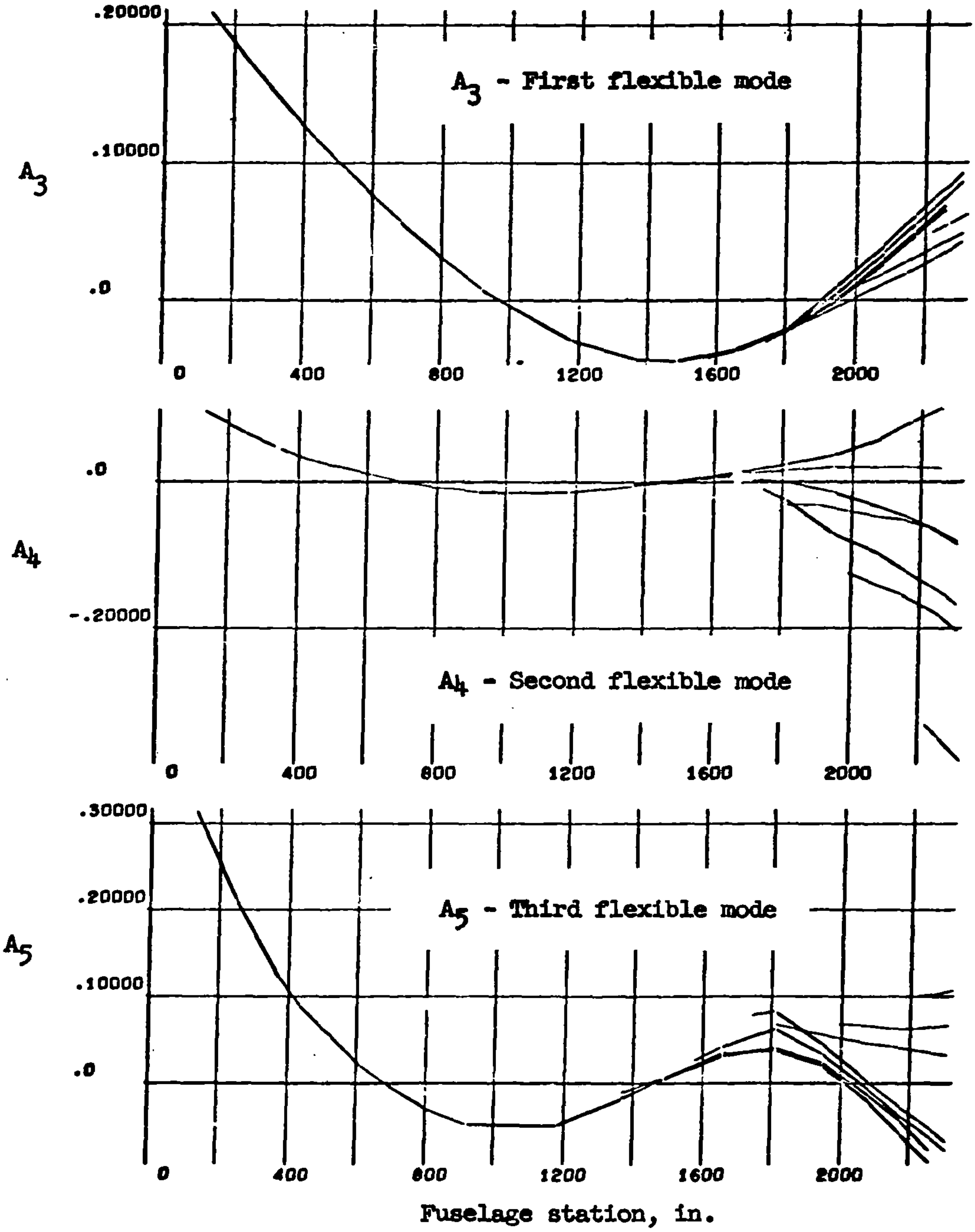

Figure 20.- Flexible mode shapes for Condition 3-2.

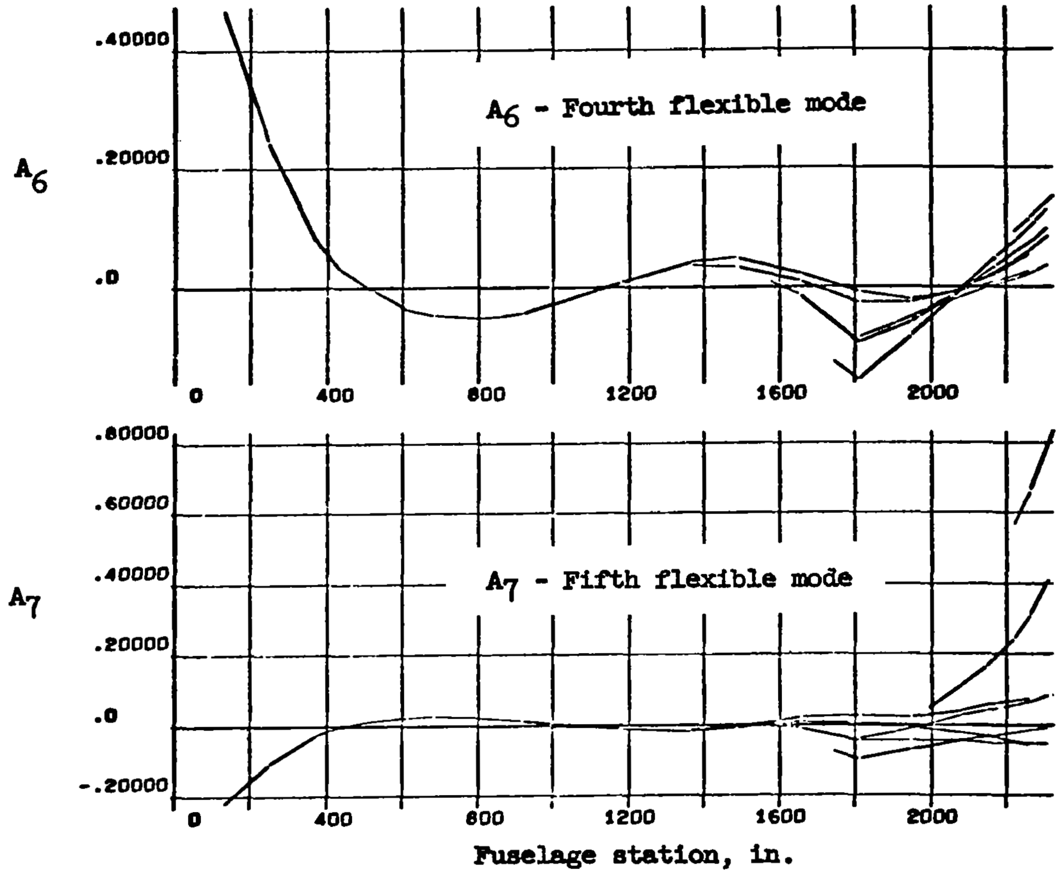

Figure 20.- Concluded.

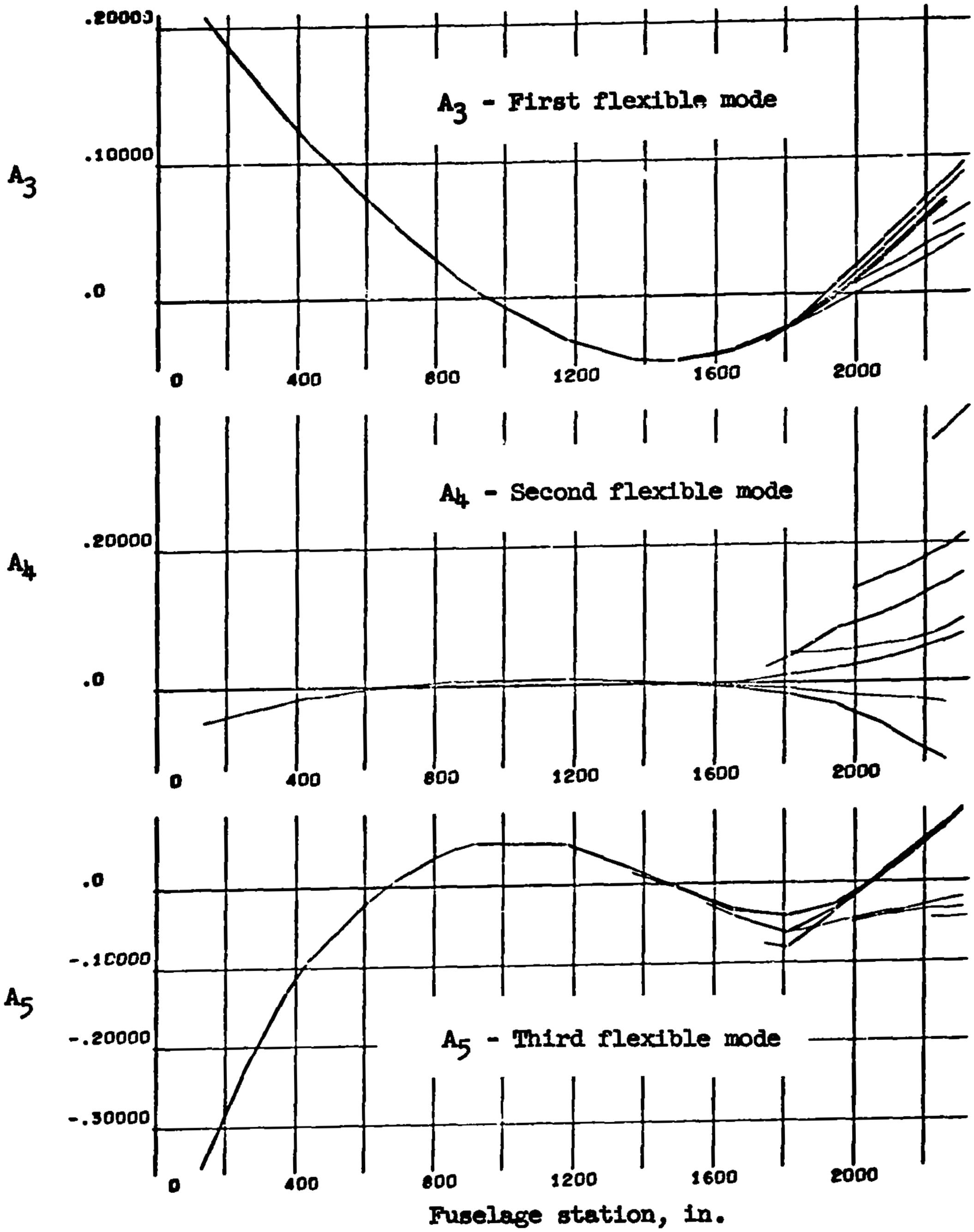

Figure 21.- Flexible mode shapes for Condition 3-3.

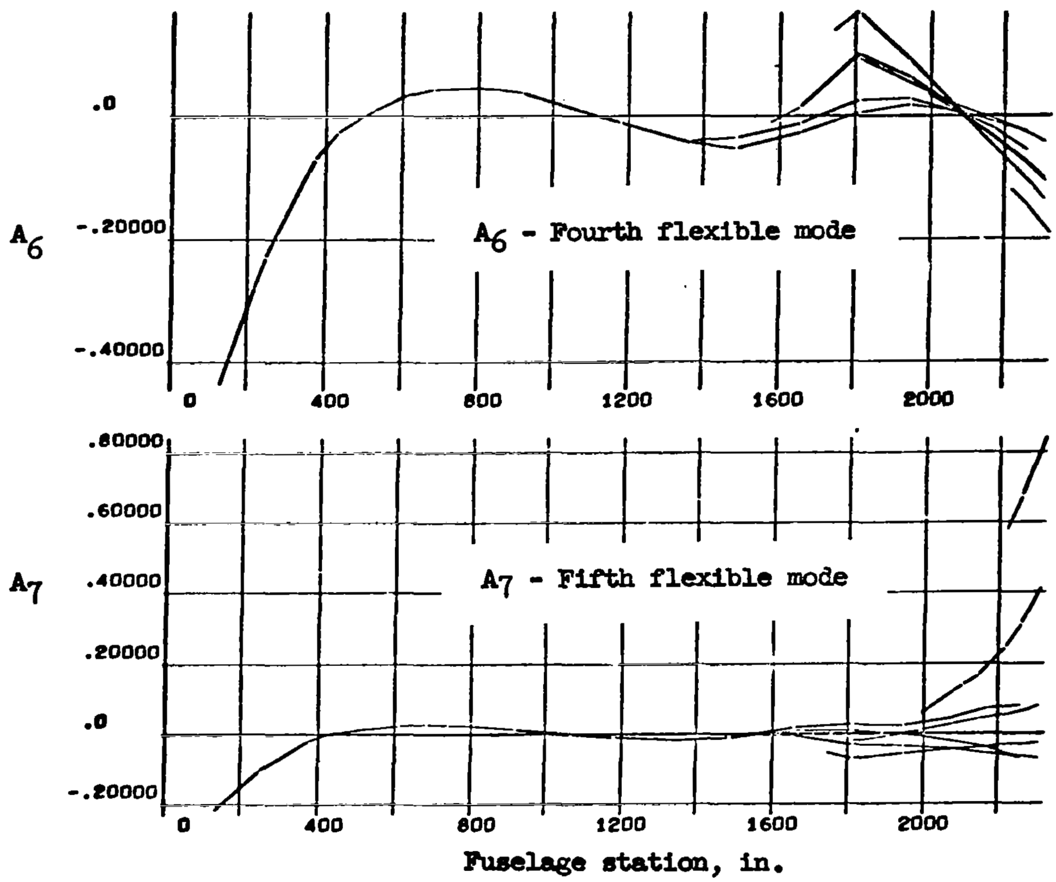

Figure 21.- Concluded.

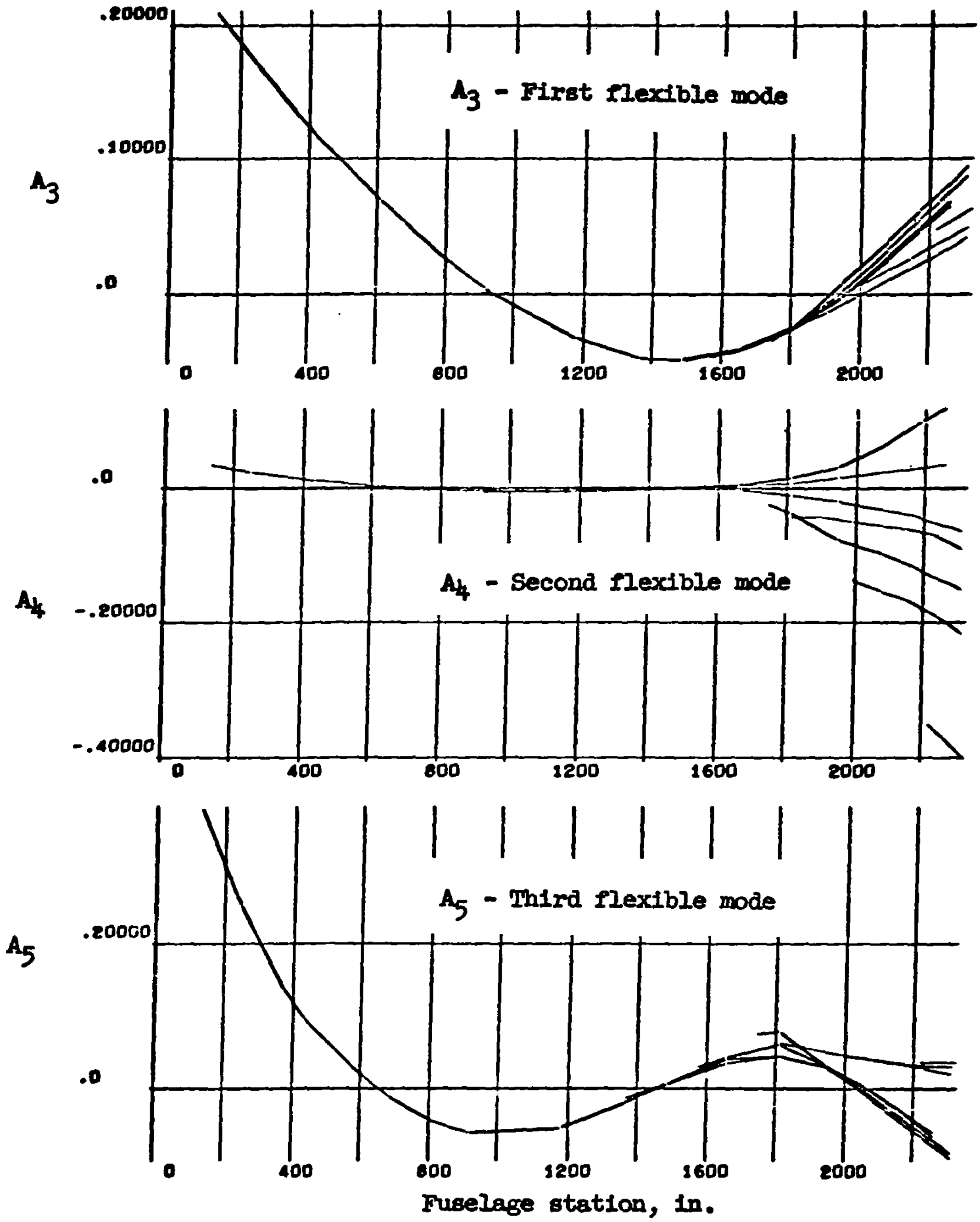

Figure 22.- Flexible mode shapes for Condition 3-4.

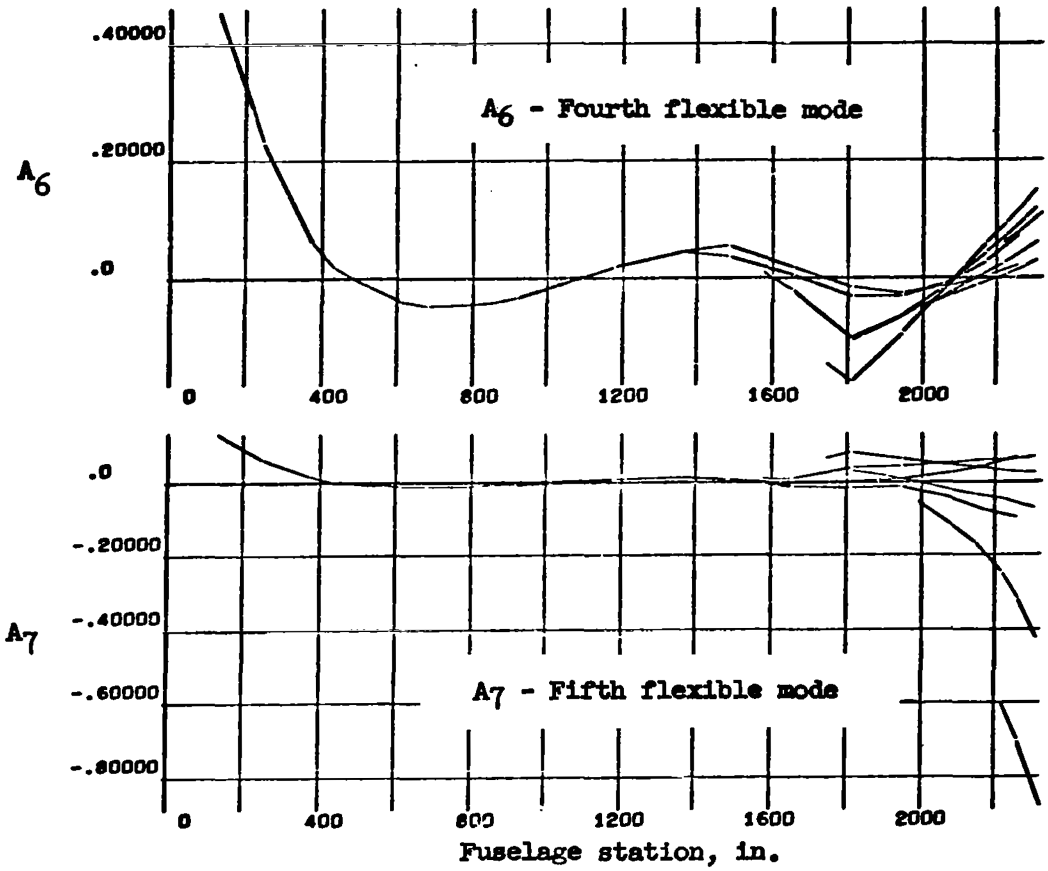

Figure 22.- Concluded.

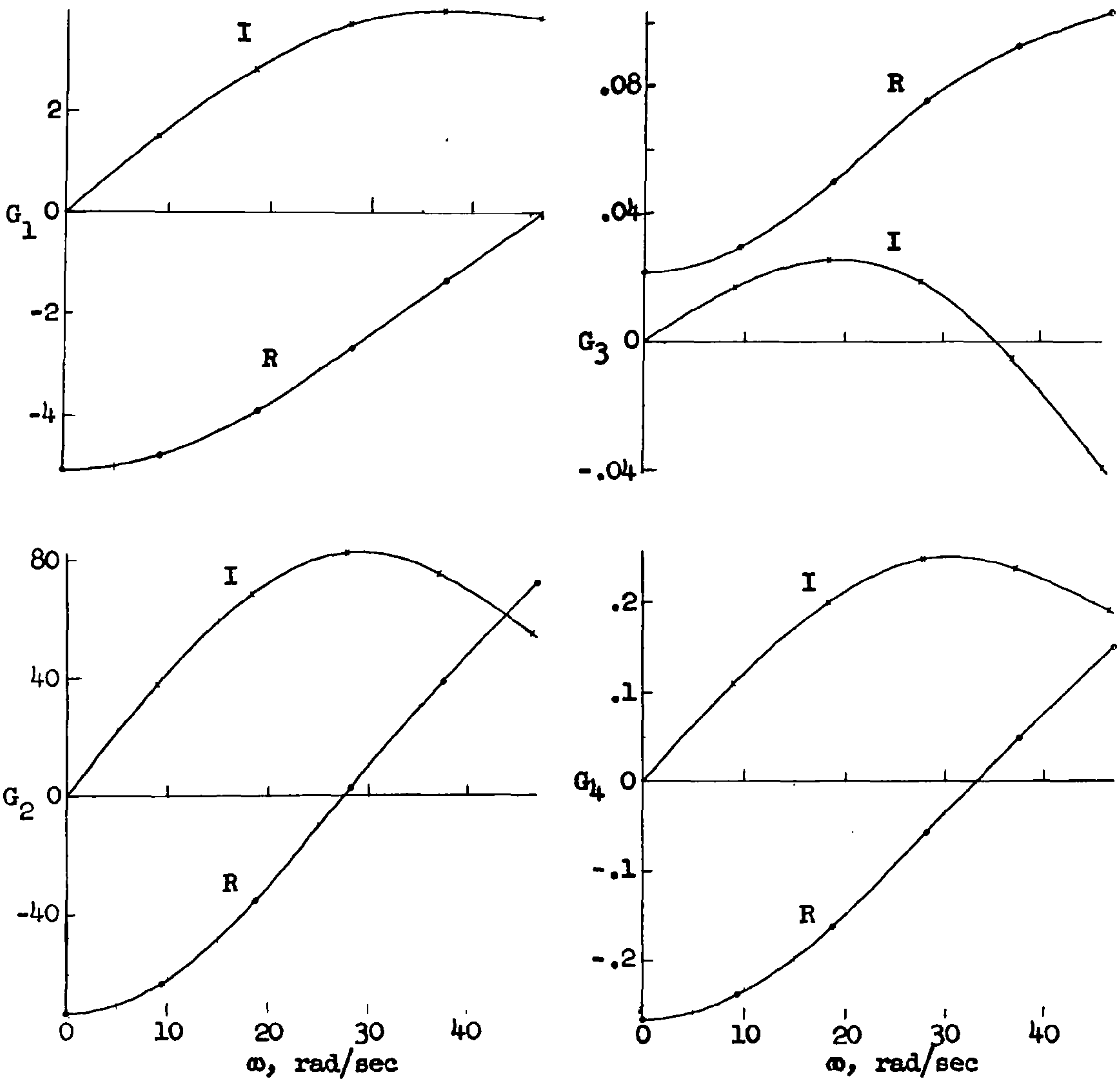

Figure 23.- Generalized forces due to gust, Condition 1-1.

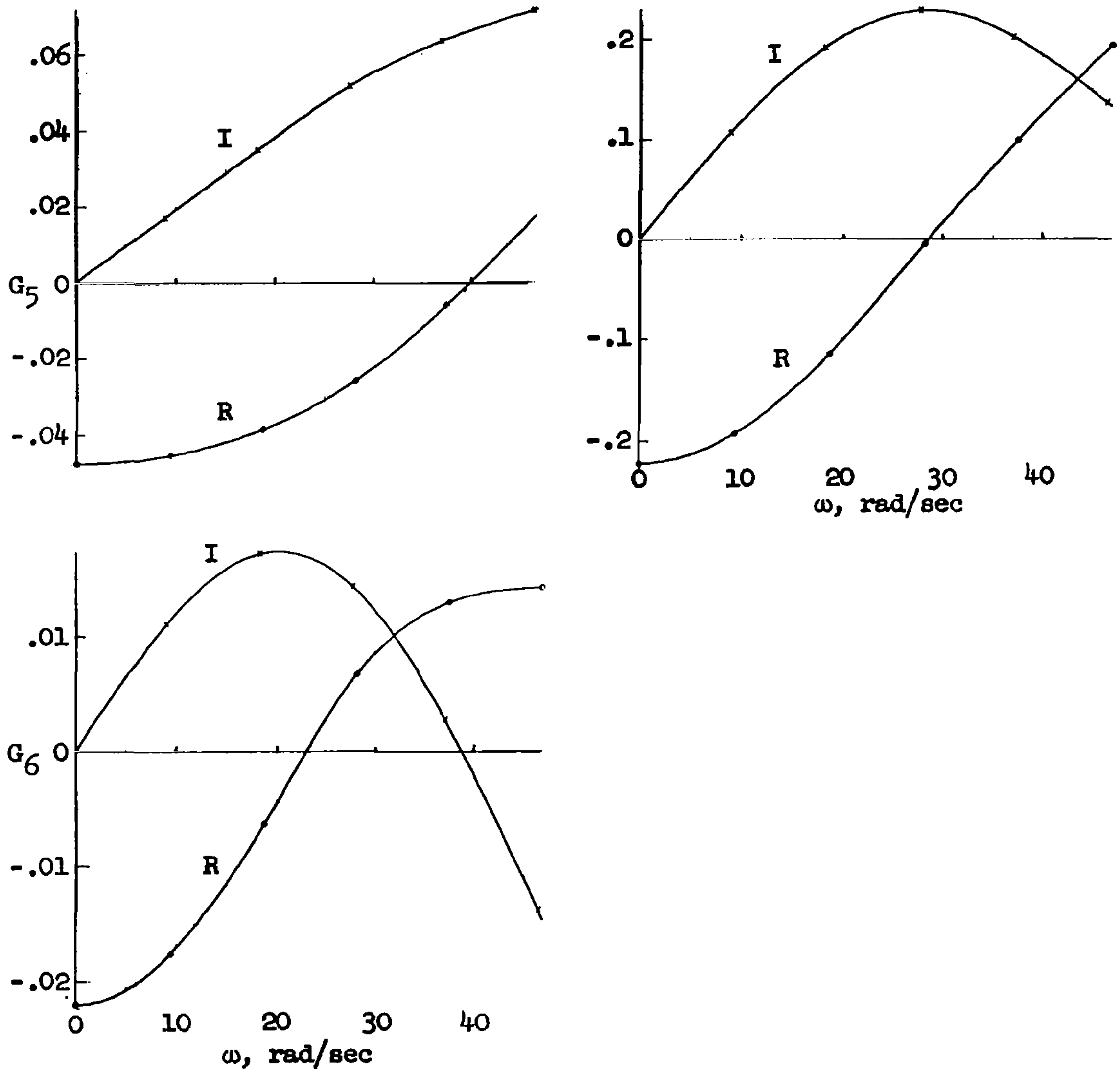

Figure 23.- Concluded.

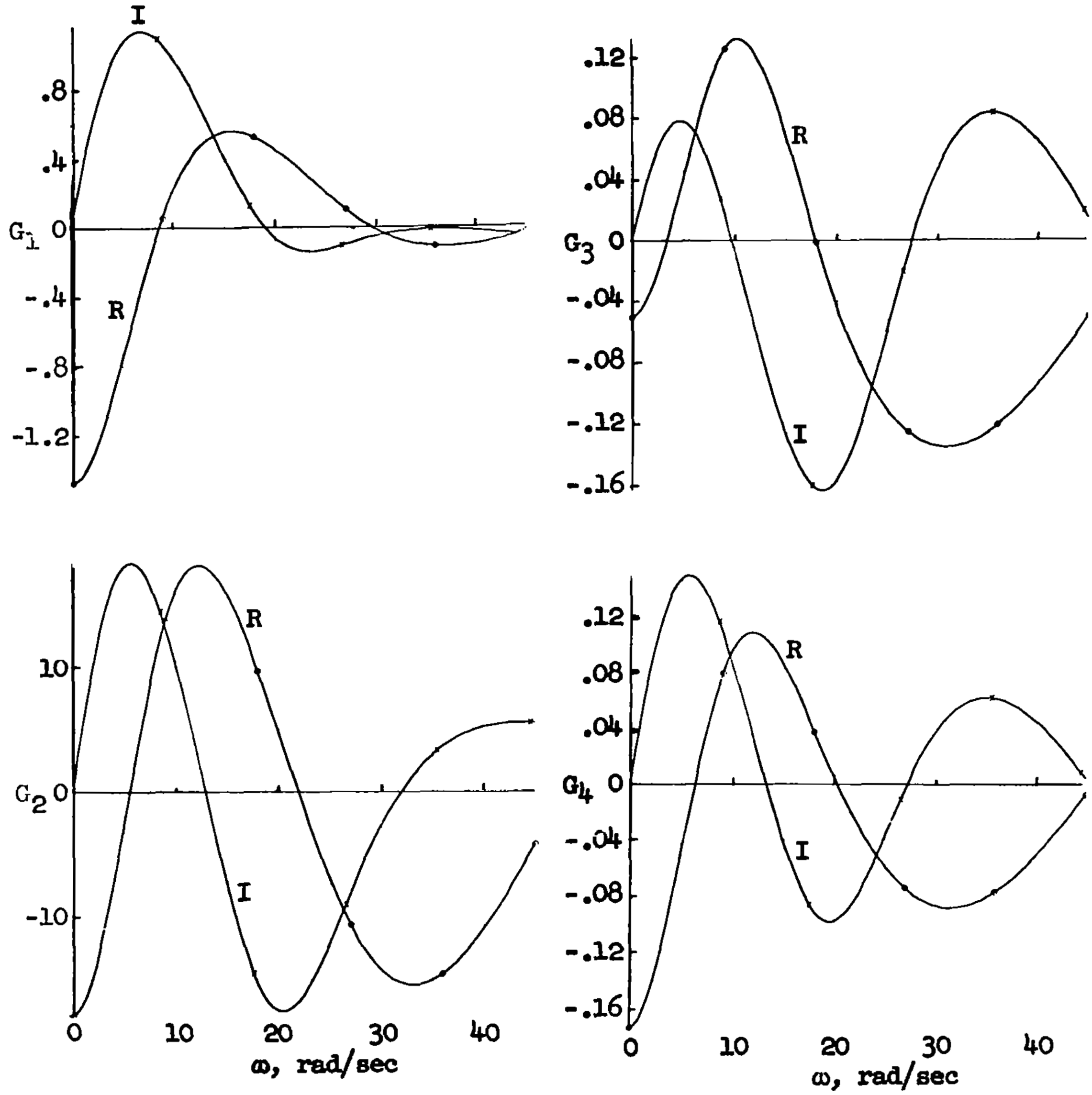

Figure 24.- Generalized forces due to gust, Condition 2-1.

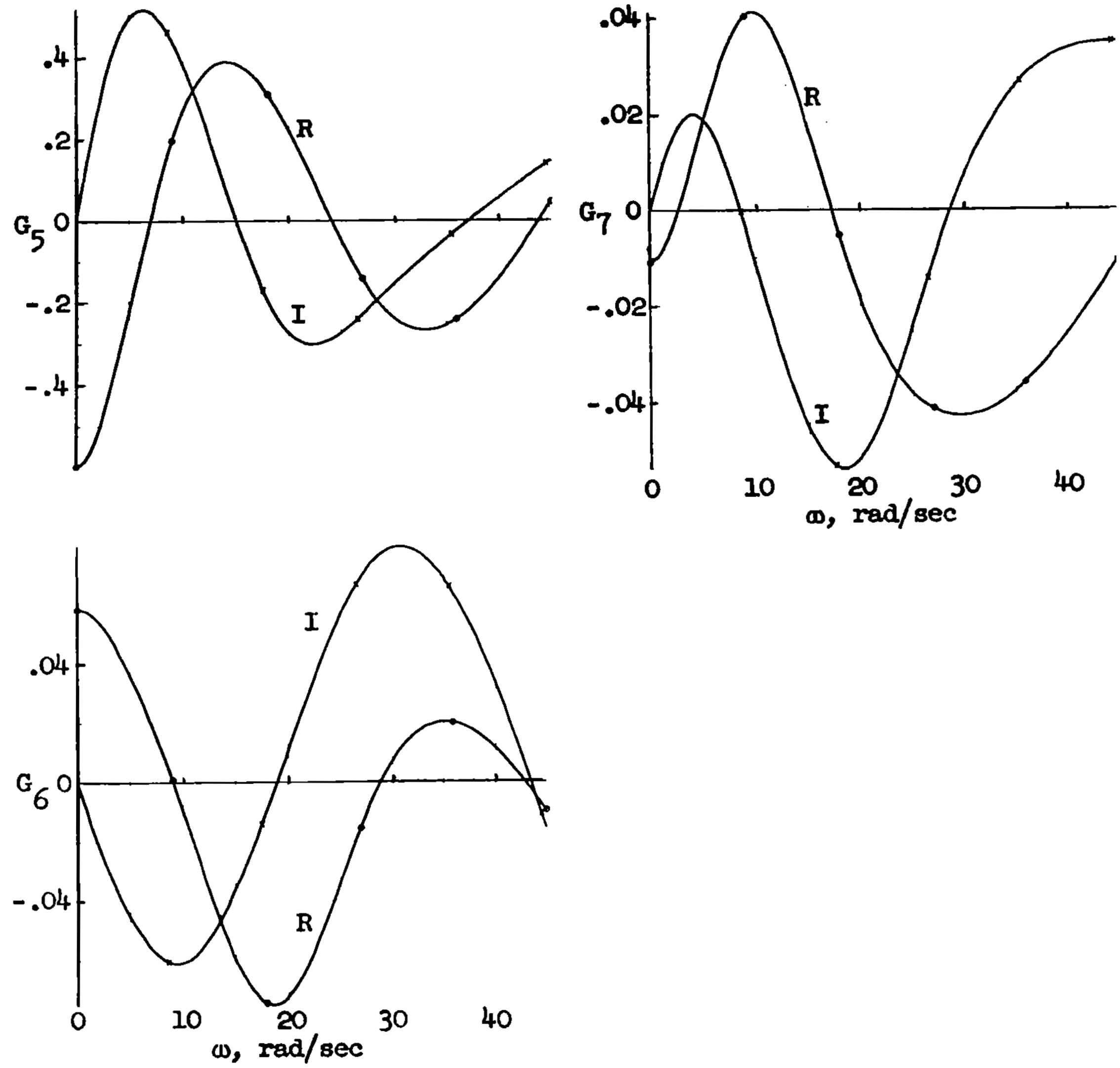

Figure 24.- Concluded.

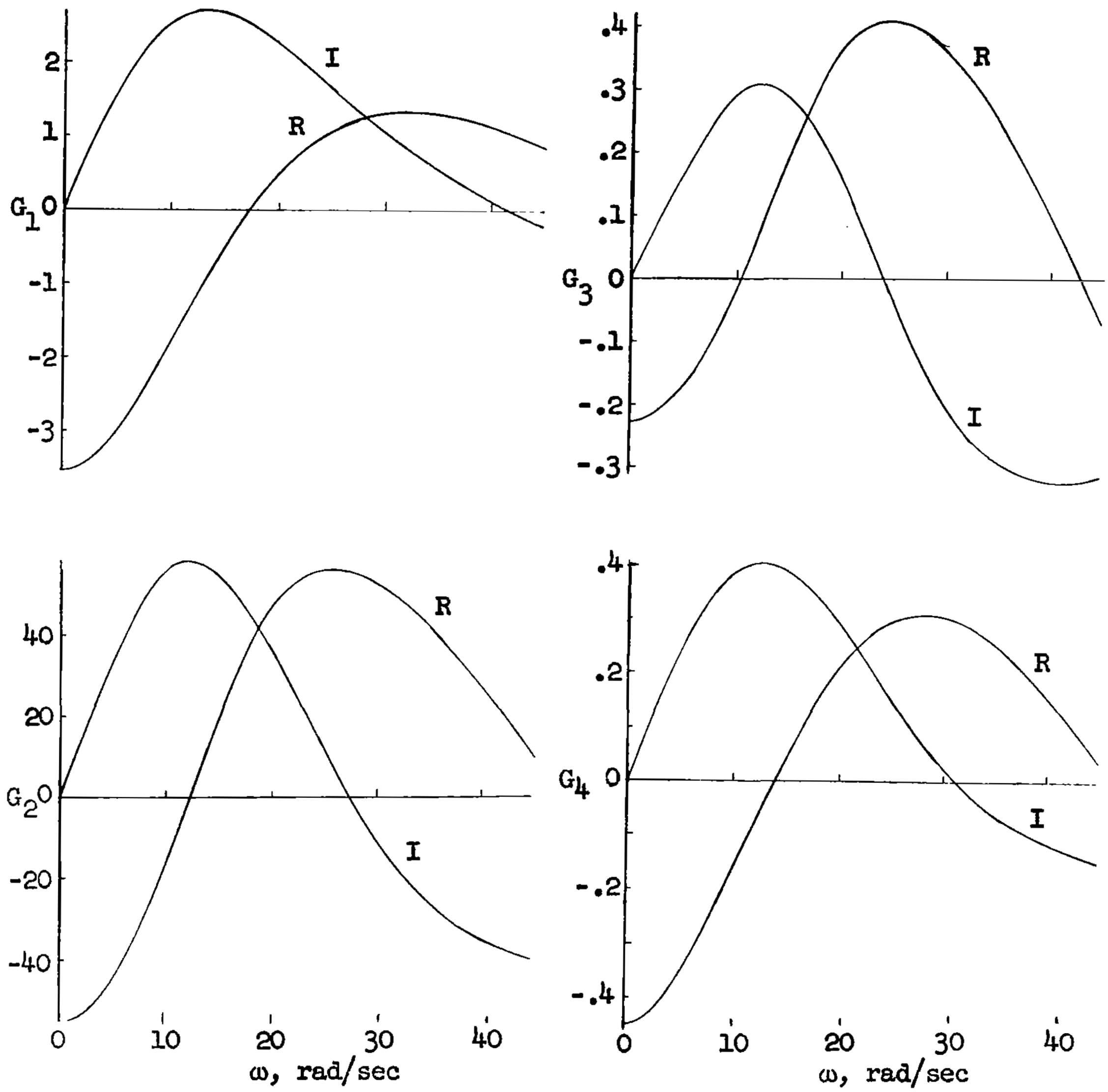

Figure 25.- Generalized forces due to gust, Condition 2-2.

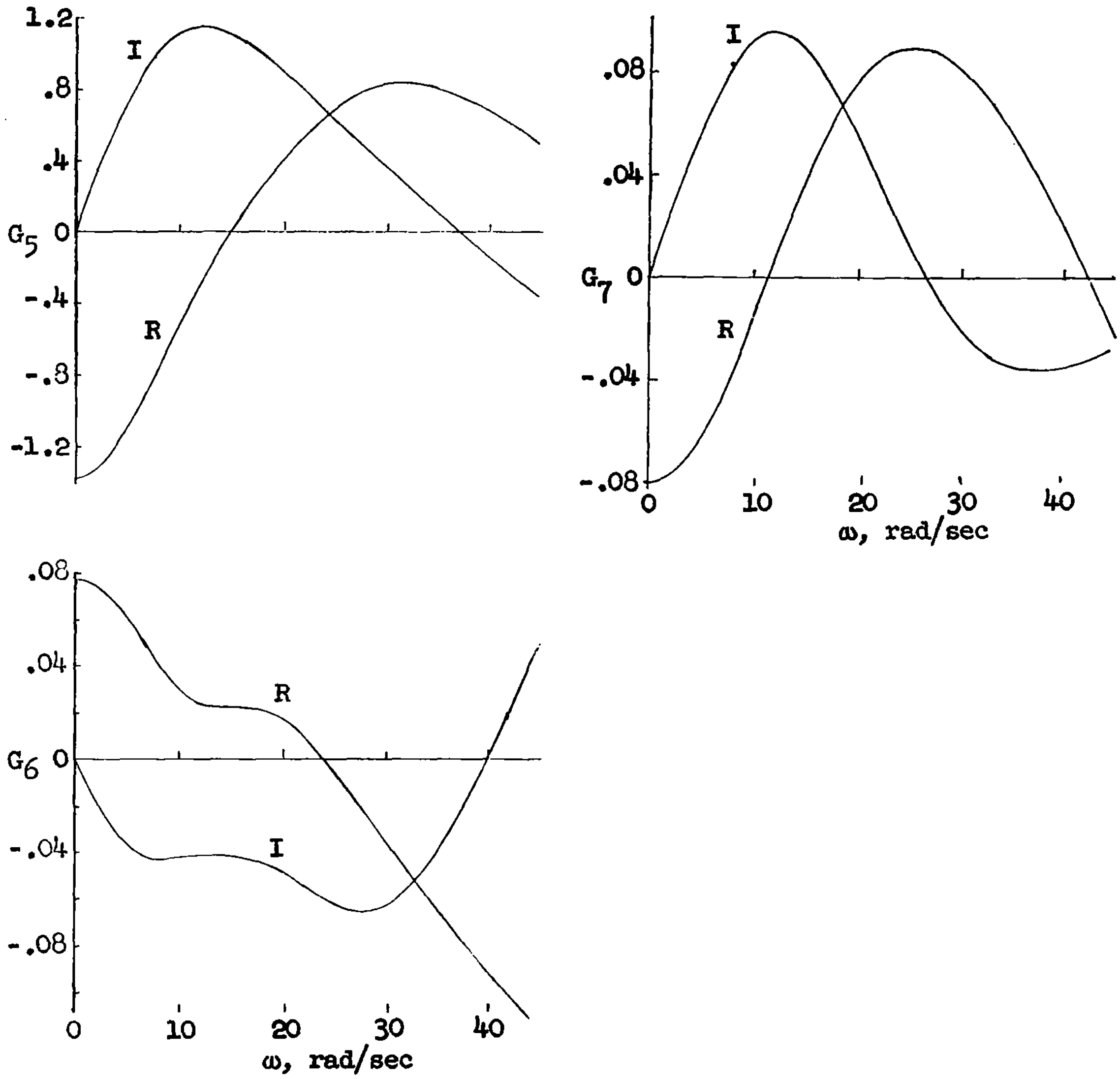

Figure 25.- Concluded.

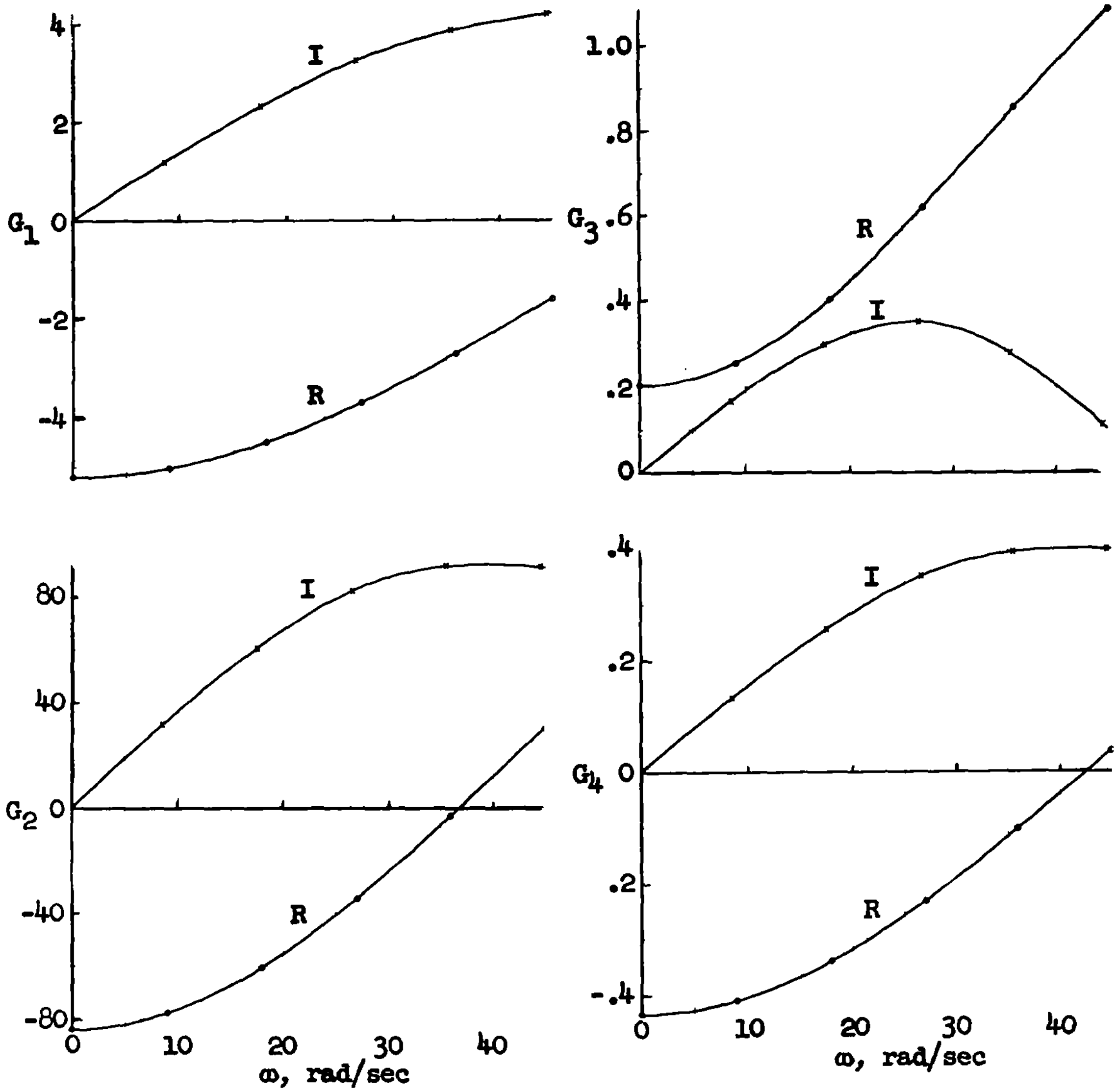

Figure 26.- Generalized forces due to gust, Condition 2-3.

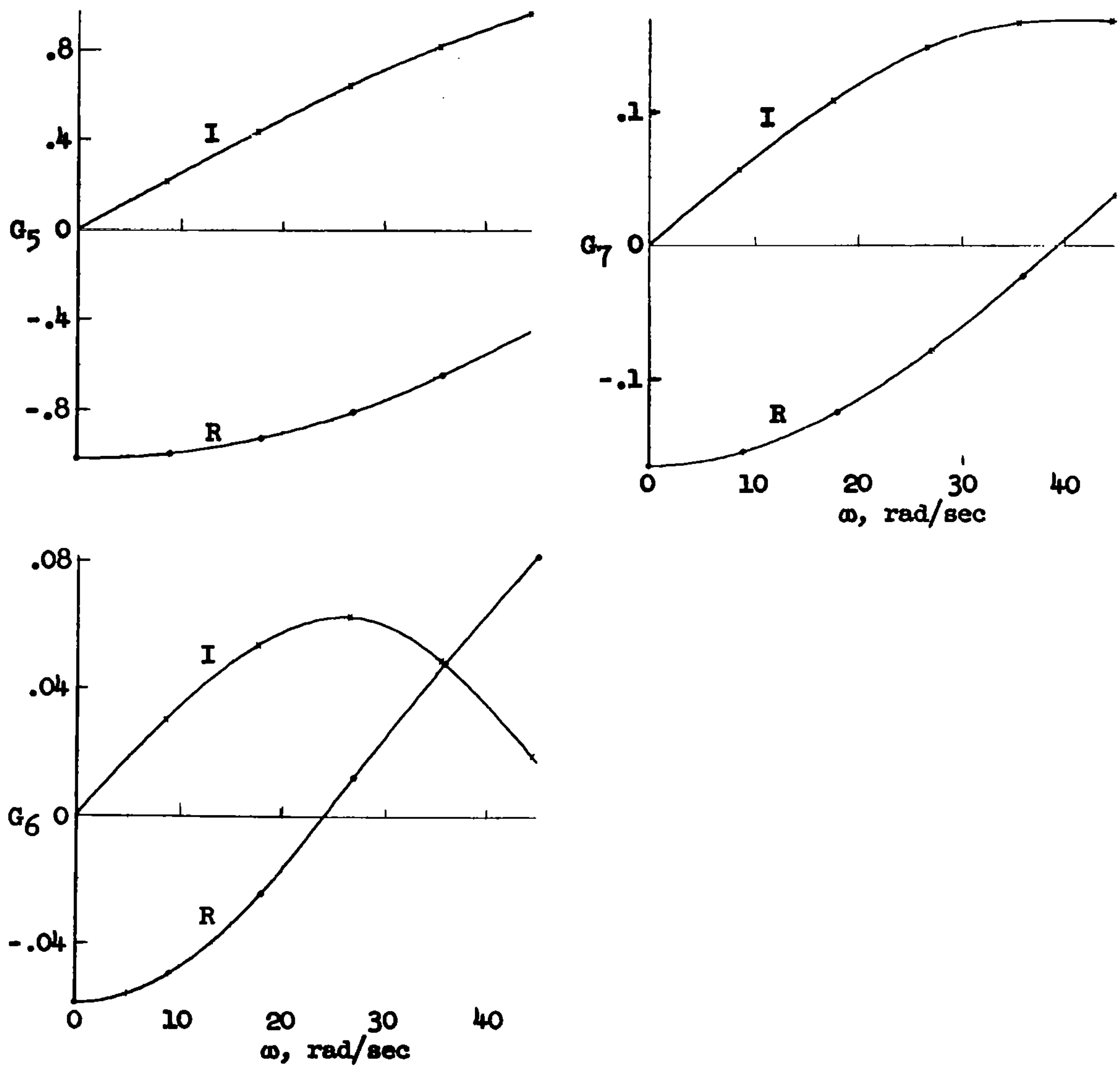

Figure 26.- Concluded.

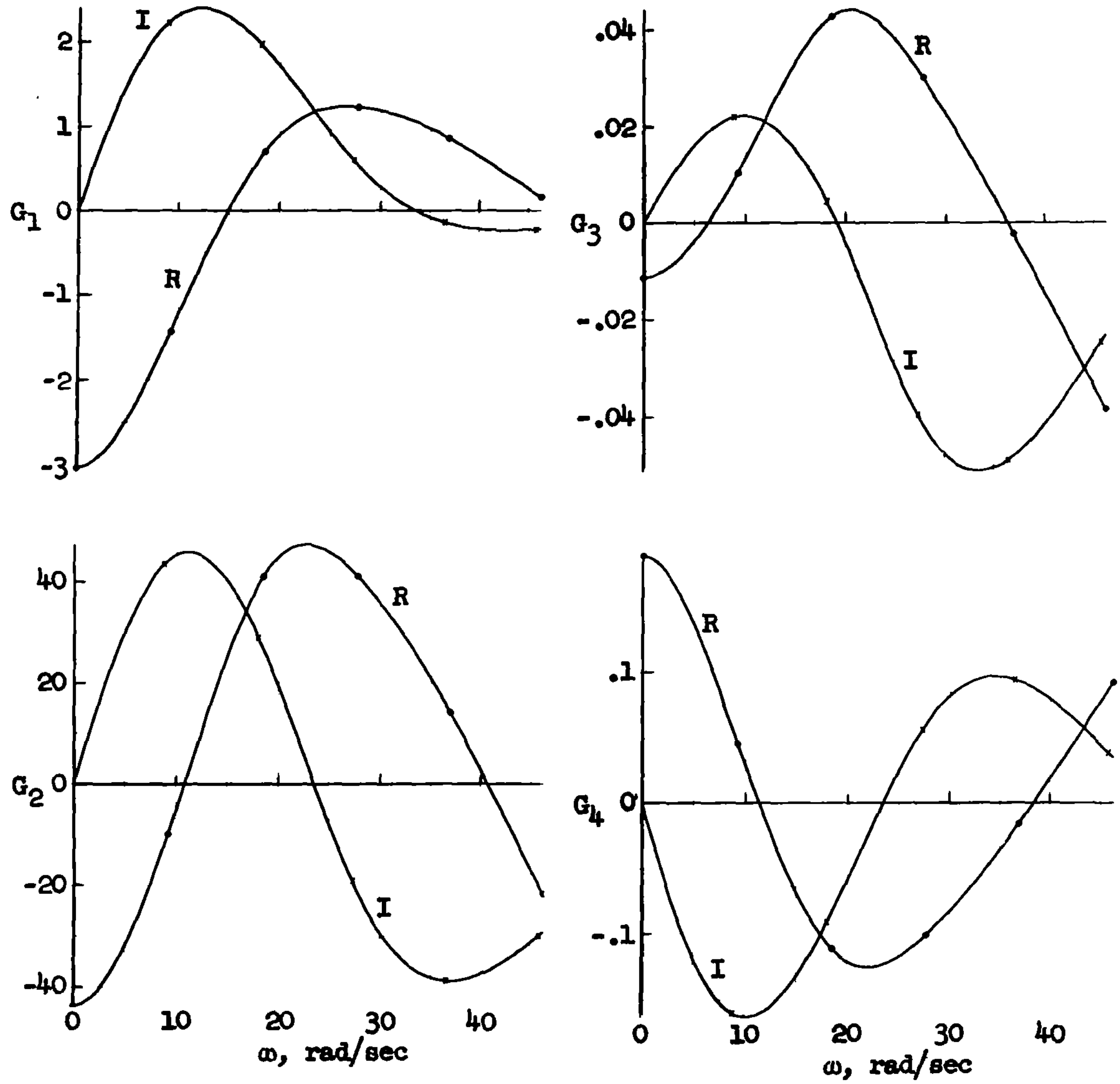

Figure 27.- Generalized forces due to gust, Condition 3-1.

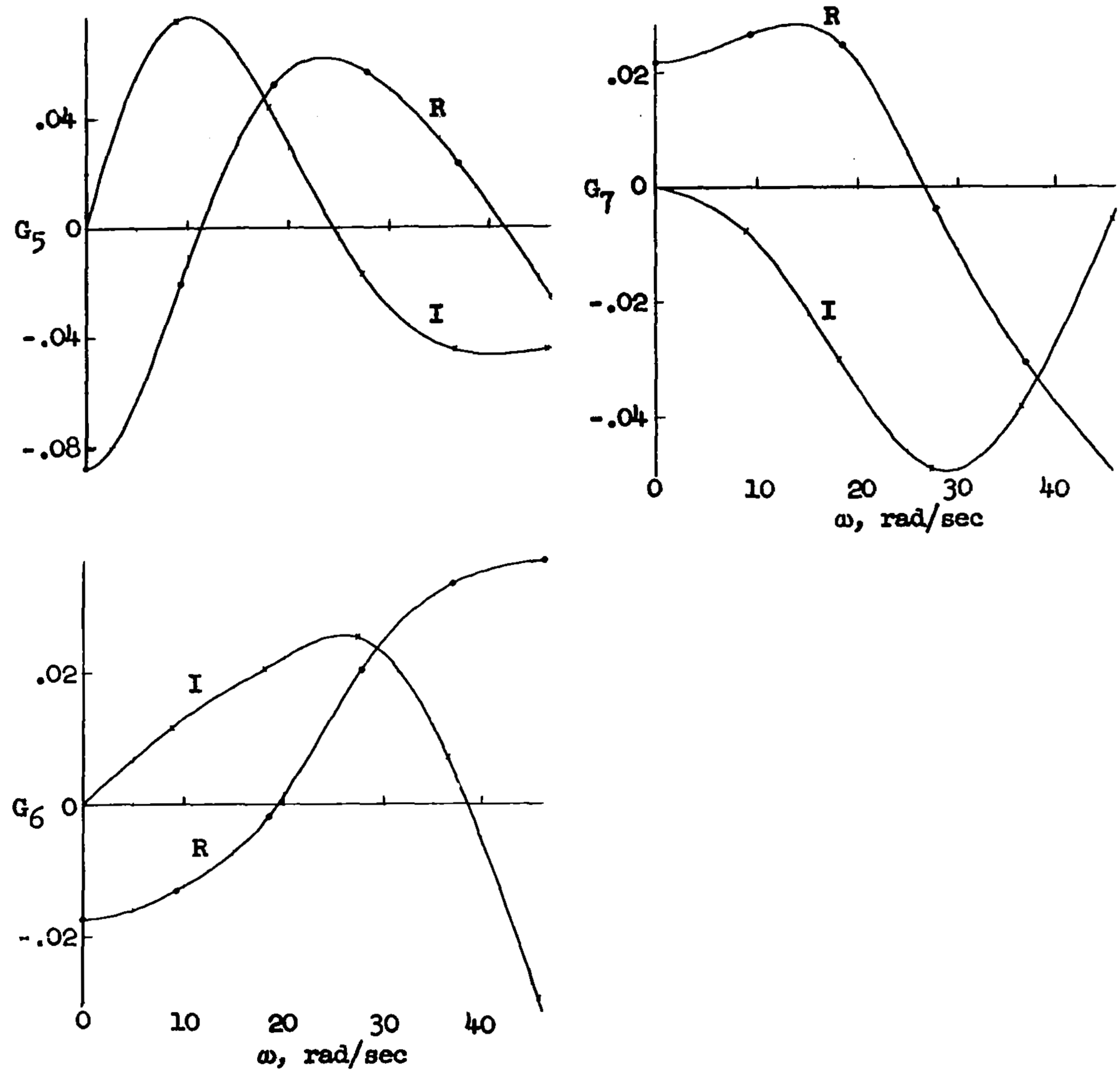

Figure 27.- Concluded.

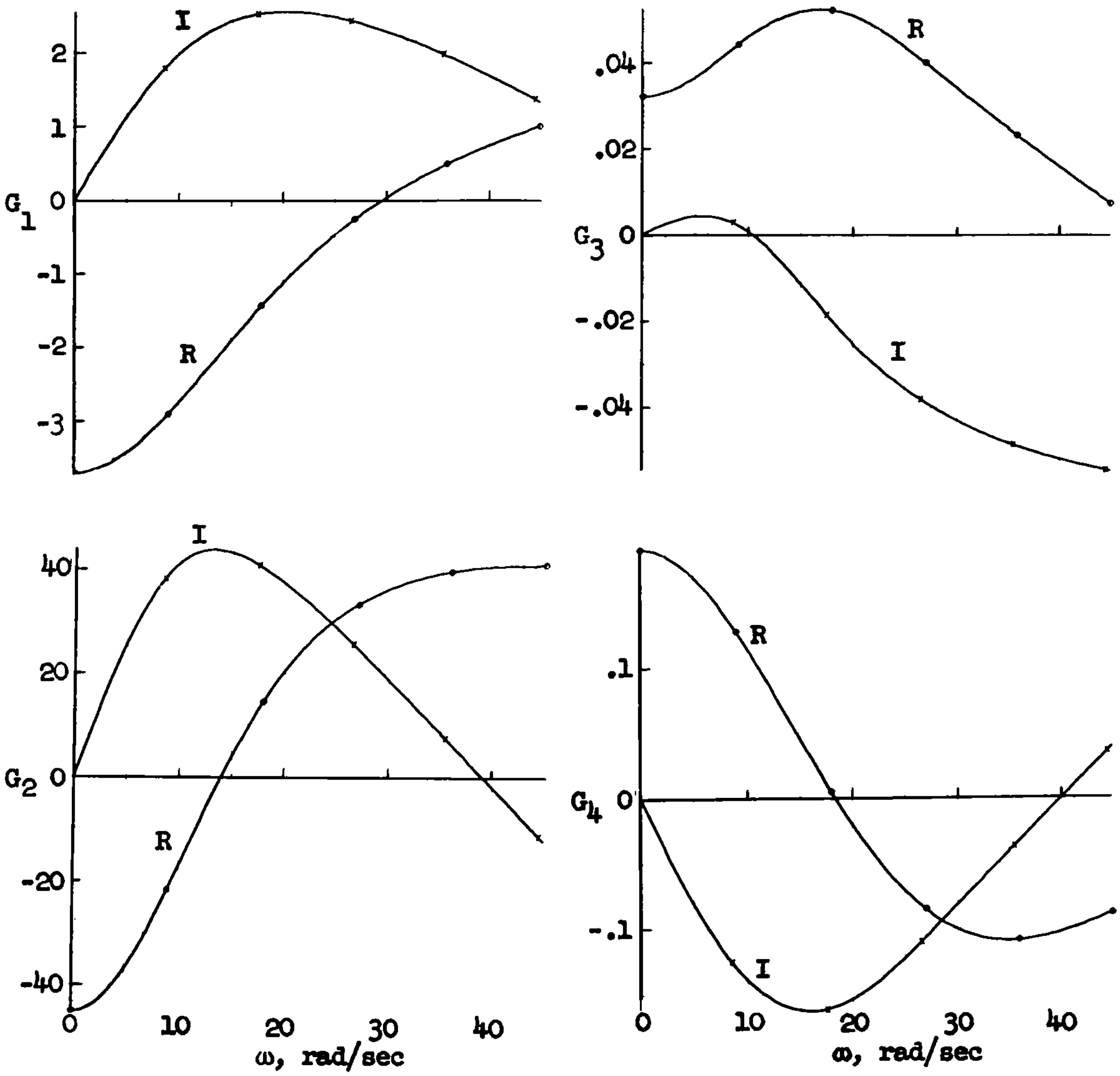

Figure 28.- Generalized forces due to gust, Condition 3-2.

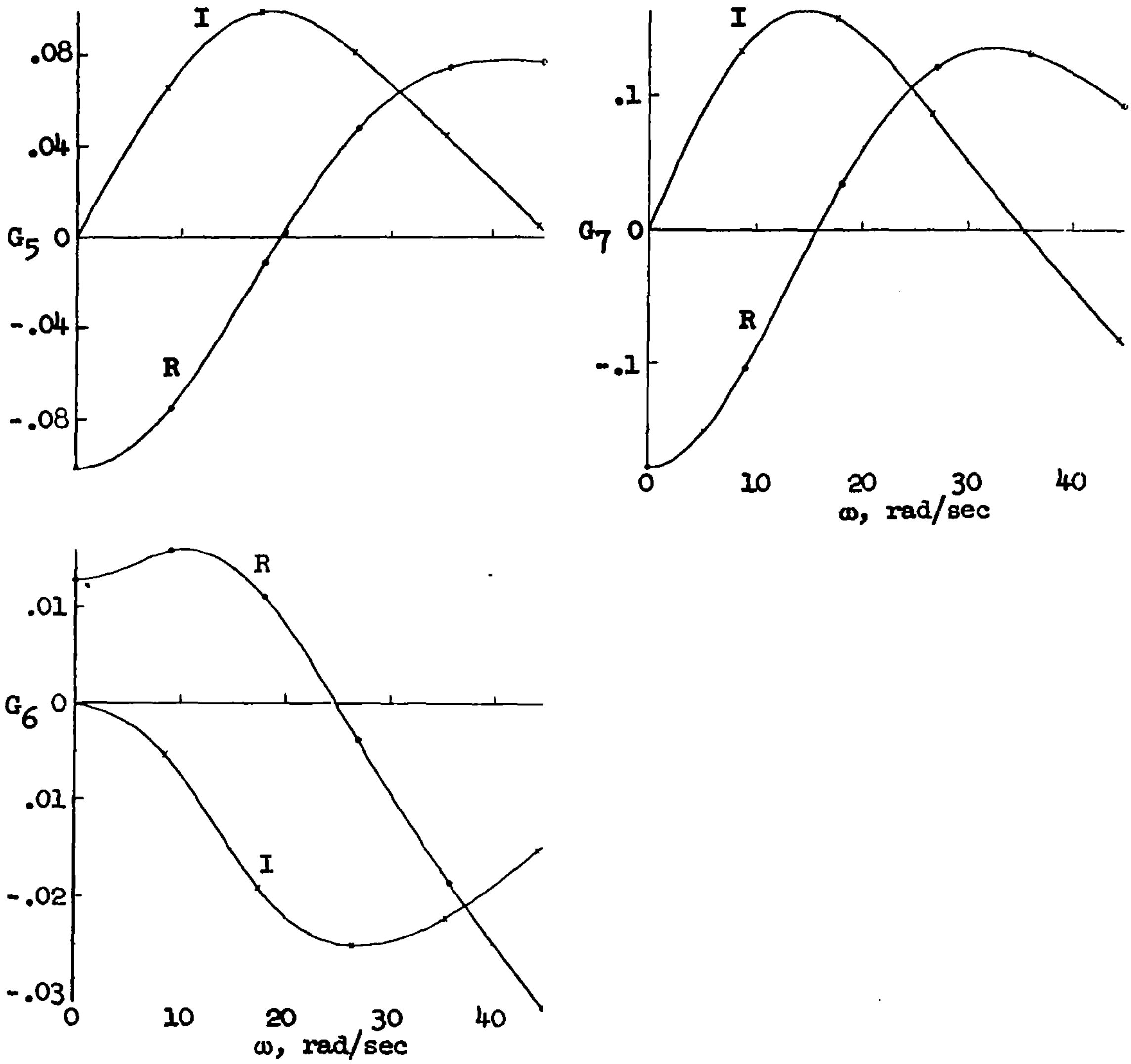

Figure 28.- Concluded.

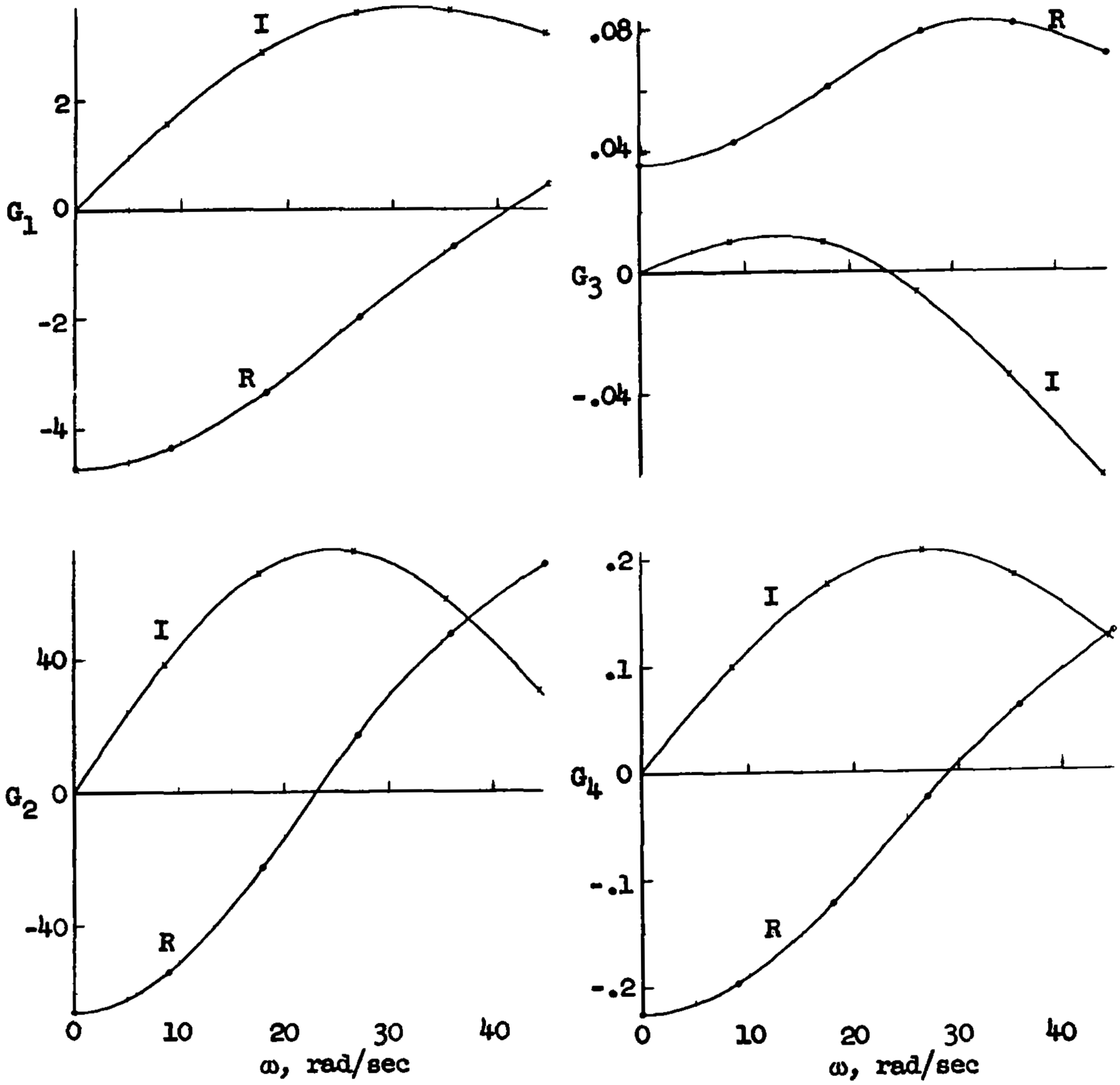

Figure 29.- Generalized forces due to gust, Condition 3-3.

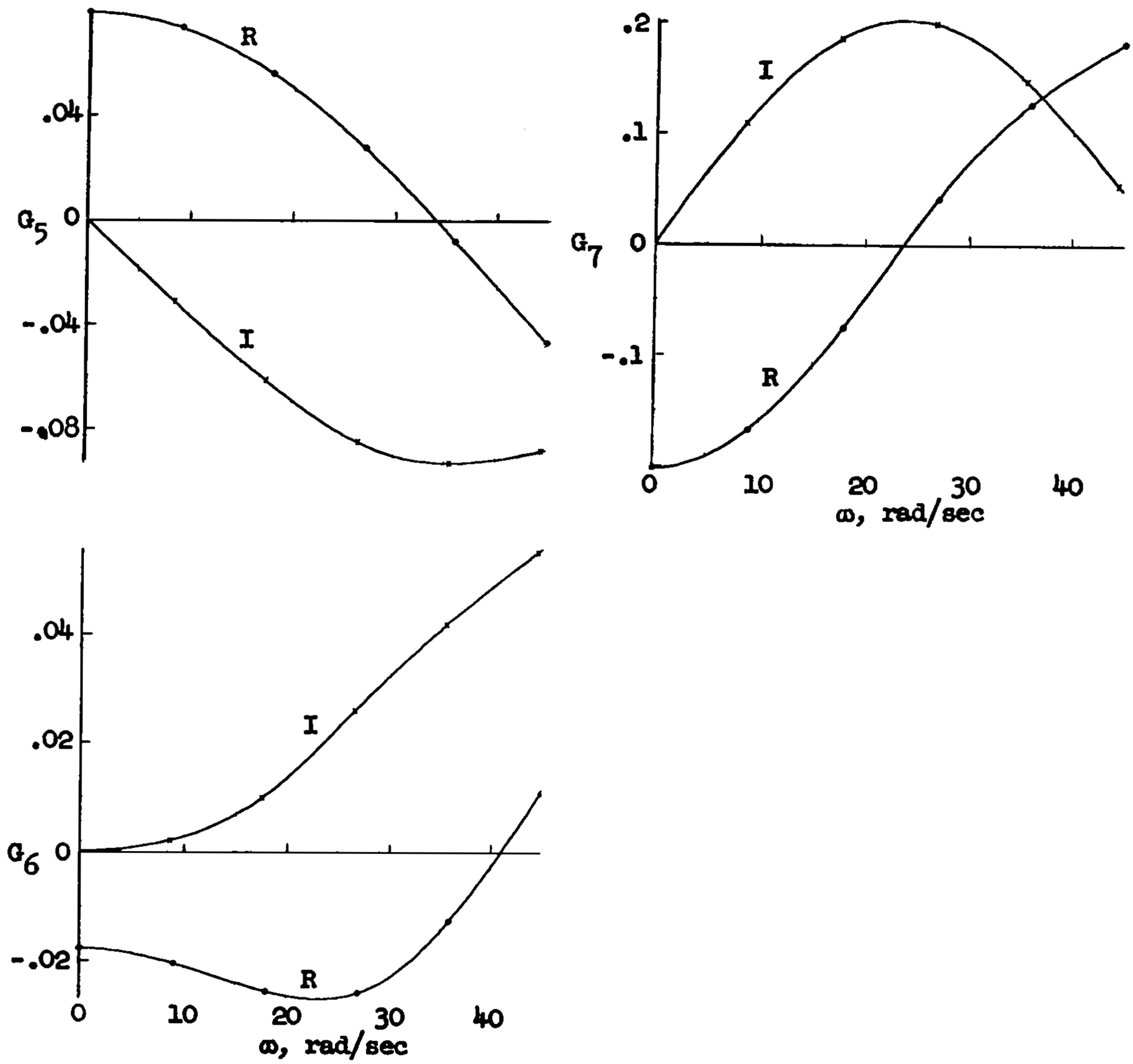

Figure 29.- Concluded.

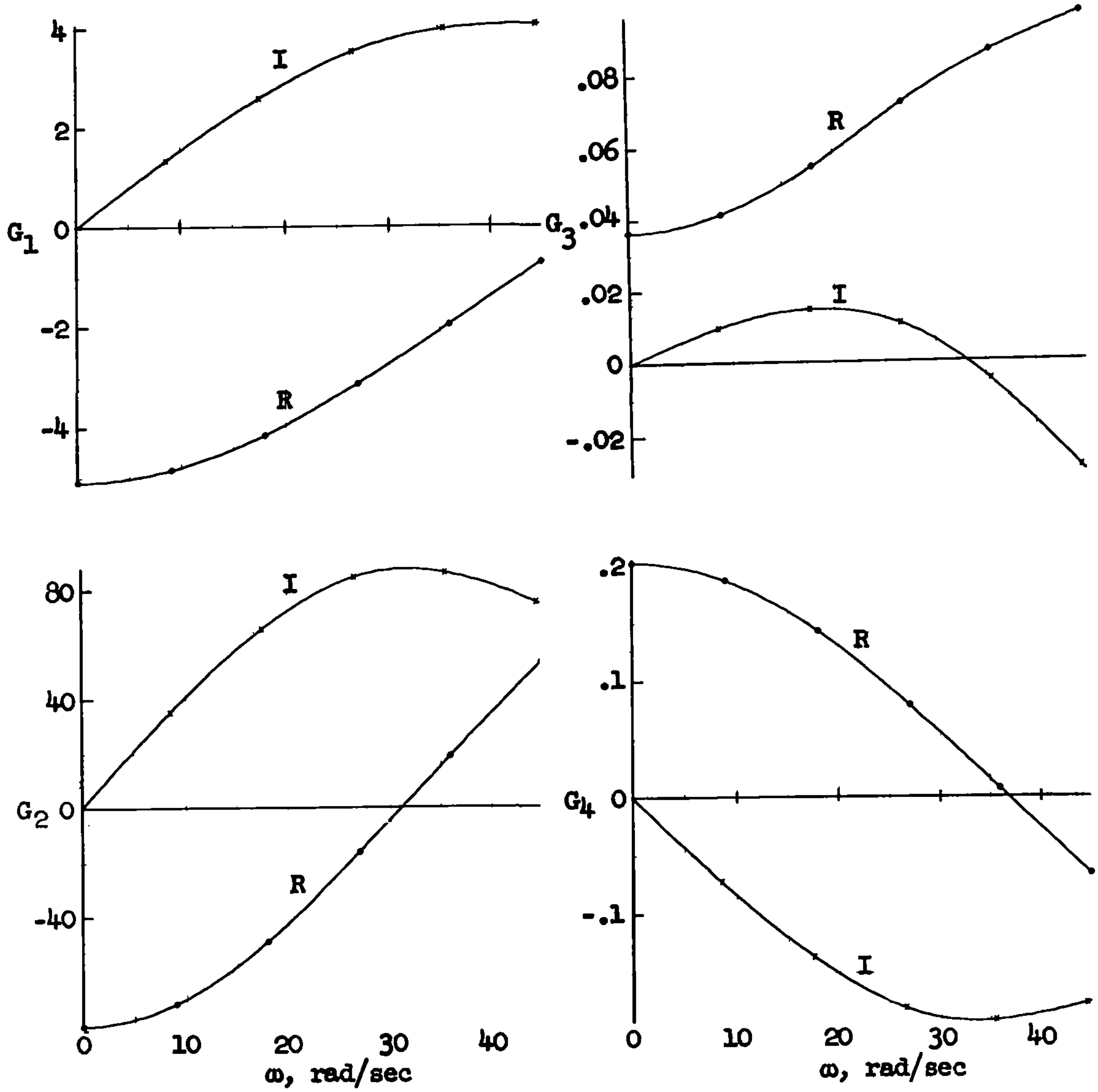

Figure 30.- Generalized forces due to gust, Condition 3-4.

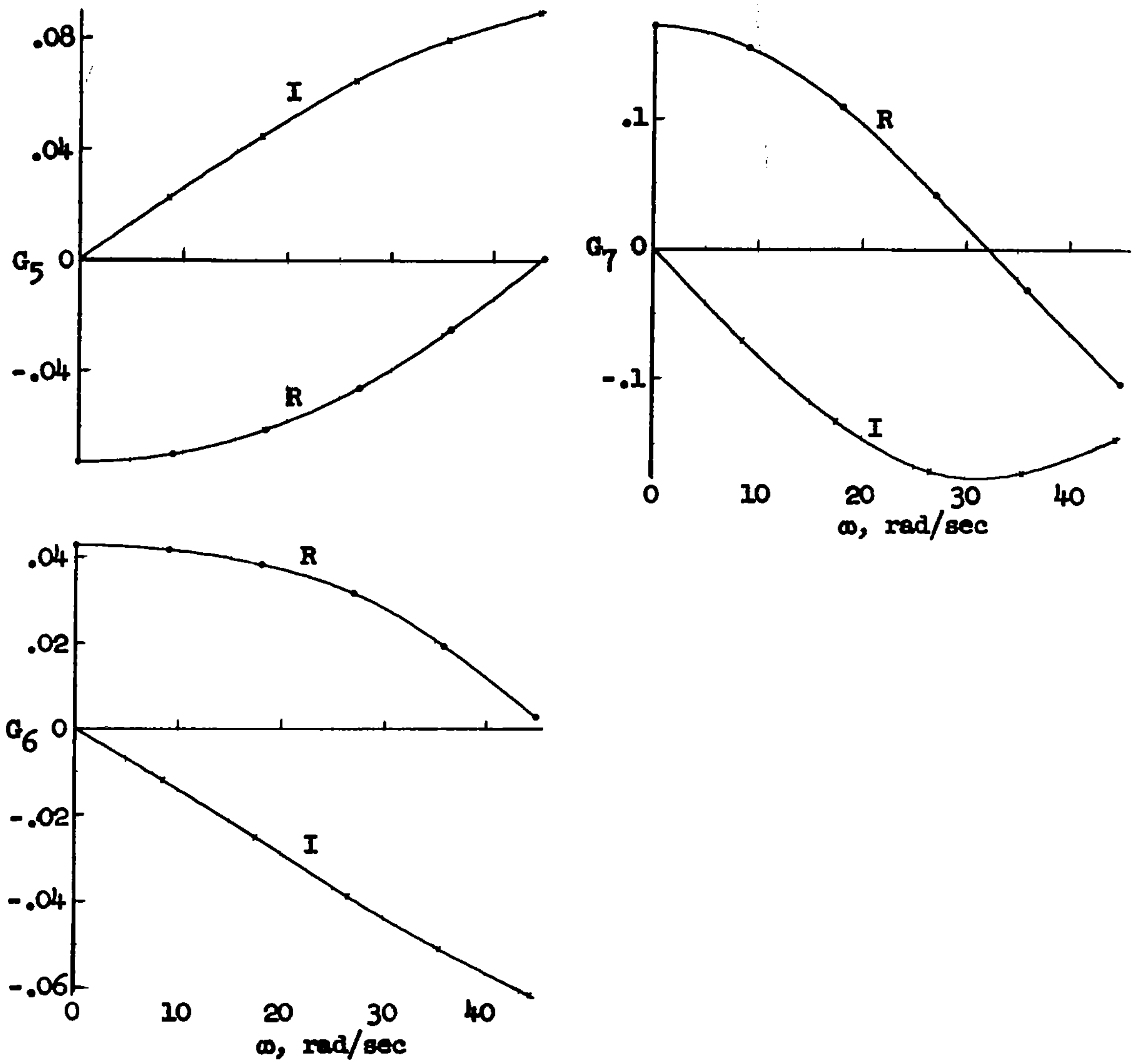

Figure 30.- Concluded.